

# **Integrative In Silico Drug Discovery: Targeting Tyrosinase with Natural Compounds for therapeutic management of Vitiligo**

**A Thesis Submitted  
In Partial Fulfillment of the  
Requirements for the Degree of**

**MASTER OF  
TECHNOLOGY**

**by**

**KHUSHI BHATIA  
(23/BIO/02)**

**Under the Supervision of  
PROF. YASHA HASIJA  
Delhi Technological University**



**Department of Biotechnology**

**DELHI TECHNOLOGICAL UNIVERSITY**  
**(Formerly Delhi College of Engineering)**  
**Shahbad Daultpur, Main Bawana Road, Delhi-110042. India**

**June, 2025**

## ACKNOWLEDGEMENT

First and foremost, I express my heartfelt gratitude to the Almighty for granting me the strength, health, and determination to complete this research work.

I extend my sincere thanks to my supervisor, **Prof. Yasha Hasija**, whose guidance, support, and insightful feedback were instrumental throughout the course of this thesis. Her constant encouragement and deep knowledge in the field of bioinformatics have helped shape this work and my academic journey.

I am also thankful to the **Department of Biotechnology, Delhi Technological University**, for providing me with the infrastructure, resources, and academic environment necessary to carry out this research.

I would like to express my appreciation to all the faculty members and technical staff of the department for their valuable assistance and cooperation whenever needed.

A special thanks to my peers and friends for their continuous motivation, stimulating discussions, and moral support throughout the course of my study. Their presence made this journey more enriching and enjoyable.

Finally, I am deeply indebted to my parents and family for their unwavering support, patience, and encouragement during every stage of this work. Their sacrifices and belief in me have been the greatest source of strength.

This thesis would not have been possible without the contribution and support of all the above-mentioned individuals. I remain grateful to each one of them.



## **DELHI TECHNOLOGICAL UNIVERSITY**

(Formerly Delhi College of Engineering)

Shahbad Daultpur, Main Bawana Road, Delhi-42

### **CANDIDATE'S DECLARATION**

I **Khushi Bhatia** hereby certify that the work which is being presented in the thesis entitled **“Integrative In Silico Drug Discovery: Targeting Tyrosinase with Natural Compounds for therapeutic management of Vitiligo”** in partial fulfilment of the requirements for the award of the Degree Master of Technology, submitted in the Department of **Biotechnology**, Delhi Technological University is an authentic record of my own work carried out during the period from **January, 2025** to **May, 2025** under the supervision of **Prof Yasha Hasija**.

The matter presented in the thesis has not been submitted by me for the award of any other degree of this or any other Institute.

**Candidate's Signature**



# DELHI TECHNOLOGICAL UNIVERSITY

(Formerly Delhi College of Engineering)

Shahbad Daultapur, Main Bawana Road, Delhi-42

## **CERTIFICATE BY THE SUPERVISOR(s)**

Certified that **Khushi Bhatia (23/BIO/02)** has carried out their search work presented in this thesis entitled **“Integrative In Silico Drug Discovery: Targeting Tyrosinase with Natural Compounds for therapeutic management of Vitiligo”** for the award of **Master of Technology** from Department of Information Technology, Delhi Technological University, Delhi, under my supervision. The thesis embodies results of original work, and studies are carried out by the student herself and the contents of the thesis do not form the basis for the award of any other degree to the candidate or to anybody else from this or any other University/Institution.

**Signature**

**Prof. Yasha Hasija**

**Head of Department**

**Delhi Technological University**

**Date:**

## ABSTRACT

Vitiligo is a complex skin condition marked by the progressive disappearance of melanocytes, the pigment-producing cells of the epidermis. This results in irregular white patches on the skin which significantly affect a patient's quality of life. Despite various clinical interventions ranging from topical agents to phototherapy, current treatments frequently fall short in terms of consistency and safety. Among the biomolecular targets implicated in pigment biosynthesis, tyrosinase—a critical enzyme in melanin production—has emerged as a focal point for therapeutic intervention. This research investigates the potential of select natural compounds to modulate tyrosinase activity using an integrated *in silico* framework.

The study follows a structured methodology that combines molecular docking, pharmacokinetic filtering and molecular dynamics simulation to evaluate and validate efficacy of the compounds (ligands). The three-dimensional structure of tyrosinase was retrieved and prepared for docking studies. A curated list of natural compounds—including Hinokinin, Lichexanthone, Tabernaemontanine, Dregamine, and Herboxidiene—was examined for binding potential. Using AutoDock, these compounds were docked to the active site of the enzyme. Binding site residues were predicted through PrankWeb, while interactions were analyzed using tools such as LigPlot and Protein Plus. Docking poses were refined and assessed based on root-mean-square deviation clustering and binding conformation stability.

To assess the pharmacological viability of each compound, a series of ADME (Absorption, Distribution, Metabolism, and Excretion) evaluations were conducted via the SwissADME platform. These analyses helped identify candidates with favourable properties such as high intestinal absorption, blood-brain barrier permeability and minimal inhibitory effects on cytochrome P450 enzymes. Compounds that met these pharmacokinetic criteria proceeded to molecular dynamics simulations, run over a 5 ns period using a cloud-based system, to capture their behaviour in a biologically relevant environment.

From the set of compounds studied, Hinokinin and Tabernaemontanine emerged as strong candidates, exhibiting high binding affinity, favourable ADME profiles and structural stability in dynamic simulation environments. While Dregamine and Herboxidiene also showed meaningful interaction with tyrosinase, they demonstrated relatively less structural retention during simulation. Lichexanthone, though modest in docking score, displayed pharmacokinetic advantages and sustained simulation stability, supporting its inclusion for future development.

This study underscores the value of computational modelling in early-stage drug discovery, particularly in dermatological applications. The integration of docking, pharmacokinetics and dynamic simulations presents a comprehensive route to filter promising candidates before experimental trials. In addition to contributing potential leads for vitiligo therapy, this research framework may be adapted for broader applications in targeting melanin-associated disorders.

Looking ahead, these computational insights require experimental validation to substantiate therapeutic utility. Follow-up studies involving biochemical assays, cell-based models and eventually animal trials will be critical in determining efficacy and safety. Further, structure-activity relationship (SAR) analysis and derivatization of lead compounds may help enhance target specificity. Expanding the natural compound library and applying AI-driven predictive screening could also accelerate discovery. Ultimately, this research offers a foundation for

developing natural, plant-based, non-toxic therapeutic options that address the clinical gap in vitiligo treatment.

## LIST OF PUBLICATIONS

K. Bhatia and Y. Hasija, "Revolutionizing Patient Care: AI-Driven Wearable Technology for Continuous Remote Health Monitoring," 2025 International Conference on Cognitive Computing in Engineering, Communications, Sciences and Biomedical Health Informatics (IC3ECSBHI), Greater Noida, India, 2025, pp. 404-409

doi: 10.1109/IC3ECSBHI63591.2025.10990913.

The screenshot shows the IEEE Xplore digital library interface. At the top, there's a navigation bar with links to IEEE.org, IEEE Xplore, IEEE SA, IEEE Spectrum, and More Sites. A search bar is prominently displayed with a dropdown menu set to 'All' and a search icon. Below the search bar, the breadcrumb trail reads 'Conferences > 2025 International Conference...'. The article title 'Revolutionizing Patient Care: AI-Driven Wearable Technology for Continuous Remote Health Monitoring' is displayed in a large, bold font. Below the title, it indicates the publisher as IEEE and provides links for 'Cite This' and 'PDF'. The authors 'Khushi Bhatia ; Yasha Hasija' are listed, along with a link for 'All Authors'. A row of icons for rights, sharing, citation, and notifications is visible. The abstract section is divided into two parts: 'Abstract' and 'Document Sections'. The 'Abstract' text describes Remote Patient Monitoring (RPM) and the role of AI-integrated wearable devices like PPG, ECG, and EDA sensors. The 'Document Sections' list includes: I. Introduction, II. Working Mechanism, III. Key Innovations in AI-Powered Wearables, and IV. Challenges and Limitations.

IEEE.org | IEEE Xplore | IEEE SA | IEEE Spectrum | More Sites

IEEE Xplore® Browse My Settings Help Institutional Sign In

All

ADVANCED SEARCH

Conferences > 2025 International Conference...

### Revolutionizing Patient Care: AI-Driven Wearable Technology for Continuous Remote Health Monitoring

Publisher: IEEE Cite This PDF

Khushi Bhatia ; Yasha Hasija All Authors

Abstract

Document Sections

I. Introduction

II. Working Mechanism

III. Key Innovations in AI-Powered Wearables

IV. Challenges and Limitations

Abstract:

Remote patient monitoring (RPM) refers to the ability of healthcare professionals to be able to monitor the well-being of their patients remotely without having to keep them under continuous in-person observation. Wearable devices that are integrated with Artificial Intelligence are a blessing in disguise when it comes to remote health monitoring. PPG sensors, ECG sensors, accelerometers, pulse oximeter and EDA sensor are some of these AI integrated wearable devices used for continuous remote health monitoring which are discussed in this article. We delved into their specific working mechanism, how the data is collected, stored and transferred and how the use of artificial intelligence algorithms come into all of this. These devices have applications in fields such as cloud computing and big data analytics for health management which are discussed along with key innovations. Certain issues such as data accuracy, data privacy and regulations are also addressed along with future directions which can be pursued that may have the potential to revolutionize the field of remote health monitoring even more

## TABLE OF CONTENTS

• LIST OF TABLES.....	11
• LIST OF TABLES.....	12
• LIST OF ABBREVIATIONS.....	15
• CHAPTER 1 – INTRODUCTION.....	16-18
○ 1.1 VITILIGO.....	16
○ 1.2 CLINICAL MANAGEMENT AND LIMITATIONS.....	16
○ 1.3 TYROSINASE AND MELANIN BIOSYNTHESIS.....	16
○ 1.4 DRUG DISCOVERY FROM NATURAL PRODUCTS.....	17
○ 1.5 IN SILICO APPROACHES IN MODERN DRUG DESIGN.....	17
○ 1.6 OBJECTIVES OF THE STUDY.....	18
• CHAPTER 2 - LITERATURE REVIEW.....	19-24
○ 2.1 VITILIGO: CLINICAL AND BIOLOGICAL CONTEXT.....	19
○ 2.2 CURRENT THERAPEUTIC APPROACHES AND LIMITATIONS.....	19
○ 2.3 TYROSINASE: FUNCTION AND THERAPEUTIC RELEVANCE.....	20
○ 2.4 NATURAL COMPOUNDS IN MELANOGENESIS MODULATION...	20
○ 2.5 MOLECULAR DOCKING IN DRUG DISCOVERY.....	21
○ 2.6 IN SILICO ADME AND DRUG-LIKENESS SCREENING.....	22
○ 2.7 OVERVIEW OF SELECTED NATURAL COMPOUNDS.....	22
▪ 2.7.1 HINOKININ.....	22
▪ 2.7.2 LICHEXANTHONE.....	23
▪ 2.7.3 TABERNAEMONTANINE.....	23
▪ 2.7.4 DREGAMINE.....	23
▪ 2.7.5 HERBOXIDIENE.....	24
○ 2.8 GAPS IN CURRENT RESEARCH.....	24
• CHAPTER 3 – METHODOLOGY.....	25-39
○ 3.1 OVERVIEW.....	25
○ 3.2 SOFTWARE AND TOOLS USED.....	25



○ 3.3 PROTEIN STRUCTURE RETRIEVAL AND PREPARATION.....	26
○ 3.4 LIGAND SELECTION AND PREPARATION.....	27
○ 3.5 BINDING SITE PREDICTION USING PRANKWEB.....	30
○ 3.6 MOLECULAR DOCKING.....	31
○ 3.7 POST-DOCKING ANALYSIS.....	32
▪ 3.7.1 RMSD-BASED CLUSTERING.....	32
▪ 3.7.2 VISUALIZATION AND INTERACTION MAPPING.....	33
○ 3.8 ADME AND DRUG-LIKENESS PREDICTION.....	33
▪ 3.8.1 LIPINSKI'S RULE OF FIVE.....	33
▪ 3.8.2 TOPOLOGICAL POLAR SURFACE AREA (TPSA).....	34
▪ 3.8.3 LOGP (LIPOPHILICITY).....	34
▪ 3.8.4 WATER SOLUBILITY.....	34
▪ 3.8.5 GASTROINTESTINAL (GI) ABSORPTION.....	34
▪ 3.8.6 BLOOD-BRAIN BARRIER (BBB) PERMEABILITY.....	34
▪ 3.8.7 CYP450 INHIBITION.....	35
▪ 3.8.8 BOILED-EGG PLOT.....	35
○ 3.9 MOLECULAR DYNAMICS (MD) SIMULATIONS.....	35
▪ 3.9.1 PREPARATION OF INPUT FILES.....	36
▪ 3.9.2 FORCE FIELD ASSIGNMENT.....	36
▪ 3.9.3 SYSTEM SOLVATION AND IONIZATION.....	36
▪ 3.9.4 ENERGY MINIMIZATION.....	36
▪ 3.9.5 EQUILIBRATION PHASE.....	37
▪ 3.9.6 PRODUCTION RUN.....	37
▪ 3.9.7 TRAJECTORY ANALYSIS.....	38
• CHAPTER 4 - RESULTS AND DISCUSSION.....	39-107
○ 4.1 OVERVIEW.....	39
○ 4.2 HINOKININ.....	39
▪ 4.2.1 DOCKING RESULTS.....	39
▪ 4.2.2 BINDING SITE INTERACTIONS.....	40
▪ 4.2.3 ADME ANALYSIS.....	43

▪ 4.2.4 Molecular Dynamics (MD) Simulation Results.....	47
○ 4.3 TABERNAEMONTANINE.....	52
▪ 4.3.1 DOCKING RESULTS.....	52
▪ 4.3.2 BINDING SITE INTERACTIONS.....	53
▪ 4.3.3 ADME ANALYSIS.....	57
▪ 4.3.4 MOLECULAR DYNAMICS (MD) SIMULATION RESULTS....	61
○ 4.4 DREGAMINE.....	65
▪ 4.4.1 DOCKING RESULTS.....	65
▪ 4.4.2 BINDING SITE INTERACTIONS.....	66
▪ 4.4.3 ADME ANALYSIS.....	70
▪ 4.4.4 MOLECULAR DYNAMICS (MD) SIMULATION RESULTS....	74
○ 4.5 HERBOXIDIENE.....	77
▪ 4.5.1 DOCKING RESULTS.....	77
▪ 4.5.2 BINDING SITE INTERACTIONS.....	89
▪ 4.5.3 ADME ANALYSIS.....	83
▪ 4.5.4 MOLECULAR DYNAMICS (MD) SIMULATION RESULTS....	88
○ 4.6 LICHEXANTHONE.....	92
▪ 4.6.1 DOCKING RESULTS.....	92
▪ 4.6.2 BINDING SITE INTERACTIONS.....	93
▪ 4.6.3 ADME ANALYSIS.....	98
▪ 4.6.4 MOLECULAR DYNAMICS (MD) SIMULATION RESULTS...	102
• CHAPTER 5 – CONCLUSION AND FUTURE SCOPE.....	108-110
○ 5.1 CONCLUSION.....	108
○ 5.2 FUTURE SCOPE.....	109
• REFERENCES.....	111-113
• LIST OF PUBLICATIONS.....	114
• PLAGIARISM REPORT.....	115-118

## LIST OF TABLES

Table No.	Title
Table 3.1	List of Software and Tools used
Table 3.2	List of Amino Acid Residues of active binding site
Table 3.3	Grid Box parameters of Molecular Docking
Table 3.4	Coordinates of Grid Box Center
Table 3.5	Parameters of Molecular Docking
Table 3.6	Parameters applied for Equilibration phase
Table 3.7	Parameters applied for MD Production run
Table 4.1	RMSD Summary for Hinokinin
Table 4.2	ADME Profile of Hinokinin
Table 4.3	RMSD Summary for Tabernaemontanine
Table 4.4	ADME Profile of Tabernaemontanine
Table 4.5	RMSD Summary for Dregamine
Table 4.6	ADME Profile of Dregamine
Table 4.7	RMSD Summary for Herboxidiene
Table 4.8	ADME Profile of Herboxidiene
Table 4.9	RMSD Summary for Lichexanthone
Table 4.10	ADME Profile of Lichexanthone

## LIST OF FIGURES

Figure No.	Title
Fig 3.1	Prepared structure of Tyrosinase visualized on PyMol
Fig 3.2	Structure of Hinokinin
Fig 3.3	Structure of Lichexanthone
Fig 3.4	Structure of Tabernaemontanine
Fig 3.5	Structure of Dregamine
Fig 3.6	Structure of Herboxidiene
Fig 3.7	Grid Box in AutoDock
Fig 4.1	Visualization of docking interactions between Tyrosinase and Hinokinin
Fig 4.2	Binding site interactions of Tyrosinase-Hinokinin complex
Fig 4.3	2D interaction diagram of Tyrosinase-Hinokinin complex
Fig 4.4	ADME properties of Hinokinin predicted by SwissADME
Fig 4.5	Boiled-egg plot of Hinokinin
Fig 4.6	RMSD of Protein Backbone Atoms Over Time (Hinokinin)
Fig 4.7	RMSF of Protein Residues (Hinokinin)
Fig 4.8	2D RMSD Heatmap (Hinokinin)
Fig 4.9	Ligand–Protein Interaction Distance Over Time (Hinokinin)
Fig 4.10	Protein–Ligand Interaction Energy (Hinokinin)
Fig 4.11	Radius of Gyration (Hinokinin)
Fig 4.12	Principal Component Analysis (Hinokinin)
Fig 4.13	Visualization of docking interactions between Tyrosinase and Tabernaemontanine
Fig 4.14	Binding site interactions (Tabernaemontanine)
Fig 4.15	2D interaction diagram of Tyrosinase-Tabernaemontanine (LigPlot)
Fig 4.16	2D interaction diagram of Tyrosinase-Tabernaemontanine (Protein Plus)
Fig 4.17	ADME properties of Tabernaemontanine
Fig 4.18	Boiled-egg plot of Tabernaemontanine

Fig 4.19	RMSD of Protein Backbone Atoms (Tabernaemontanine)
Fig 4.20	RMSF of Protein Residues (Tabernaemontanine)
Fig 4.21	2D RMSD Heatmap (Tabernaemontanine)
Fig 4.22	Protein–Ligand Interaction Energy (Tabernaemontanine)
Fig 4.23	Radius of Gyration (Tabernaemontanine)
Fig 4.24	Principal Component Analysis (Tabernaemontanine)
Fig 4.25	Visualization of binding interactions (Dregamine)
Fig 4.26	Binding site interactions (Dregamine)
Fig 4.27	2D interaction diagram of Tyrosinase–Dregamine (LigPlot)
Fig 4.28	2D interaction diagram (Protein Plus) – Dregamine
Fig 4.29	ADME properties of Dregamine
Fig 4.30	Boiled-egg plot of Dregamine
Fig 4.31	RMSD of Protein Backbone Atoms Over Time (Dregamine)
Fig 4.32	RMSF of Protein Residues (Dregamine)
Fig 4.33	2D RMSD Heatmap (Dregamine)
Fig 4.34	Protein–Ligand Interaction Energy (Dregamine)
Fig 4.35	Radius of Gyration (Dregamine)
Fig 4.36	PCA (Dregamine)
Fig 4.37	Visualization of binding interactions (Herboxidiene)
Fig 4.38	Binding site interactions (Herboxidiene)
Fig 4.39	2D interaction diagram – LigPlot (Herboxidiene)
Fig 4.40	2D interaction diagram – Protein Plus (Herboxidiene)
Fig 4.41	ADME properties of Herboxidiene
Fig 4.42	Boiled-egg plot of Herboxidiene
Fig 4.43	RMSD of Protein Backbone Atoms Over Time (Herboxidiene)
Fig 4.44	RMSF of Protein Residues (Herboxidiene)
Fig 4.45	2D RMSD Heatmap (Herboxidiene)
Fig 4.46	Ligand–Protein Interaction Distance Over Time (Herboxidiene)
Fig 4.47	Protein–Ligand Interaction Energy (Herboxidiene)

Fig 4.48	Radius of Gyration (Herboxidiene)
Fig 4.49	Principal Component Analysis (Herboxidiene)
Fig 4.69	Visualization of Binding interactions (Lichexanthone)
Fig 4.70	Binding site interactions (Lichexanthone)
Fig 4.71	2D interaction diagram – LigPlot (Lichexanthone)
Fig 4.72	2D interaction diagram – Protein Plus (Lichexanthone)
Fig 4.73	ADME properties of Lichexanthone
Fig 4.74	Boiled-egg plot of Lichexanthone
Fig 4.75	RMSD of Protein Backbone Atoms Over Time (Lichexanthone)
Fig 4.76	RMSF of Protein Residues (Lichexanthone)
Fig 4.77	2D RMSD Heat Map (Lichexanthone)
Fig 4.78	Ligand–Protein Interaction Distance Over Time (Lichexanthone)
Fig 4.79	Protein–Ligand Interaction Energy (Lichexanthone)
Fig 4.80	Radius of Gyration (Lichexanthone)
Fig 4.81	Principal Component Analysis (Lichexanthone)

## LIST OF ABBREVIATIONS

UV – ultraviolet

ADME – Absorption, Distribution, Metabolism and Excretion

MD – Molecular Dynamics

RMSD – Root Mean Square Deviation

ROS – reactive oxygen species

GWAS – Genome wide association studies

PUVA – Psoralen + UVA

NB-UVB – Narrowband UVB

SBDD – structure-based drug design

BBB – blood–brain barrier

LGA – Lamarckian Genetic Algorithm

SIB – Swiss Institute of Bioinformatics

TPSA – Topological Polar Surface Area

SVM – support vector machine

CYP – cytochrome P450

BOILED – Brain Or IntestinaL EstimatedD

OpenFF – Open Force Field

RMSF – Root Mean Square Fluctuation

$K_i$  – Inhibition Constant

R<sub>g</sub> – Radius of gyration

GI – Gastrointestinal

P-gp – P-glycoprotein

PAINS – Pan-Assay INterference Compounds

HIA – Human intestinal absorption

CNS – central nervous system

PCA – Principal Component Analysis

SA – Synthetic Accessibility

vdW – van der Waals

# **CHAPTER 1**

## **INTRODUCTION**

### **1.1 VITILIGO**

Vitiligo is a chronic, progressive, and often stigmatized dermatological condition characterized by depigmented macules and patches resulting from the selective destruction of melanocytes—the pigment-producing cells of the skin [1]. It affects approximately 0.5% to 2% of the global population, with no preference for gender or ethnicity. While the disease is not life-threatening, its psychosocial implications are significant. Individuals with vitiligo often experience anxiety, depression, and social withdrawal due to its visible manifestations.

The precise etiology of vitiligo remains elusive, although it is widely accepted that the pathogenesis is multifactorial. The most supported theories include autoimmune mechanisms, oxidative stress, neural factors, genetic predispositions, and cytotoxicity [2]. Among these, oxidative stress is believed to play a crucial initiating role in melanocyte degeneration, leading to immune dysregulation and the development of vitiliginous lesions.

### **1.2 CLINICAL MANAGEMENT AND LIMITATIONS**

The therapeutic landscape for vitiligo includes topical corticosteroids [3], calcineurin inhibitors [4], phototherapy (narrowband UVB) [5], psoralen plus UVA (PUVA) [6], surgical techniques (e.g., melanocyte transfer) [7], and depigmentation therapy [8] for extensive cases. However, these therapies have variable success rates, long treatment durations, high recurrence rates, and in some cases, significant side effects.

Moreover, because there are not any treatments that work for all patients, it is evident that new targeted medicines are urgently needed to halt the disease progression and return normal pigment.

### **1.3 TYROSINASE AND MELANIN BIOSYNTHESIS**

Melanin, the pigment responsible for skin, hair, and eye colour, plays a protective role against ultraviolet (UV) radiation-induced damage [9]. The biosynthesis of melanin, known as melanogenesis, is a complex multi-step process catalyzed by several key enzymes. Tyrosinase is the most critical and rate-limiting enzyme in this pathway [10].

Tyrosinase catalyzes two essential reactions: the hydroxylation of L-tyrosine to L-DOPA (L-3,4-dihydroxyphenylalanine), and the subsequent oxidation of L-DOPA to dopaquinone [11]. These initial steps set off a cascade of reactions leading to the synthesis of either eumelanin or pheomelanin. Any dysregulation in tyrosinase expression or activity can disrupt melanogenesis, potentially contributing to pigmentary disorders such as vitiligo and melasma [12].



Tyrosinase is a key factor which is why it may be targeted by therapies designed to impact pigmentation. Stopping tyrosinase helps reduce hyperpigmentation [13] and boosting its activity can help fight vitiligo and other hypopigmentary diseases [14].

## **1.4 DRUG DISCOVERY FROM NATURAL PRODUCTS**

For a long time, natural products have given scientists many important pharmaceuticals. Many healthcare drugs created to fight cancer, infections and inflammation are based on phytochemicals [15]. Because they have many different forms and are biologically similar to humans, they are chosen for drug research.

Many compounds from plants have been found to have effects on tyrosinase in pigmentation disorders. For example, arbutin [16] and kojic acid [17] are well-known tyrosinase inhibitors in skin care. Nevertheless, finding agents that increase pigmentation by stabilizing tyrosinase is a new focus in finding ways to manage vitiligo.

In this study, five naturally occurring compounds—Hinokinin [18], Lichexanthone [19], Tabernaemontanine [20], Dregamine [21] and Herboxidiene [22]—were chosen for docking experiments due to their active properties and because they represent a range of structural types. Antioxidant, anti-inflammatory and anticancer actions linked to these compounds could make them helpful in vitiligo treatment.

## **1.5 IN SILICO APPROACHES IN MODERN DRUG DESIGN**

Drug discovery focused on structure depends heavily on molecular docking [23]. It requires estimating which is the best way for a small molecule to fit and bind to important biological proteins such as enzymes or receptor proteins. Docking simulations allow us to see how the ligand and receptor interact, form hydrogen bonds and what the energy pattern looks like in the complex [24].

Docking, virtual screening, prediction of ADME (Absorption, Distribution, Metabolism and Excretion) and Molecular Dynamics (MD) simulations using computational methods greatly cut down the time, money and risk during experimental drug development. During early-stage of drug discovery, they help choose those drug candidates with the greatest potential for testing [25].

For this project, molecular docking was applied to examine how the selected natural compounds connect to human tyrosinase. To carry out the docking protocol, the validated AutoDock [26] tool for molecular docking was used to check binding energies and determine interaction models at the active site. The protein structure for tyrosinase was obtained from the RCSB Protein Data Bank (PDB ID: 5M8L), while the ligand structures were gathered from PubChem.

## **1.6 OBJECTIVES OF THE STUDY**

The specific objectives of this study are:

- To identify natural compounds with potential tyrosinase-modulating activity for the treatment of vitiligo.
- To perform molecular docking of tyrosinase with five selected compounds using AutoDock.
- To evaluate the binding affinities and interaction patterns of each compound.
- To analyze Root Mean Square Deviation (RMSD) data to assess the docking stability.
- To perform ADME analysis using SwissADME to predict the pharmacokinetic properties and drug-likeness of the compounds.
- To identify potential lead molecules for future experimental validation.
- To validate the molecular docking results by checking the stability of docked complexes using Molecular Dynamics (MD) simulations.

## CHAPTER 2

### LITERATURE REVIEW

#### 2.1 VITILIGO: CLINICAL AND BIOLOGICAL CONTEXT

Vitiligo is a skin condition that is present in about 70 million people globally [27]. As a result of melanocyte loss over time, people develop well-defined white patches on the skin and membranes inside the mouth, nose and eyes [28]. This condition can happen at any time, but it usually develops before individuals turn 30. Although vitiligo does not injure the body or transmit disease, but it can cause depression, create social barriers for the patients and bring on anxiety [29].

The exact cause of vitiligo remains elusive, but researchers have proposed several contributing mechanisms:

- **Autoimmunity:** It is generally accepted that the immune system attacks melanocytes unintentionally. An increase in CD8+ cytotoxic T cells and antibodies that attack melanocyte-related molecules supports this idea [30].
- **Oxidative Stress:** Higher amounts of hydrogen peroxide and reactive oxygen species (ROS) have been spotted in vitiliginous skin, which could lead to melanocyte apoptosis [31].
- **Neural Hypothesis:** It states that a possible cause for melanoma may be an imbalance in brain chemicals that results in poisonous substances harming the melanin-forming cells [32].
- **Genetic Susceptibility:** Several loci, including NLRP1, PTPN22 and TYR, have been identified by GWAS to play a significant role [33].
- **Melanocyte Adhesion Defects:** New evidence indicates that vitiligo causes melanocytes to separate easily from the basal layer and ultimately contribute to cell loss [34].

Since vitiligo is caused by various factors, it is hard to treat since various mechanisms in the body must be addressed.

#### 2.2 CURRENT THERAPEUTIC APPROACHES AND LIMITATIONS

The therapeutic modalities for vitiligo can be categorized into medical, surgical, and adjunctive treatments. The most commonly employed treatments include:

- **Topical corticosteroids and calcineurin inhibitors:** Used to suppress local immune responses.
- **Phototherapy:** Narrowband UVB (NB-UVB) is considered the gold standard for generalized vitiligo, promoting melanocyte proliferation and migration.

- **PUVA (Psoralen + UVA):** Utilizes light-sensitive compounds combined with UVA exposure, though it has more side effects.
- **Surgical interventions:** Techniques such as suction blister grafting and melanocyte transplantation are used in stable vitiligo.
- **Depigmentation therapies:** Applied in extensive cases to achieve uniformity in skin tone.

Even though their degrees of effectiveness are not always clear, these therapies are linked to frequent relapses, lengthy treatments and possible side effects that include skin atrophy, irritation and an increased risk for cancer with phototherapy. More importantly, none of the current treatments are designed to recover tyrosinase function, defend the melanocytes from damage or reverse oxidation in the skin. Therefore, there is a need for new methods that target molecular aspects involved in melanin production and cell durability.

## 2.3 TYROSINASE: FUNCTION AND THERAPEUTIC RELEVANCE

Tyrosinase is a multifunctional, glycosylated, copper-containing oxidase responsible for catalyzing the first two rate-limiting steps in melanin biosynthesis [35]. These include:

1. The hydroxylation of L-tyrosine to L-DOPA.
2. The oxidation of L-DOPA to dopaquinone.

Subsequent steps lead to the production of either eumelanin (black/brown pigment) or pheomelanin (red/yellow pigment), depending on the availability of cysteine and other factors [36]. The enzyme's activity is critically dependent on two copper ions (CuA and CuB) at its active site, coordinated by histidine residues [37].

Tissue loss in vitiligo is partly caused by the lowered or changed action of tyrosinase which reduces the production of melanin [38]. ROS and UV can increase melanocyte apoptosis by adding stress to the tyrosinase protein [39].

When tyrosinase is modulated, pigmentation can be easily controlled. Although the goal of both pharmaceutical and cosmetics is generally to decrease tyrosinase for skin whitening and melasma, the goal in vitiligo is just the opposite—to support the survival and pigment of melanocytes by boosting tyrosinase activity.

## 2.4 NATURAL COMPOUNDS IN MELANOGENESIS MODULATION

Nature has provided many therapeutic agents for a very long time. More than half of the drugs now approved come from or are inspired by, natural resources [40]. These include plant alkaloids, flavonoids, terpenoids, lignans, xanthones, and marine compounds [41]. Several of these have been shown to affect pigmentation by:

- Acting directly on enzymes like tyrosinase and TRP-1.

- Modulating signaling pathways such as MITF, Wnt/ $\beta$ -catenin, and PKA/CREB.
- Providing antioxidant protection to melanocytes under oxidative stress.

For instance:

- Psoralens, found in *Psoralea corylifolia*, are used in PUVA therapy to promote melanogenesis [42].
- Ginsenosides from *Panax ginseng* are known to enhance tyrosinase expression [43].
- Baicalein, a flavonoid, has shown melanogenic activity by upregulating MITF [44].

Despite what has been found, very few natural substances have been properly examined for their ability to stimulate tyrosinase in vitiligo. This points out the need for new studies to fill a key information gap. Each of the five compounds were chosen mainly because they come from five different structural classes, allowing for a wider search for new tyrosinase regulators.

## 2.5 MOLECULAR DOCKING IN DRUG DISCOVERY

Molecular docking is a computational simulation technique that predicts the preferred binding orientation of a small molecule (ligand) to a target macromolecule (usually a protein) [45]. It plays a central role in modern structure-based drug design (SBDD) and is particularly useful for:

- Ranking compounds based on predicted binding energy.
- Mapping active sites and important binding residues.
- Visualizing ligand–protein interactions such as hydrogen bonding, hydrophobic contacts, and metal coordination.

AutoDock has become one of the most common docking tools as it offers flexibility, reliability and is freely available to use [46]. A Lamarckian Genetic Algorithm is used to improve binding poses and a semi-empirical free energy force field is applied to calculate the binding affinity [47].

In the context of pigmentation research, docking studies have been used to:

- Discover novel tyrosinase inhibitors and activators.
- Study binding modes of flavonoids, alkaloids, and synthetic molecules.
- Simulate oxidative damage models in melanocytes.

By means of molecular docking, researchers can quickly and affordably sort through various natural products and identify those forming significant and specific connections with tyrosinase to be examined further.

## 2.6 IN SILICO ADME AND DRUG-LIKENESS SCREENING

Though a molecule must have the potential to bind to its target, its pharmacokinetic properties determine if it is suitable for use in medicine. In Silico ADME profiling is now a key step when looking for new medicines at the early stages of discovery. It allows researchers to foresee the behaviour of a compound inside the body which makes failures in preclinical and clinical trials less likely [48].

**SwissADME** is a widely used web-based tool that calculates a range of pharmacokinetic and drug-likeness properties [49], including:

- Gastrointestinal absorption and blood–brain barrier (BBB) permeability.
- Interaction with cytochrome P450 (CYP450) enzymes that affect drug metabolism.
- Solubility, lipophilicity, and bioavailability scores.
- Compliance with rules such as Lipinski's Rule of Five, Veber Rule, and Ghose Filter.
- Visualization of absorption and BBB potential using the BOILED-Egg plot.

With these predictions, scientists can determine how easily the substance can be ingested orally, the likelihood of toxicity and possible problems with bioaccumulation or metabolism. All five ligands were screened using ADME profiling to check their drug-likeness and find compounds that have good pharmacokinetic properties.

## 2.7 OVERVIEW OF SELECTED NATURAL COMPOUNDS

For many years, natural products have been essential in drug discovery because of how diverse they are in their structures, how much they have evolved and how much use they can have as medicines. The current study examined five natural compounds, as they demonstrate various biological activities, including antioxidant, anti-inflammatory, neuroactive and enzyme-modulatory abilities. These compounds were selected because they were known to have activity against metabolic oxidation and melanogenesis and because some of their chemical groups could interact with tyrosinase.

After reviewing a large number of databases, studies and references, each compound was picked for this study. The ability of these compounds to participate in interactions with the active site of tyrosinase through hydrogen bonding,  $\pi$ - $\pi$  stacking or metal ion coordination was considered. Each compound is examined in detail below.

### 2.7.1 HINOKININ

Hinokinin is a member of the dibenzylbutyrolactone-type lignans, found in the plants *Zanthoxylum naranjillo* and *Virola surinamensis* [18]. Lignans have consistently been connected to both controlling oxidative stress and cell protection [50]. Reports show that hinokinin has good antioxidant, anti-inflammatory, anti-protozoal and anticancer activities. Its design includes two phenylpropanoid units joined by a lactone group which allows it to take part in electron transfer and scavenging.

Oxidative stress is one of the main causes of melanocyte degeneration in the disease. Because of its antioxidant properties, Hinokinin could help safeguard melanocytes against damage caused by certain toxins. Additionally, the presence of hydroxyl and methoxy on the phenyl rings of the molecule may help form better interactions with the copper-rich part of tyrosinase. Because of these points, Hinokinin was added to the study to see if it might control tyrosinase and help reduce hypopigmentation.

### 2.7.2 LICHEXANTHONE

Lichexanthone, a natural xanthone, is mainly found in lichens, in particular *Cladia aggregata* and also in some higher plants [51]. Xanthoness possess biologically active features as polyphenols, influencing many functions such as antimicrobial, antioxidant and enzyme regulatory ones [52]. The hydroxyl and methyl groups attached to its cyclic core make it possible for lichexanthone to have both hydrophobic and polar interactions with proteins.

Xanthoness have been investigated for their ability to communicate with oxidoreductase enzymes. Though Lichexanthone has never been linked to tyrosinase in previous studies, its structure is similar to known tyrosinase inhibitors such as mangiferin and norathyriol. Also, its antioxidant property may guard melanocytes against ROS-related death. Based on these features, Lichexanthone appears to act in two ways: by targeting tyrosinase and by lowering oxidative stress.

### 2.7.3 TABERNAEMONTANINE

Plants of the *Tabernaemontana* genus are used in Traditional Medicine and from them, doctors can extract Tabernaemontanine to aid in the treatment of inflammation, disorders of the brain and nerves and skin-related diseases [53]. Indole alkaloids show structural similarity to L-tyrosine and L-DOPA, two chemical substances produced naturally by tyrosinase [54]. The shared feature could lead to these compounds being able to compete for the area on the tyrosinase where important reactions take place.

Other than its ability to bind, Tabernaemontanine has also been found to support healthy neurons and act as an antioxidant by studies conducted in both the lab and in animals [55]. Due to its structure—with lipophobic rings and polar nitrogen groups—it is well-adapted to attach to both non-polar binding sites and the metal copper ions present in tyrosinase. Therefore, it shows promise as a substance to investigate its part in defending melanocytes and encouraging melanin synthesis.

### 2.7.4 DREGAMINE

Dregamine which comes from plants in the *Tabernaemontana* family, is a monoterpenoid indole alkaloid that draws attention for its probable cytotoxicity and effect on certain microbes [56]. Dregamine possesses an indole nucleus, as it does in Tabernaemontanine which is important because it can interact with tyrosinase's active parts by either  $\pi$ -stacking or hydrogen bonding.

The stiff structure provided by Dregamine's unique spirocyclic form can influence its interactions with the key binding site (known as the active pocket) in the target enzyme. In addition, its role in neurobiology may mean it could control the distribution of pigment through nerve signals. Because of the molecule's pharmacology, lipophilicity and bioactivity, it warrants a place in the docking-based screening study.

### 2.7.5 HERBOXIDIENE

*Streptomyces chromofuscus* produces Herboxidiene, a macrocyclic polyketide that was recognized as a spliceosome inhibitor showing strong antitumor activity [57]. Although melanin biosynthesis and pigmentation changes are not linked to it, the complex structure and high reactivity of melanin make it ideal for in silico investigations.

Herboxidiene contains several hydrogen bond acceptors and donors, hydroxyl groups and a conjugated diene, all of which help it interact strongly with enzymes [58]. By looking at an atypical scaffold, this study illustrates a form of scaffold-hopping to test a new chemical for pigmentation purposes. If Herboxidiene is discovered as active, it may serve as the first class of modulators acting on tyrosinase in a distinct way.

## 2.8 GAPS IN CURRENT RESEARCH

The review of current literature highlights several critical gaps:

- Most research focuses on inhibiting tyrosinase for skin-lightening purposes; little is done to find activators or stabilizers, which are more relevant for vitiligo.
- There is an underrepresentation of marine and microbial natural products in pigmentation studies.
- Many promising natural compounds lack comprehensive ADME profiling, limiting their development potential.
- The integration of in silico docking and pharmacokinetic analysis for tyrosinase-targeting agents remains underexplored.

To find new leads from natural products, this research uses docking, compares structures using RMSD and carries out ADME evaluations. Using multiple techniques together helps find results more quickly and enhances the value of computational predictions for real-world use.



## CHAPTER 3

### METHODOLOGY

#### 3.1 OVERVIEW

This chapter describes in detail the process used in this study to identify and assess how well the five natural products interact with the human tyrosinase enzyme using molecular docking. The process includes preparing proteins and ligands, finding potential active sites, molecular docking using AutoDock 4.2, checking interaction and analysis of visualization and making drug-related predictions using ADME methods. All the experiments were done computationally using a combination of open-source and specialized computational tools.

#### 3.2 SOFTWARE AND TOOLS USED

The study utilized a range of freely available and research-grade software for molecular docking, visualization, and ADME prediction. Each tool played a specific role in the docking workflow, from data retrieval to final visualization:

Table 3.1 – List of Software and Tools used

Software/Tool	Application
PubChem	Retrieval of ligand structures in SDF format
RCSB Protein Data Bank	Retrieval of 3D tyrosinase structure (PDB ID: 5M8L)
AutoDock 4.2	Molecular docking simulations
AutoDock Tools	Preparation of receptor and ligand files for docking
Open Babel	Energy minimization and format conversion of ligands
LigPlot+	2D interaction mapping between ligand and protein
PrankWeb	Prediction of potential binding sites on tyrosinase
PLIP	Identification of non-covalent interactions between biological macromolecules and their ligands
Protein Plus	Visualize structures and create 2D pose depictions
SwissADME	Prediction of ADME and pharmacokinetic properties

PyMOL	3D visualization of protein-ligand complexes
Discovery Studio Visualizer	Detailed molecular interaction analysis
Google Colab	Molecular Dynamics (MD) Simulations

These tools were selected for their accuracy, accessibility and widespread validation in the computational biology community.

### 3.3 PROTEIN STRUCTURE RETRIEVAL AND PREPARATION

The crystal structure of human tyrosinase was downloaded from the RCSB Protein Data Bank with PDB ID: 5M8L, which represents the catalytically active domain of the enzyme.

The protein preparation involved the following steps:

- Removal of water molecules, co-crystallized ligands, and heteroatoms to avoid non-specific interactions.
- Addition of polar hydrogens using AutoDock Tools.
- Assignment of Kollman charges to all atoms.
- Conversion of the structure to PDBQT format required for AutoDock.

Performing the above preprocessing work was important to get accurate results and maintain the necessary structure and functions of the enzyme.

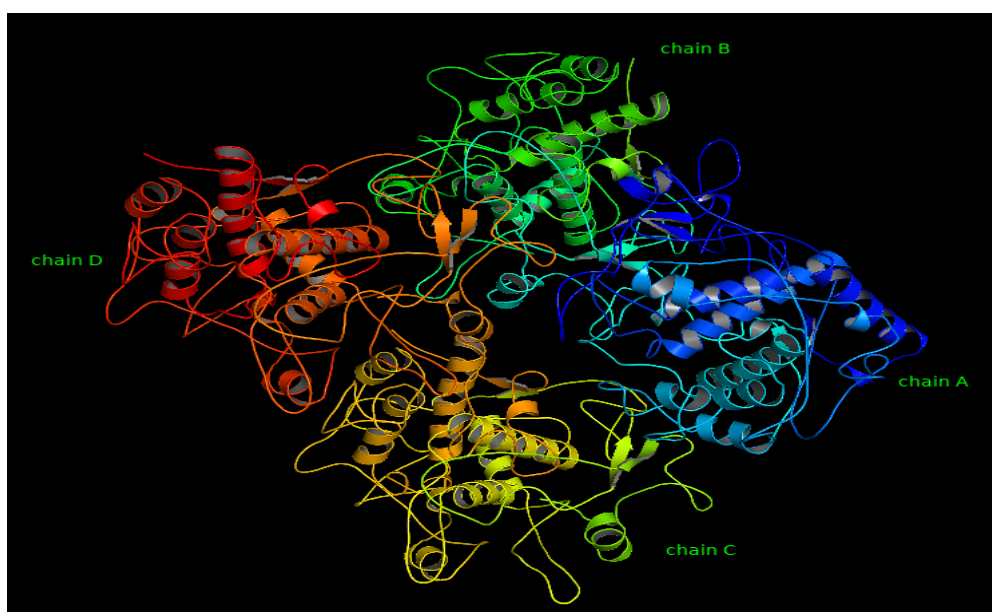


Fig 3.1 - Prepared structure of Tyrosinase visualized on PyMol

### 3.4 LIGAND SELECTION AND PREPARATION

Five natural bioactive compounds were selected for docking based on literature survey, known pharmacological activities, and structural diversity. These include:

1. **Hinokinin** (Compound CID: [442879](#))
2. **Lichexanthone** (Compound CID: [5358904](#))
3. **Tabernaemontanine** (Compound CID: [12309360](#))
4. **Dregamine** (Compound CID: [12309361](#))
5. **Herboxidiene** (Compound CID: [6438496](#))

The ligands were retrieved from the PubChem database in SDF format and processed as follows:

- Energy minimization was performed using Open Babel with the MMFF94 force field to optimize their geometries.
- The minimized structures were converted to PDB format using Open Babel.
- Using AutoDock Tools, each ligand was assigned Gasteiger charges, rotatable bonds were defined, and the final structure was saved in PDBQT format.

This preparation ensured that ligands were in their most stable conformations, maximizing the accuracy of docking predictions.

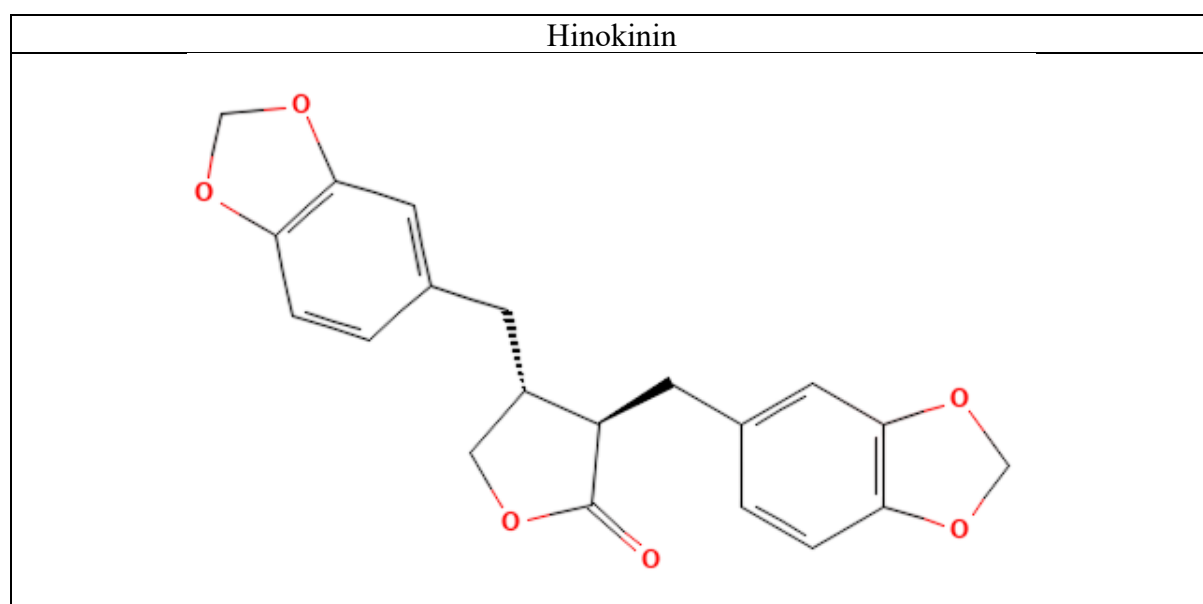


Fig 3.2 – Structure of Hinokinin

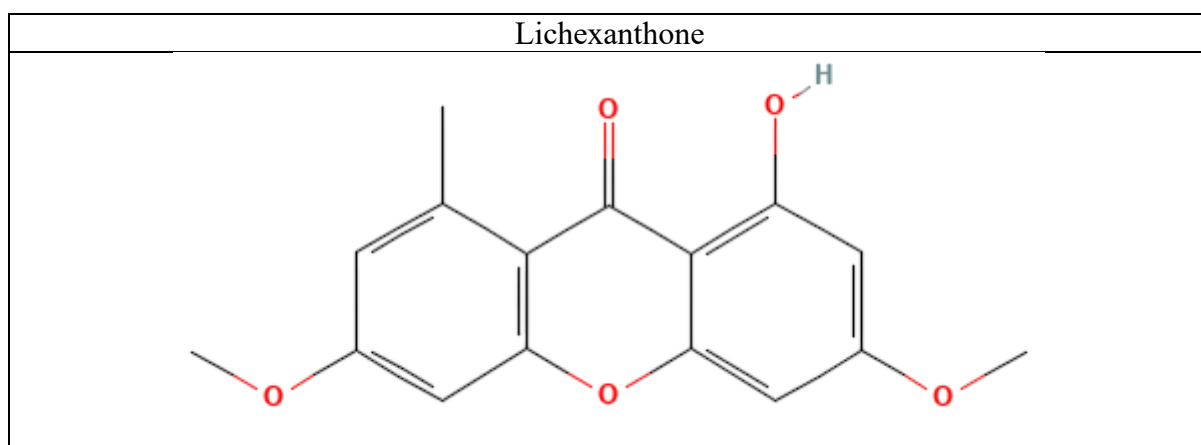


Fig 3.3 – Structure of Lichexanthone

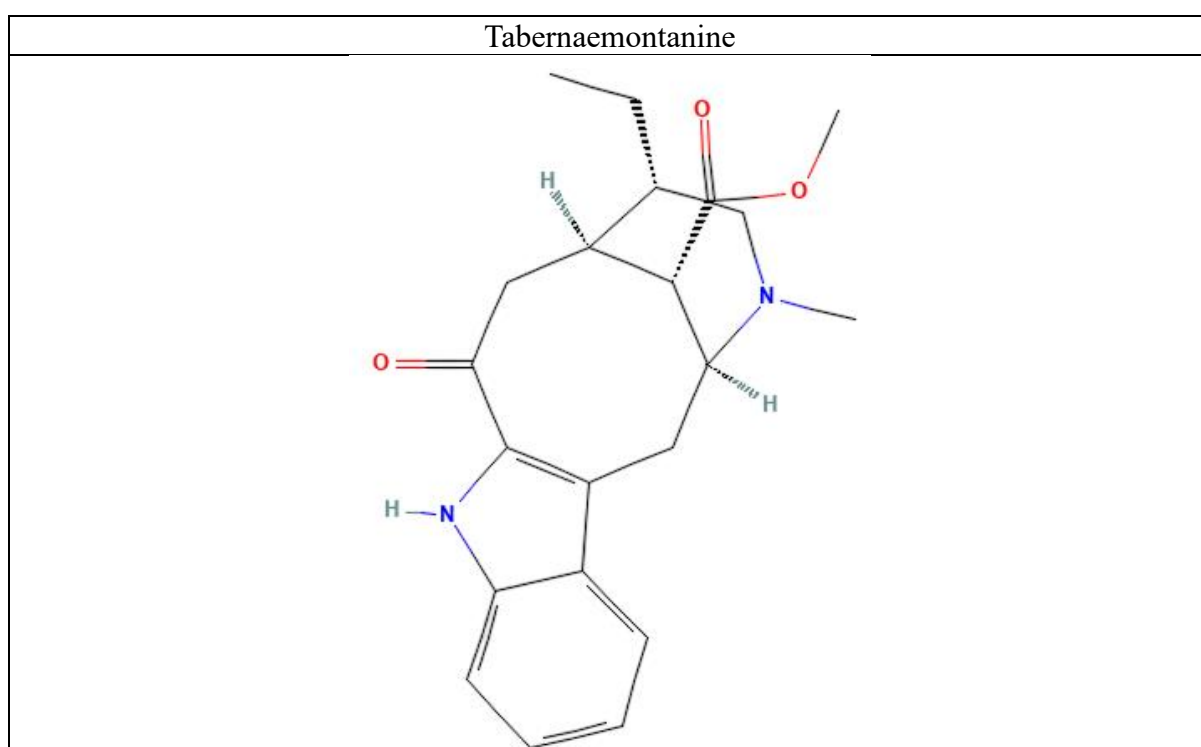


Fig 3.4 – Structure of Tabernaemontanine

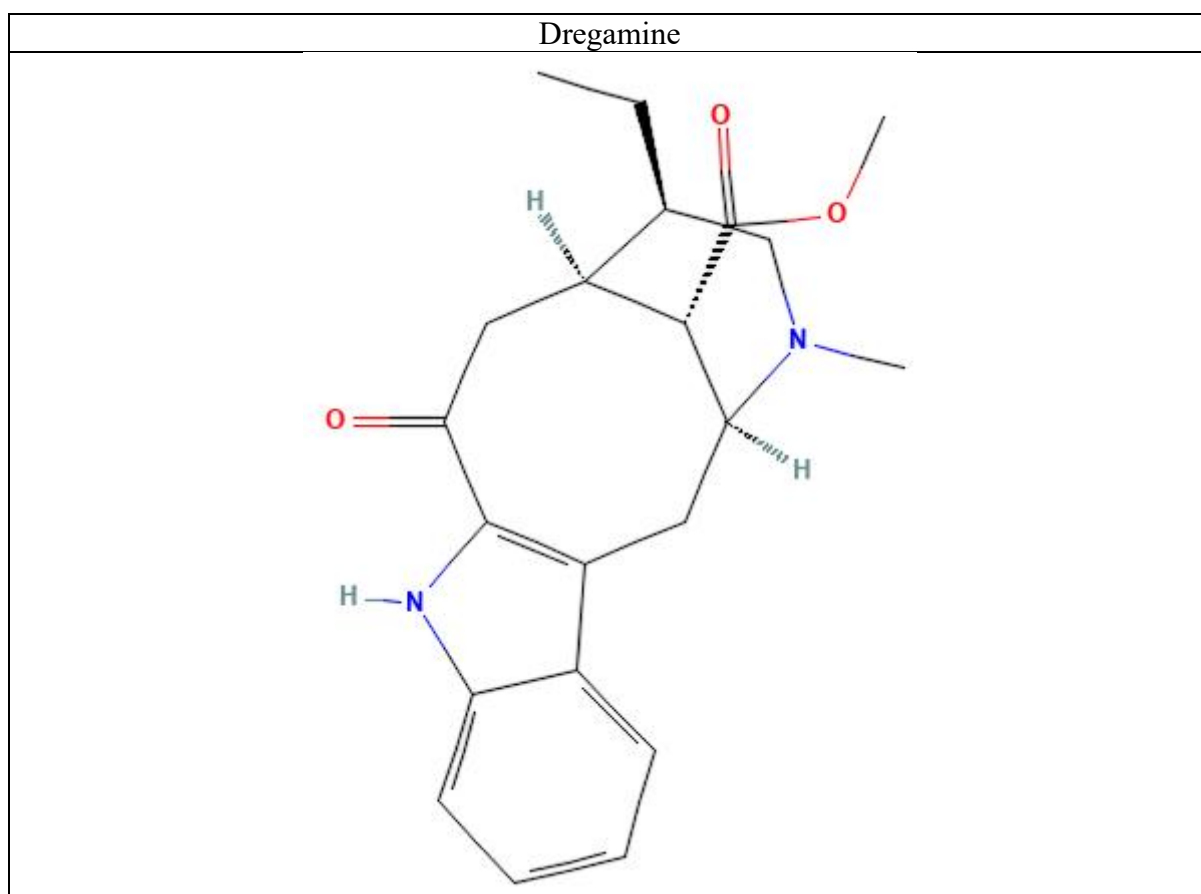


Fig 3.5 – Structure of Dregamine

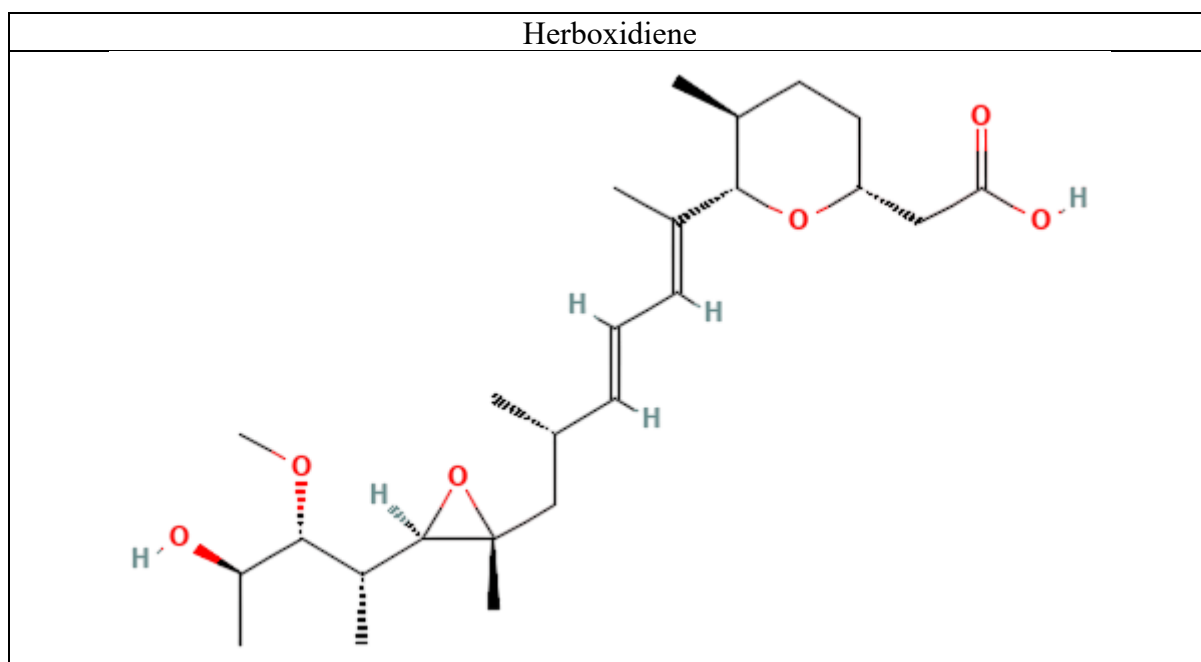


Fig 3.6 – Structure of Herboxidiene

### 3.5 BINDING SITE PREDICTION USING PRANKWEB

PrankWeb [59], a machine learning server, was used to find the active binding site of human tyrosinase by studying its protein structure and evolution.

Following amino acid residues that are part of the predicted active site were recognized after the top-ranked binding pocket was selected using calculations:

Table 3.2 – List of Amino Acid Residues of active binding site

<b>Binding Site Residues</b>
<b>C_98, C_99, C_100, C_101, C_105, C_106, C_107, C_108, C_112, C_113, C_114, C_115, C_156, C_158, C_226, C_229, C_230, C_233, C_234, C_444, C_445, C_446, C_447, C_451, C_452, C_460</b>

Such residues encircle the dinuclear copper center of tyrosinase that helps make tyrosinase active. The site's predicted coordinates were entered to determine the docking grid box parameters.

Following are the parameters applied on the grid box:

Table 3.3 – Grid Box parameters of Molecular Docking

Total grid points per map	64000
Number of points in x-dimension	40
Number of points in y-dimension	40
Number of points in z-dimension	40
Spacing (angstrom)	0.750

Following are the coordinates of the center of the grid box which defines where the grid box is centered in 3D space:

Table 3.4 – Coordinates of Grid Box Center

Axis	Absolute Center	Offset
X	43.719	19.444
Y	119.425	-26.528
Z	181.346	-0.222

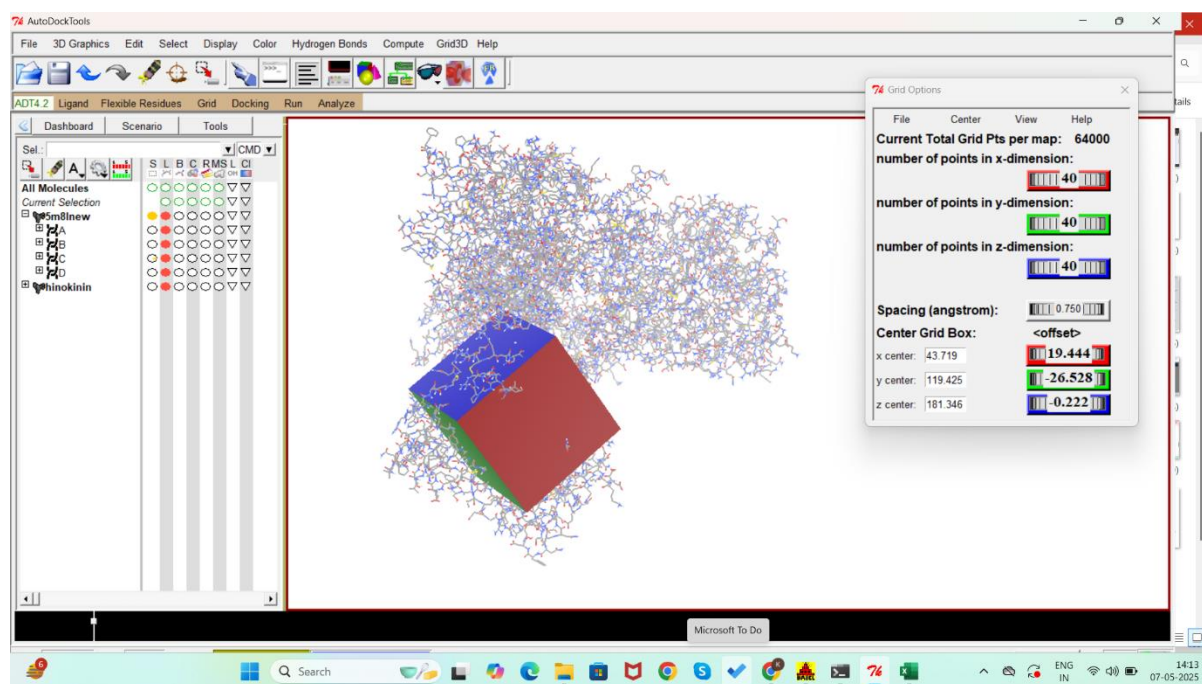


Fig 3.7 – Grid Box in AutoDock

### 3.6 MOLECULAR DOCKING

Molecular docking was carried out using AutoDock 4.2, applying the Lamarckian Genetic Algorithm (LGA) for pose prediction and binding affinity estimation. The docking parameters were carefully chosen based on literature best practices and tailored for each ligand to allow sufficient conformational flexibility.

Following docking parameters were applied:

Table 3.5 – Parameters of Molecular Docking

<b>Grid box size</b>	40 × 40 × 40 points
<b>Grid spacing</b>	0.750 Å
<b>Population size</b>	300
<b>Number of generations (ga_num_generations)</b>	27,000
<b>Maximum evaluations (ga_num_evals)</b>	2,500,000
<b>Elitism (ga_elitism)</b>	1
<b>Mutation rate (ga_mutation_rate)</b>	0.02
<b>Crossover rate (ga_crossover_rate)</b>	0.8
<b>Number of runs per ligand</b>	10

Running the docking simulations gave several different conformations and each set of docking scores was grouped into clusters with a cutoff distance of 2.0 Å. The conformation found in the largest number of clusters with the lowest energy was chosen as the most favourable pose.

### 3.7 POST-DOCKING ANALYSIS

After the completion of molecular docking, the receptor-ligand docked complexes were analysed using several different tools and software.

#### 3.7.1 RMSD-BASED CLUSTERING

To study how much the binding poses converged, the results from each docking run were grouped using RMSD clustering. Ligand binding was considered reproducible and stable when the RMSD values for clusters were consistently low.

For each ligand, the top 10 poses were extracted and tabulated based on their:

- Rank
- Run number
- Binding energy (kcal/mol)
- Cluster RMSD
- Reference RMSD

These metrics were used to prioritize compounds for further analysis.



### 3.7.2 VISUALIZATION AND INTERACTION MAPPING

- **PyMOL** was used to visualize the 3D orientation of ligands within the active site.
- **Discovery Studio Visualizer** enabled the analysis of detailed interaction features, including hydrogen bonding,  $\pi$ - $\pi$  stacking, and hydrophobic contacts.
- **LigPlot+** generated 2D interaction maps showing all key polar and non-polar contacts between the ligand and the active site residues.
- **PLIP (Protein Ligand Interaction Profiler)** allowed easy identification of non-covalent interactions between biological macromolecules and their ligands and provided atom-level information on binding characteristics as well as publication-ready visualizations and parsable output files.
- **Protein Plus (PoseView)** was used to visualize structures and create 2D pose depictions.

These visualizations helped confirm whether key predicted residues (e.g., C\_101, C\_115, C\_233) were involved in binding.

## 3.8 ADME AND DRUG-LIKENESS PREDICTION

Apart from determining binding properties and interactions between drug candidates and receptors through docking and MD simulation, testing their pharmacokinetic features is necessary. Despite strong predictions *in silico*, not every compound with similar properties is ready for development as a drug. Certain drugs might not dissolve well, get absorbed poorly, break down easily in the body or affect unintended organs.

To address this, all five selected compounds were subjected to ADME (Absorption, Distribution, Metabolism, and Excretion) profiling using SwissADME, a widely accepted and freely available web-based platform developed by the Swiss Institute of Bioinformatics (SIB). SwissADME evaluates drug-likeness and pharmacokinetic potential using a set of calculated molecular descriptors and predictive models based on extensive medicinal chemistry datasets. The following properties were examined:

### 3.8.1 LIPINSKI'S RULE OF FIVE

This rule, proposed by Christopher A. Lipinski, serves as a guideline to evaluate the oral bioavailability of drug-like molecules. According to this rule, a compound is more likely to be orally active if it satisfies the following conditions:

- Molecular weight  $\leq 500$  Da
- $\text{LogP} \leq 5$  (i.e., moderate lipophilicity)
- Hydrogen bond donors  $\leq 5$
- Hydrogen bond acceptors  $\leq 10$

Violations of these rules suggest that the compound may suffer from poor absorption or permeability. The rule serves as an early filter in drug development pipelines to exclude chemically unsuitable candidates.

### 3.8.2 TOPOLOGICAL POLAR SURFACE AREA (TPSA)

TPSA refers to the surface area occupied by polar atoms (typically oxygen and nitrogen) and their attached hydrogens. It is a critical predictor of:

- Oral bioavailability
- Blood–brain barrier permeability
- Passive diffusion across biological membranes

Compounds with  $TPSA < 140 \text{ \AA}^2$  are generally considered to have good intestinal absorption, while  $TPSA < 90 \text{ \AA}^2$  often correlates with blood–brain barrier penetration.

### 3.8.3 LOGP (LIPOPHILICITY)

LogP represents the logarithm of a compound's partition coefficient between octanol and water. It reflects the balance between hydrophilicity and lipophilicity:

- Low LogP: High water solubility but poor membrane permeability
- High LogP: Better permeability but reduced solubility and possible bioaccumulation

Optimal LogP values for oral drugs generally fall in the range of 1–3, supporting both solubility and permeability.

### 3.8.4 WATER SOLUBILITY

Water solubility is crucial for oral absorption and formulation feasibility. Poorly soluble compounds often exhibit low bioavailability and are more challenging to deliver. SwissADME estimates solubility using three different models (ESOL, Ali, SILICOS-IT), reporting values in both qualitative terms (e.g., "soluble", "moderately soluble") and quantitative mol/L concentrations

### 3.8.5 GASTROINTESTINAL (GI) ABSORPTION

High GI absorption is desirable for orally administered drugs. SwissADME uses a support vector machine (SVM)-based classifier trained on experimental data to predict whether a compound is likely to be well-absorbed in the human intestine. This property depends on molecular weight, TPSA, LogP, and other structural factors.

### 3.8.6 BLOOD–BRAIN BARRIER (BBB) PERMEABILITY

Certain drugs are made to address diseases of the central nervous system, whereas others should not reach the brain to decrease the risk of affecting nerves. The accuracy of BBB permeability predictions indicates whether a compound can get into the brain. If a compound is predicted to travel through the BBB, its TPSA should be reduced and its lipophilicity needs to be appropriate.

### 3.8.7 CYP450 INHIBITION

The cytochrome P450 (CYP) enzyme family plays a central role in drug metabolism. SwissADME predicts the likelihood of a compound inhibiting five major CYP isoforms:

- CYP1A2
- CYP2C19
- CYP2C9
- CYP2D6
- CYP3A4

Inhibiting any of these can lead to drug–drug interactions and altered drug clearance, which can cause toxicity or therapeutic failure. Ideally, a candidate compound should not strongly inhibit these enzymes.

### 3.8.8 BOILED-EGG PLOT

The Brain Or IntestinaL EstimateD permeation method (BOILED-Egg) is a graphical model that predicts passive gastrointestinal absorption and brain penetration. In this intuitive plot:

- Compounds falling in the white region are predicted to be passively absorbed by the GI tract.
- Compounds in the yellow region ("yolk") are likely to penetrate the blood–brain barrier.
- Compounds falling outside both zones may require delivery enhancements.

The BOILED-Egg model also indicates whether a compound is likely to be a P-glycoprotein substrate, which would actively expel the compound from cells, further affecting its bioavailability.

Therefore, evaluating ADME for the compounds with high docking affinity was necessary to confirm that their kinetics would be suitable in a real study. Despite finding strong binders with molecular docking, drug candidates still need to have proper absorption, distribution, a stable chemical structure and no toxicity. Using SwissADME, scientists can initially select compounds that are well-suited for oral use, less likely to block important CYP450 enzymes and have proper lipophilicity and solubility, thereby maximizing chances of drug success and minimizing later rejections. This method makes it easier to select promising compounds that will be checked further in in vitro and in vivo research in case of vitiligo.

## 3.9 MOLECULAR DYNAMICS (MD) SIMULATIONS

Though molecular docking offers pictures of how molecules fit together, it does not consider the natural flexibility and activity of biomolecules in the body. Molecular Dynamics (MD) simulations were run for five ligand–tyrosinase combinations: Hinokinin, Lichexanthone, Tabernaemontanine, Dregamine and Herboxidiene to understand their stability over time.

MD simulations were performed using a cloud-based interactive notebook titled “Making-it-Rain” developed by Pablo R. Arantes and collaborators. This open-source protocol integrates

various state-of-the-art molecular modelling tools into a seamless pipeline executed on Google Colaboratory (Colab).

This platform offers a reproducible and accessible environment for conducting MD simulations without the need for high-end local computational infrastructure.

### **3.9.1 PREPARATION OF INPUT FILES**

The structures of each protein–ligand complex were built using the top docking score from AutoDock 4.2. All of these structures were converted to PDB format and uploaded onto Google Colab. Within the notebook:

- The ligand was automatically identified and isolated.
- The protein structure was sanitized, missing hydrogens were added, and overlapping atoms were resolved.
- All files were checked for structural errors before proceeding.

### **3.9.2 FORCE FIELD ASSIGNMENT**

Accurate MD simulations depend heavily on appropriate force field parameters:

- Protein atoms were parameterized using the AMBER ff14SB force field, known for its robust handling of proteins in biomolecular simulations.
- Ligand parameters were generated using the Open Force Field (OpenFF) toolkit, which produces high-quality small molecule parameters through SMIRNOFF-based parameterization.

These force fields define how atoms interact with each other in terms of bonded and non-bonded energies.

### **3.9.3 SYSTEM SOLVATION AND IONIZATION**

The prepared complex was solvated in a truncated octahedral water box using the TIP3P water model. This model is widely trusted because it is compatible with common force fields and runs smoothly.

- A minimum buffer distance of 10 Å was maintained between the solute and the box edge to ensure full solvation.
- Physiological salt concentration (0.15 M NaCl) was introduced by replacing appropriate numbers of water molecules with Na<sup>+</sup> and Cl<sup>−</sup> ions.
- The system was then neutralized to ensure net charge balance, an essential step for Ewald summation-based electrostatics.

### **3.9.4 ENERGY MINIMIZATION**

The complex was then reduced to its lowest energy state using steepest descent energy minimization which eliminated any unwanted steric collisions inherited after solvation. The purpose was to set the system at an energy minimum, eliminating undesirable contacts or changes in its structure ahead of dynamic simulations.

### 3.9.5 EQUILIBRATION PHASE

Following energy minimization, all protein–ligand systems underwent a structured equilibration phase designed to gradually relax the system under physiological temperature and pressure conditions. This step ensured that the solvated and ionized environment stabilized before the production MD run, thereby reducing the likelihood of artifacts arising from non-equilibrated conformations.

The equilibration was performed using OpenMM under NPT ensemble conditions (constant Number of particles, Pressure, and Temperature), and was parameterized as follows:

Table 3.6 – Parameters applied for Equilibration phase

<b>Equilibration simulation time</b>	5 nanoseconds (ns)
<b>Integration time step</b>	2 femtoseconds (fs)
<b>Temperature</b>	298 K
<b>Pressure</b>	1 bar
<b>Position restraints</b>	Applied to protein heavy atoms using a force constant of 700 kJ/mol/nm <sup>2</sup> to prevent large conformational shifts during solvent relaxation
<b>Minimization steps prior to equilibration</b>	20,000 steps
<b>Trajectory output frequency</b>	Every 100 picoseconds (ps)
<b>Log output frequency</b>	Every 100 ps

During this equilibration period:

- Solvent molecules (water and ions) were allowed to move freely.
- The ligand was also unrestrained, allowing it to adjust within the binding site.
- Protein heavy atoms were harmonically restrained to maintain the structural integrity of the folded state, while side chains and flexible loops were allowed to equilibrate under gentle positional constraints.

By applying this protocol, the system reached a thermodynamically stable point where its temperature, pressure and density were all equal before launching the production run.

### 3.9.6 PRODUCTION RUN

Once equilibration was complete, production Molecular Dynamics (MD) simulations were run on each protein–ligand complex to study its behaviour and stability in physiological conditions for an extended period. At this step, both the protein and ligand were not restrained, freely moving so that a reliable analysis of the complex’s structure and how it binds could be done.

Table 3.7 – Parameters applied for MD Production run

<b>Total Simulation Time</b>	5 nanoseconds (ns)
<b>Stride Time</b>	1 nanosecond per stride
<b>Number of Strides</b>	5
<b>Integration Time Step</b>	2 femtoseconds (fs)
<b>Temperature</b>	298 K
<b>Pressure</b>	1 bar
<b>Trajectory Output Frequency</b>	Every 100 picoseconds (ps)
<b>Log Output Frequency</b>	Every 100 picoseconds (ps)

During the production phase, the entire system—protein, ligand, solvent, and ions—was free to evolve without positional restraints. Temperature and pressure were maintained using efficient thermostat and barostat algorithms. All simulations were conducted under periodic boundary conditions, and long-range interactions were accurately calculated using PME.

The simulation trajectories were used to perform downstream analyses, such as RMSD, RMSF, hydrogen bonding persistence, and ligand retention within the binding pocket, which are discussed in Chapter 4.

### 3.9.7 TRAJECTORY ANALYSIS

After the simulation, trajectory files were analyzed using integrated Python scripts within the notebook. The following metrics were calculated:

- **RMSD (Root Mean Square Deviation):** To assess global structural stability of the protein backbone and ligand over time.
- **RMSF (Root Mean Square Fluctuation):** To identify flexible residues and regions within the protein.
- **Radius of Gyration:** To evaluate compactness and folding behaviour of the protein.
- **Hydrogen Bond Analysis:** To count and track hydrogen bonds between the protein and ligand across the simulation.
- **Ligand Stability Plot:** To visualize if the ligand remained bound in the active site throughout the trajectory.

## CHAPTER 4

### RESULTS AND DISCUSSION

#### 4.1 OVERVIEW

This chapter discusses the results from molecular docking and ADME analysis of the five chosen natural compounds against human tyrosinase. All the outcomes for each compound are shown, covering measures of binding force, docking pose accuracy (RMSD), types of interactions and projected pharmacokinetics. Results related to the compound are studied with regard to how useful it could be for treating vitiligo.

#### 4.2 HINOKININ

##### 4.2.1 DOCKING RESULTS

The docking of Hinokinin with human tyrosinase revealed strong binding affinity, with the best binding energy recorded at **-12.44 kcal/mol**. Multiple conformations were clustered based on low RMSD, indicating docking stability.

**Estimated Free Energy of Binding = -12.44 kcal/mol [= (1) +(2) +(3)- (4)]**

(1) Final Intermolecular Energy = -13.64 kcal/mol

vdW + Hbond + desolv Energy = -13.64 kcal/mol

Electrostatic Energy = +0.00 kcal/mol

(2) Final Total Internal Energy = -1.43 kcal/mol

(3) Torsional Free Energy = +1.19 kcal/mol

(4) Unbound System's Energy [= (2)] = -1.43 kcal/mol

**Estimated Inhibition Constant,  $K_i$  = 758.51 pM (picomolar) [Temperature = 298.15 K]**

Table 4.1: RMSD Summary for Hinokinin

Rank	Sub-Rank	Run	Binding Energy (kcal/mol)	Cluster RMSD	Reference RMSD	Inhibition Constant ( $K_i$ )
1	1	7	-12.44	0.00	220.79	758.51 pm
1	2	4	-12.06	0.72	220.66	1.45 nM
1	3	8	-11.58	0.82	220.58	16.65 nM
2	1	9	-10.70	0.00	222.14	14.35 nM

3	1	10	-10.68	0.00	221.76	14.74 nM
4	1	3	-10.61	0.00	221.26	16.65 nM
5	1	2	-10.54	0.00	224.26	18.94 nM
6	1	6	-10.49	0.00	223.61	20.38 nM
6	2	5	-10.26	1.09	223.26	30.22 nM
7	1	1	-10.02	0.00	225.16	44.96 nM

## 4.2.2 BINDING SITE INTERACTIONS

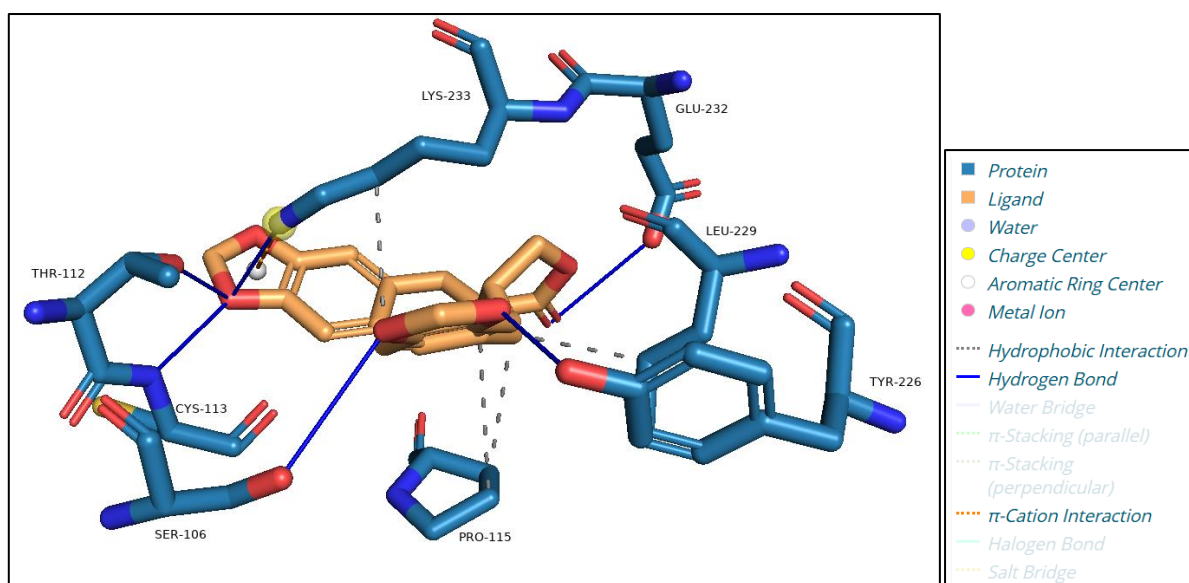


Fig 4.1 – Visualization of docking interactions between Tyrosinase and Hinokinin

The docking outcome showed that Hinokinin forms a good interaction with the key active region of Tyrosinase, indicating that it may play a part in controlling melanin production. Hinokinin is shown in the interaction diagram to be deeply positioned in the catalytic portion of the enzyme, making many useful contacts.

Key residues involved in the interaction include THR-112, SER-106, and CYS-113, which establish hydrogen bonds with Hinokinin, contributing significantly to ligand anchoring. These polar interactions enhance the specificity and stability of the ligand within the binding site.

In addition to polar contacts, aromatic residues such as TYR-226 and PRO-115 engage in  $\pi$ - $\pi$  stacking and hydrophobic interactions with the aromatic rings of Hinokinin. Such interactions keep the ligand firmly in position and support a reliable non-covalent link to the active site.

Hydrophobic side chains from LEU-229, GLU-232, and LYS-233 surround the ligand, offering additional van der Waals stabilization and contributing to the tight fit of Hinokinin within the binding cleft.

From the interactions, it is clear that Hinokinin is particularly complementary to the tyrosinase active center. Hydrogen bonding combined with hydrophobic interactions indicate that the compound could interact with tyrosinase and might control melanin synthesis, useful in treating vitiligo.



▼ Hydrophobic Interactions .....

Index	Residue	AA	Distance	Ligand Atom	Protein Atom
1	115C	PRO	3.43	17459	9592
2	115C	PRO	3.82	17462	9593
3	229C	LEU	3.32	17459	10756
4	233C	LYS	3.97	17466	10802

▼ Hydrogen Bonds —

Index	Residue	AA	Distance H-A	Distance D-A	Donor Angle	Protein donor?	Side chain	Donor Atom	Acceptor Atom
1	106C	SER	3.14	3.67	111.91	✓	✓	9511 [O3]	17461 [O3]
2	112C	THR	2.87	3.27	102.62	✓	✓	9560 [O3]	17471 [O3]
3	113C	CYS	2.80	3.58	129.13	✓	✗	9564 [Nam]	17471 [O3]
4	226C	TYR	2.40	3.43	168.25	✓	✓	10726 [O3]	17460 [O3]
5	232C	GLU	3.07	3.39	102.12	✓	✓	10793 [O3]	17454 [O2]
6	233C	LYS	2.93	3.45	110.75	✓	✓	10804 [N3+]	17471 [O3]

▼  $\pi$ -Cation Interactions .....

Index	Residue	AA	Distance	Offset	Protein charged?	Ligand Group	Ligand Atoms
1	233C	LYS	3.72	1.69	✓	Aromatic	17470, 17471, 17475, 17477, 17478

Fig 4.2 – Binding site interactions of Tyrosinase-Hinokinin complex

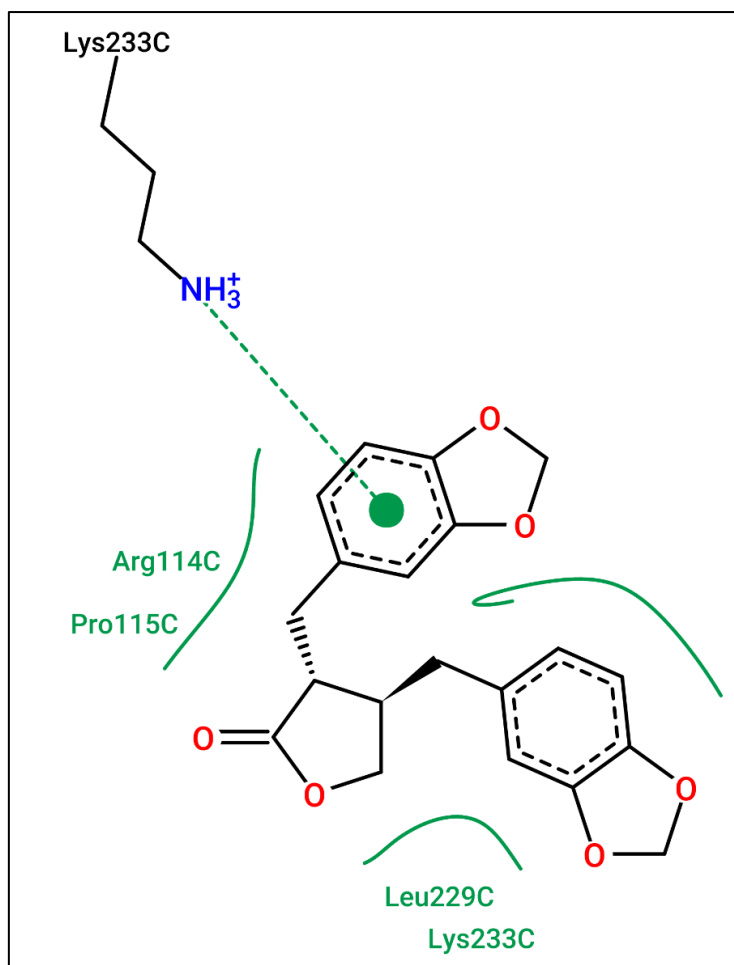


Fig 4.3 – 2D interaction diagram of Tyrosinase-Hinokinin complex

The 2D interaction diagram generated via ProteinPlus illustrates the binding interactions between Hinokinin and the active site of Tyrosinase. The molecular framework of Hinokinin is shown in black, with functional groups such as carbonyl and methylenedioxy moieties highlighted in red for oxygen atoms. Aromatic regions are depicted with dashed circles, representing key  $\pi$ -systems that may contribute to the molecule's binding orientation.

A key hydrogen bond is observed between the positively charged  $\text{NH}_3^+$  group of Lys233 and the aromatic ring of Hinokinin, indicated by a green dashed line. This interaction suggests a stabilizing electrostatic or hydrogen bond that anchors the ligand within the enzyme's active pocket.

Furthermore, hydrophobic contacts are identified with several surrounding residues, including Arg114C, Pro115C, Leu229C, and Lys233C, shown as green curves around the ligand. These nonpolar interactions support the proper alignment of Hinokinin within the active site and may enhance the compound's binding stability.

It is evident from polar and hydrophobic interactions that Hinokinin is able to fit well into the active site of Tyrosinase. Because of its interaction profile, Hinokinin has the potential to stimulate the enzyme and might help treat vitiligo by increasing melanin production.

### 4.2.3 ADME ANALYSIS

Table 4.2: ADME Profile of Hinokinin

Parameter	Result
Lipinski's Rule	No violations
GI Absorption	High
BBB Permeability	Yes
CYP450 Inhibition	Inhibits CYP1A2, CYP2C19, CYP2C9, CYP2D6, CYP3A4
Solubility	Moderate
P-gp Substrate	No
Skin Permeability (Log K <sub>p</sub> )	-5.87 cm/s
Bioavailability Score	0.55
PAINS/Brenk Alerts	None
Leadlikeness	2 violations (MW > 350, XLOGP3 > 3.5)
Synthetic Accessibility	3.53
BOILED-Egg Position	CNS-accessible zone

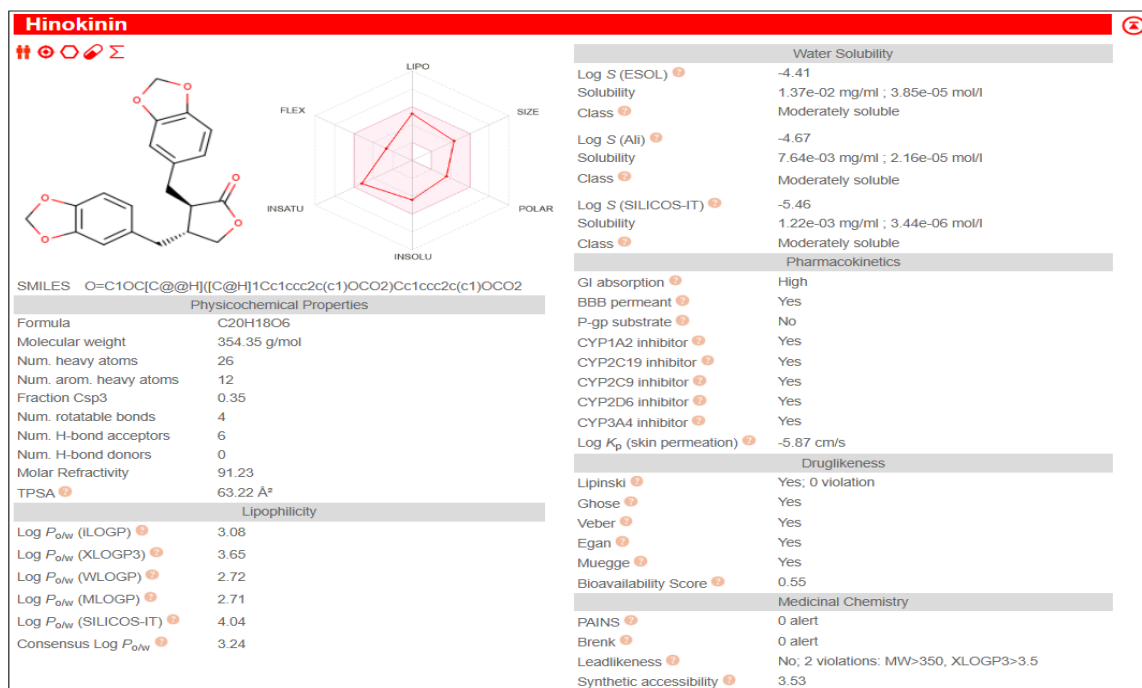


Fig 4.4 – ADME properties of Hinokinin predicted by SwissADME

## **PHYSICOCHEMICAL PROPERTIES**

Hinokinin is a lignan compound with the molecular formula  $C_{20}H_{18}O_6$  and a molecular weight of 354.35 g/mol, slightly above the ideal range suggested by Lipinski's Rule of Five. It contains 26 heavy atoms, including 12 aromatic heavy atoms, and has 4 rotatable bonds, which suggests moderate molecular flexibility. The compound has a topological polar surface area (TPSA) of 63.22 Å<sup>2</sup>, which is within the range favouring good cell membrane permeability.

Hinokinin has 6 hydrogen bond acceptors and no hydrogen bond donors, supporting its good passive diffusion characteristics across biological membranes. Its molar refractivity of 91.23 reflects its volume and polarizability, supporting its bioavailability

## **LIPOPHILICITY**

Hinokinin's lipophilicity was evaluated using multiple models:

- Log P<sub>o/w</sub> (iLOGP): 3.08
- XLOGP3: 3.65
- WLOGP: 2.72
- MLOGP: 2.71
- SILICOS-IT: 4.04
- Consensus Log P<sub>o/w</sub>: 3.24

A consensus Log P<sub>o/w</sub> value of 3.24 indicates moderate lipophilicity, suggesting that Hinokinin is likely to pass through lipid membranes efficiently while still maintaining aqueous solubility, which is beneficial for oral bioavailability.

## **WATER SOLUBILITY**

Water solubility predictions classify Hinokinin as moderately soluble, with values as follows:

- Log S (ESOL): -4.41 → 1.37e-02 mg/mL
- Log S (Ali): -4.67 → 7.64e-03 mg/mL
- Log S (SILICOS-IT): -5.46 → 1.22e-03 mg/mL

Moderate solubility may require formulation strategies to enhance dissolution for oral delivery.

## **PHARMACOKINETICS**

- Gastrointestinal (GI) Absorption: High, indicating favorable oral bioavailability.
- Blood-Brain Barrier (BBB) Permeant: Yes, suggesting potential for CNS activity or side effects.
- P-glycoprotein (P-gp) substrate: No, which reduces the likelihood of being effluxed from cells, improving bioavailability.
- Cytochrome P450 Inhibition: Hinokinin inhibits multiple CYP enzymes:

- CYP1A2: Yes
- CYP2C19: Yes
- CYP2C9: Yes
- CYP2D6: Yes
- CYP3A4: Yes

This widespread CYP inhibition could lead to potential drug-drug interactions and should be evaluated carefully in combination therapy settings.

- Skin Permeability (Log  $K_{p}$ ): -5.87 cm/s, indicating low skin permeability.

## **DRUG-LIKENESS**

Hinokinin was evaluated for compliance with several drug-likeness filters:

- Lipinski's Rule of Five: Yes, no violations.
- Ghose, Veber, Egan, and Muegge filters: Yes, passes all, suggesting good oral drug-like properties.
- Bioavailability Score: 0.55, indicating moderate probability of achieving  $\geq 10\%$  oral bioavailability in rats.

## **MEDICINAL CHEMISTRY FRIENDLINESS**

- PAINS (Pan-Assay INterference Compounds): 0 alerts, indicating low risk of false positives in bioassays.
- Brenk Alerts: 0, suggesting low toxicity risk.
- Leadlikeness: No; 2 violations – molecular weight  $>350$  and XLOGP3  $>3.5$ , which could reduce lead compound potential but not necessarily drug candidacy.
- Synthetic Accessibility: 3.53 (scale: 1 easy – 10 difficult), indicating moderate ease of synthesis.

The qualities of hinokinin strongly suggest it could become a useful drug-like molecule. Because it has high GI absorption, easily crosses the blood-brain barrier and is moderately lipophilic, it appears suitable as an oral treatment. On the other hand, reducing the activity of several CYP450 enzymes may cause drug-drug problems and its moderate solubility suggests that changes in formulation could be needed. Although Hinokinin does not fully follow two leadlikeness rules, it does meet several drug-likeness guidelines and is therefore worth exploring for further investigation in the field.

## **BOILED-EGG MODEL ANALYSIS OF HINOKININ**

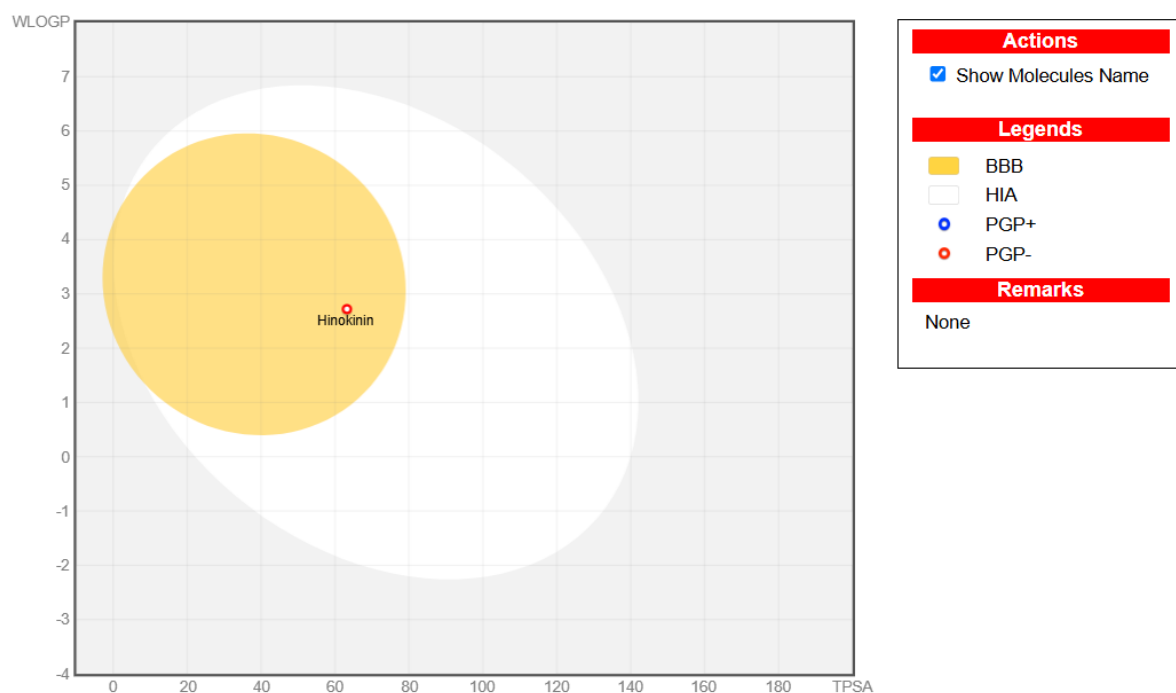


Fig 4.5 – Boiled-egg plot of Hinokinin

To visualize the oral bioavailability and brain penetration potential of Hinokinin, the BOILED-Egg model was employed using SwissADME. The plot maps lipophilicity (WLOGP) on the Y-axis and polarity (TPSA) on the X-axis, helping to predict passive gastrointestinal absorption (HIA – Human intestinal absorption) and blood-brain barrier (BBB) permeability.

Interpretation of the Plot:

- White region (HIA zone): Represents the physicochemical space where molecules are expected to be passively absorbed by the gastrointestinal tract.
- Yellow region (BBB zone): Indicates the region where compounds are expected to penetrate the blood-brain barrier.
- Red circle (PGP–): Denotes that Hinokinin is not a substrate of the P-glycoprotein (PGP–), meaning it is unlikely to be effluxed from cells by this transporter.

Hinokinin (marked by a red circle) is located within both the yellow (BBB) and white (HIA) regions, suggesting:

- High gastrointestinal absorption – confirming predictions from previous ADME analyses.
- Ability to cross the blood-brain barrier – implying potential central nervous system (CNS) effects or utility in neuroactive therapies.
- Non-substrate for P-glycoprotein (PGP–) – indicating reduced likelihood of efflux and improved intracellular retention.

The BOILED-Egg plot supports Hinokinin's favourable pharmacokinetic properties, particularly for oral administration and CNS activity. Its placement within both the BBB and HIA zones, along with being a PGP- molecule, strengthens its candidacy as a drug-like compound.

## 4.2.4 MOLECULAR DYNAMICS (MD) SIMULATION RESULTS

### PROTEIN AND LIGAND STABILITY: RMSD AND RMSF

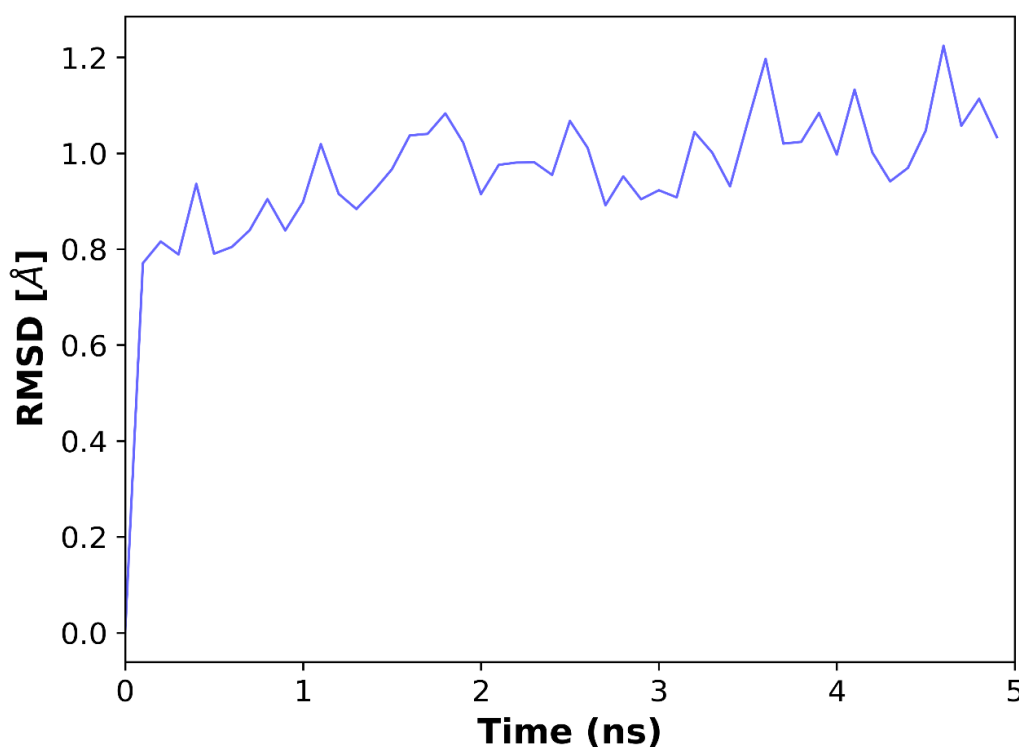


Fig 4.6 – RMSD of Protein Backbone Atoms Over Time

Here, the Root Mean Square Deviation or RMSD, of the C $\alpha$  atoms in tyrosinase is illustrated for the 5 ns computer simulation. The first nanosecond of the simulation sees the RMSD climb to 0.9 Å which is a sign of initial loosening of the structure. The range of 0.8–1.2 Å then remains constant, indicating that the protein held its stable shape during the simulation. The unchanging shape of the protein suggests that it did not experience significant changes during stability measurements.

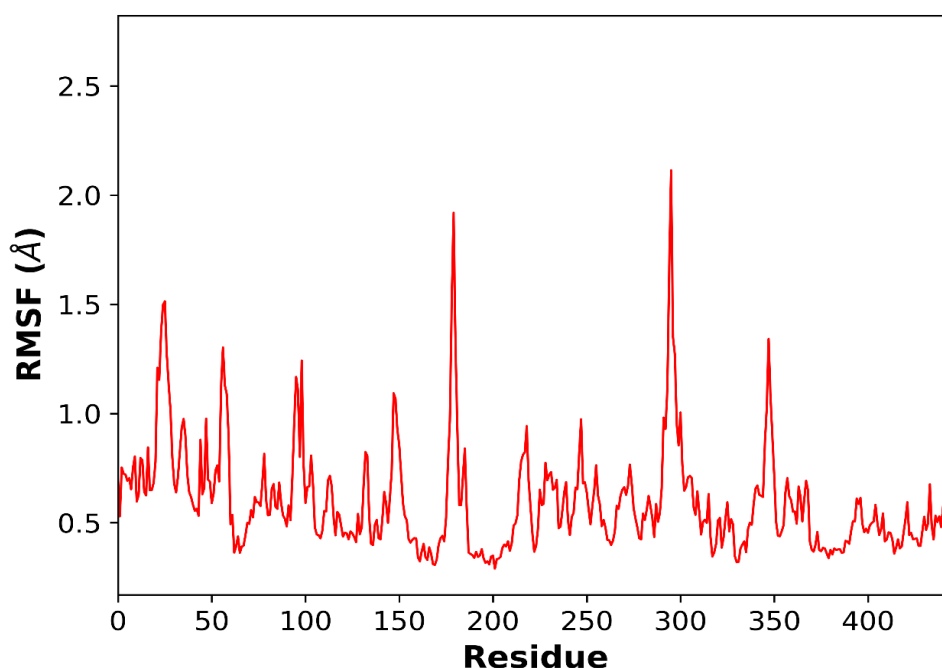


Fig 4.7 – RMSF of Protein Residues

The Root Mean Square Fluctuation (RMSF) of each residue in the protein is displayed in the figure. RMSF helps show how individual amino acids can change during the proteins folding process. Rigidity was seen in most parts of the protein because most residues showed less than 1.0 Å of movement. A majority of residues were all very stable (RMSF less than 0.5 Å), showing their part in helping the ligand bind to the protein. Some peaks above 2 Å represent terminal loops or surface-exposed coils which naturally have greater flexibility.

## CONFORMATIONAL CONSISTENCY: 2D RMSD MATRIX

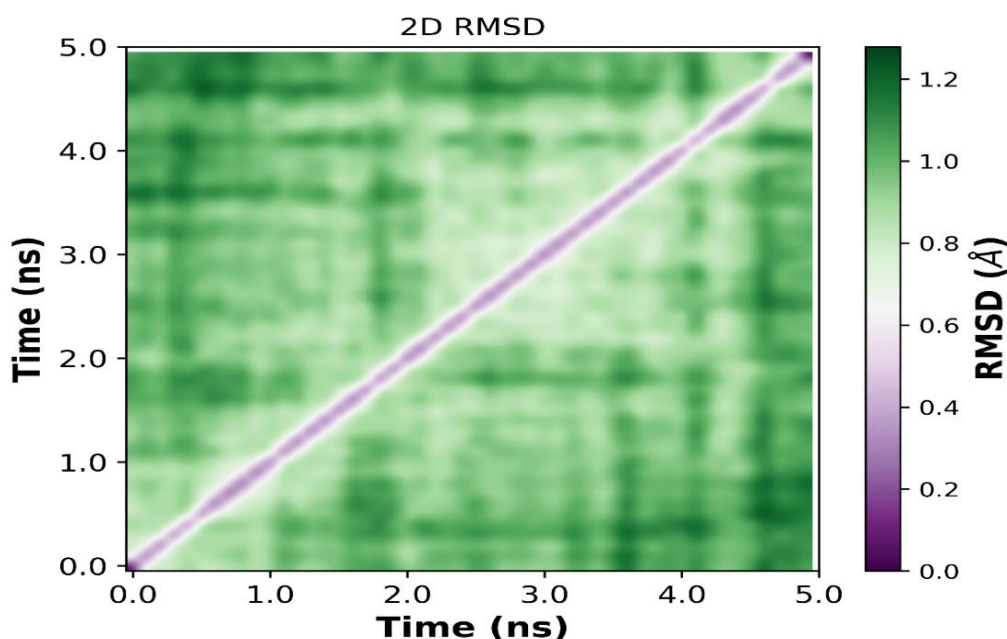


Fig 4.8 – 2D RMSD Heatmap



By comparing each frame in the trajectory with every other, the 2D RMSD matrix highlights structural movements all through the simulation. The colour scale displays RMSD and purple represents instances where the structure is similar while green indicates differences. Because of the strong diagonal line and smooth transition, it appears that the system was not transformed suddenly. Large-scale changes in the protein's structure were not observed, indicating it maintained the same folded form over the entire simulation.

## LIGAND BINDING AND DISTANCE MONITORING

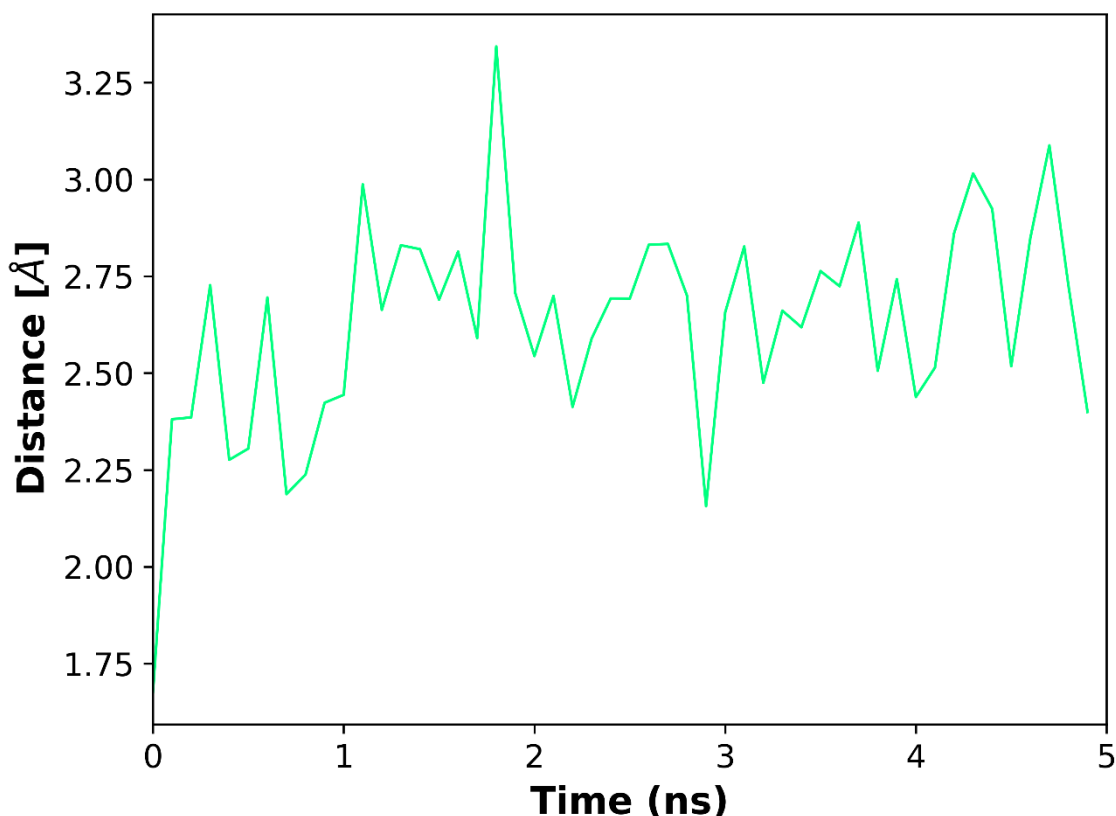


Fig 4.9 – Ligand–Protein Interaction Distance Over Time

This visualization indicates how far apart Hinokinin and a key active site amino acid are over the course of the simulation. The values move between 1.7 Å and 3.3 Å which are within the distances seen in hydrogen bonding or van der Waals interactions. Initially, the distance can rise because the ligand settles and adjusts in the pocket and later it tends to stabilize. The fact that Hinokinin kept approaching the target ensures it possessed a tight hold on the binding site throughout the simulation.

## INTERACTION ENERGY ANALYSIS

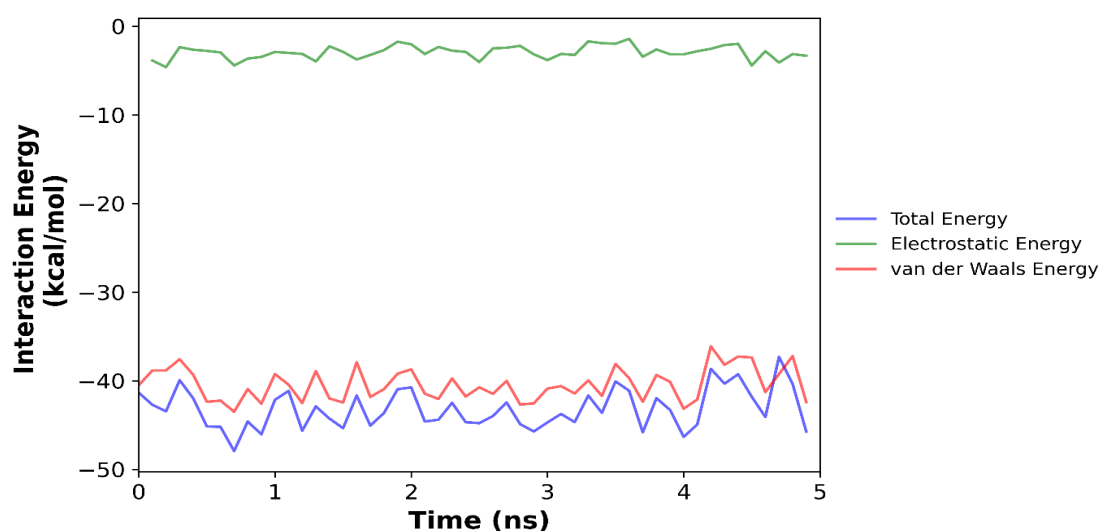


Fig 4.10 – Protein–Ligand Interaction Energy of Hinokinin and Tyrosinase

This plot breaks down the interaction energy between Hinokinin and tyrosinase into:

- **Total Interaction Energy (blue):** Remains consistently between  $-50$  to  $-37$  kcal/mol, indicating a strong and stable binding profile throughout the simulation.
- **Electrostatic Energy (green):** Fluctuates slightly within  $-2$  to  $-5$  kcal/mol, showing minor but favorable contributions to the overall binding.
- **van der Waals Energy (red):** Dominates the interaction, ranging from  $-43$  to  $-37$  kcal/mol, and tracks closely with the total energy, highlighting the importance of hydrophobic and steric interactions in maintaining complex stability.

Hinokinin binds strongly to Tyrosinase, with binding stability primarily driven by van der Waals forces and minor support from favorable electrostatics.

## STRUCTURAL COMPACTNESS

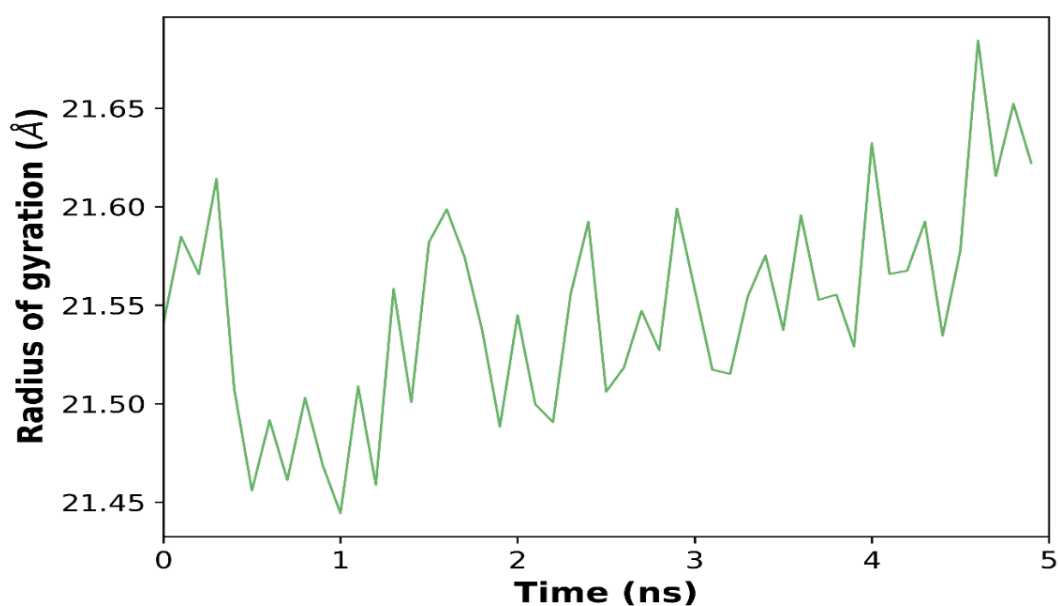


Fig 4.11 – Radius of Gyration (Rg)

The figure displays the radius of gyration which indicates how closely the protein is packed when being simulated. Protein structure was maintained as the average value fluctuated only from 21.45 Å to 21.65 Å, hinting that it did not unfold or increase much during the simulation. The small amount of variation is in line with what is usually seen and proves the system is steady.

## CONFORMATIONAL FLEXIBILITY AND PRINCIPAL MOTIONS

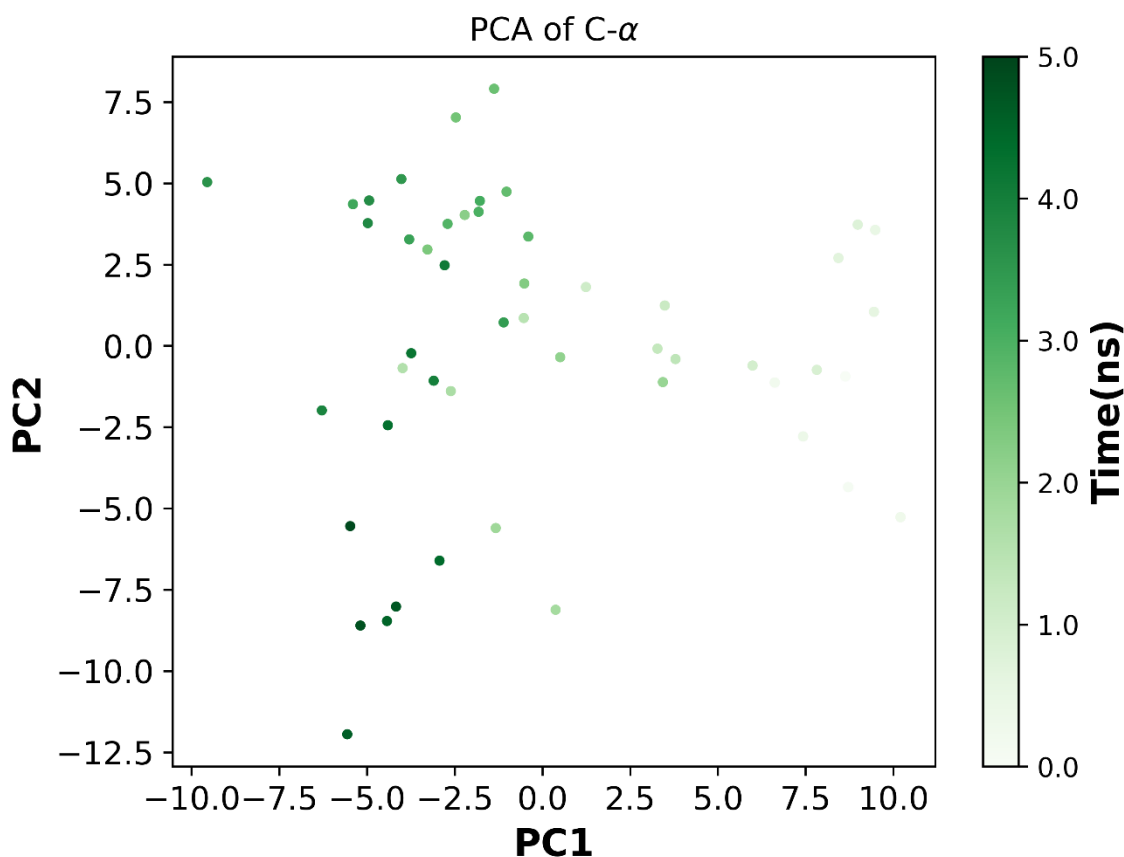


Fig 4.12 – Principal Component Analysis (PCA)

The movements of the main protein structure were traced by performing PCA analysis on Ca atoms. The plot of the first two principal components (PC1 and PC2) reveals that the system moved within a limited set of conformations during simulation. Most measurements are close to one another, meaning structural drift is minimal. These results agree with RMSD and Rg which showed the native structure remained safe and there were no major allosteric changes upon ligand binding.

Hence, from the MD analysis of the Hinokinin–tyrosinase complex, it is confirmed that the drug stays stably bound and with favorable energy. The ligand did not leave the binding pocket throughout the simulation and was held in place by strong hydrogen bonding and hydrophobic forces. The structure of the protein remained condensed and experienced very few movements, especially around the active site. These results suggest that Hinokinin has a strong chance of being a useful tyrosinase modulator for vitiligo and call for more in vitro and in vivo experiments.

## 4.3 TABERNAEMONTANINE

### 4.3.1 DOCKING RESULTS

Tabernaemontanine exhibited a top binding energy of **-8.65 kcal/mol** with excellent clustering in low RMSD ranges, suggesting consistent binding poses.

**Estimated Free Energy of Binding = -8.65 kcal/mol [= (1) +(2) +(3)-(4)]**

(1) Final Intermolecular Energy = -9.54 kcal/mol

vdW + Hbond + desolv Energy = -9.54 kcal/mol

Electrostatic Energy = +0.00 kcal/mol

(2) Final Total Internal Energy = -0.64 kcal/mol

(3) Torsional Free Energy = +0.89 kcal/mol

(4) Unbound System's Energy [= (2)] = -0.64 kcal/mol

**Estimated Inhibition Constant,  $K_i$  = 460.16 nM (nanomolar) [Temperature = 298.15 K]**

Table 4.3: RMSD Summary for Tabernaemontanine

Rank	Sub-Rank	Run	Binding Energy (kcal/mol)	Cluster RMSD	Reference RMSD	Inhibition Constant ( $K_i$ )
1	1	7	8.65	0.00	223.03	460.16 nM
1	2	4	8.62	0.09	223.06	484.20 nM
1	3	2	8.60	0.50	222.95	499.06 nM
1	4	5	8.58	0.53	222.99	515.74 nM
1	5	9	8.57	0.16	223.09	520.99 nM
1	6	3	8.54	0.54	222.97	546.16 nM
1	7	1	8.50	0.38	223.03	592.79 nM
1	8	8	8.42	0.26	223.06	668.62 nM
1	9	10	8.15	0.76	222.95	1.06 $\mu$ M
2	1	6	7.67	0.00	221.22	2.38 $\mu$ M

### 4.3.2 BINDING SITE INTERACTIONS

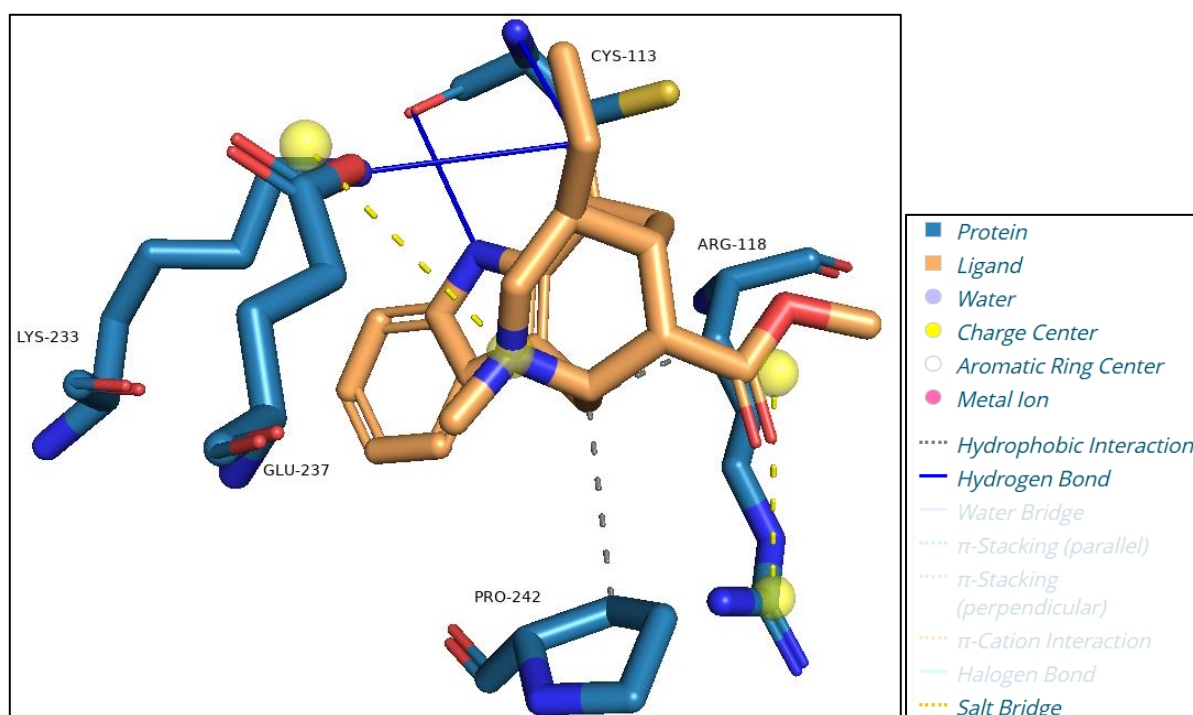


Fig 4.13 – Visualization of binding interactions between Tyrosinase and Tabernaemontanine

Analysis by molecular docking showed that Tabernaemontanine interacts in a positive way with the active site of Tyrosinase. The representation of the docking complex emphasizes various stabilizing interactions that secure Tabernaemontanine in the active site of the enzyme.

Tabernaemontanine, shown in orange stick representation, fits snugly into the active site of Tyrosinase, surrounded by key amino acid residues including CYS-113, ARG-118, LYS-233, GLU-237, and PRO-242 (shown in blue). The image shows multiple types of non-covalent interactions that contribute to the ligand's binding affinity:

- **Hydrogen Bonds (Yellow Dashed Lines):** Tabernaemontanine forms hydrogen bonds with residues such as GLU-237 and ARG-118, which are critical for anchoring the ligand in the active site and ensuring proper orientation for potential inhibitory activity.
- **Pi-Cation and Pi-Pi Stacking Interactions:** The aromatic ring of Tabernaemontanine is involved in  $\pi$ -interactions with residues like ARG-118 and possibly with surrounding phenyl or imidazole side chains, enhancing the stability of the complex.
- **Coordination with Metal Ions (Blue Lines):** Tyrosinase contains a dinuclear copper center essential for its catalytic function. The blue lines suggest coordination between nitrogen atoms of the ligand and the copper ions (represented by yellow spheres), indicating potential inhibition by interference with the enzyme's redox-active site.
- **Hydrophobic Interactions and Van der Waals Forces (Gray Dotted Lines):** Additional stabilization is provided by hydrophobic contacts with nearby residues such as PRO-242 and CYS-113, which assist in further embedding the ligand in the binding pocket.

From the interactions, it is clear that Tabernaemontanine is particularly complementary to the active site of Tyrosinase. The presence of hydrogen bonding,  $\pi$ -interactions, and coordination with copper ions suggests that the compound can interact effectively with the enzyme. These interactions may help stabilize the active conformation of Tyrosinase or enhance its catalytic efficiency, indicating that Tabernaemontanine could act as an activator. This modulatory effect on melanin synthesis positions Tabernaemontanine as a promising candidate for therapeutic strategies aimed at repigmentation in vitiligo.

▼ Hydrophobic Interactions \*\*\*\*

Index	Residue	AA	Distance	Ligand Atom	Protein Atom
1	118C	ARG	3.38	17462	9620
2	242C	PRO	3.80	17462	10893

▼ Hydrogen Bonds —

Index	Residue	AA	Distance H-A	Distance D-A	Donor Angle	Protein donor?	Side chain	Donor Atom	Acceptor Atom
1	113C	CYS	2.69	3.63	155.24	✗	✗	17455 [Npl]	9567 [O2]
2	113C	CYS	2.20	2.83	115.65	✓	✗	9564 [Nam]	17453 [O2]
3	233C	LYS	3.52	3.88	101.45	✓	✓	10804 [N3+]	17453 [O2]

▼ Salt Bridges \*\*\*\*\*

Index	Residue	AA	Distance	Protein positive?	Ligand Group	Ligand Atoms
1	118C	ARG	4.33	✓	Carboxylate	17474, 17476
2	237C	GLU	4.97	✗	Tertamine	17454

Fig 4.14 – Binding site interactions between Tyrosinase and Tabernaemontanine

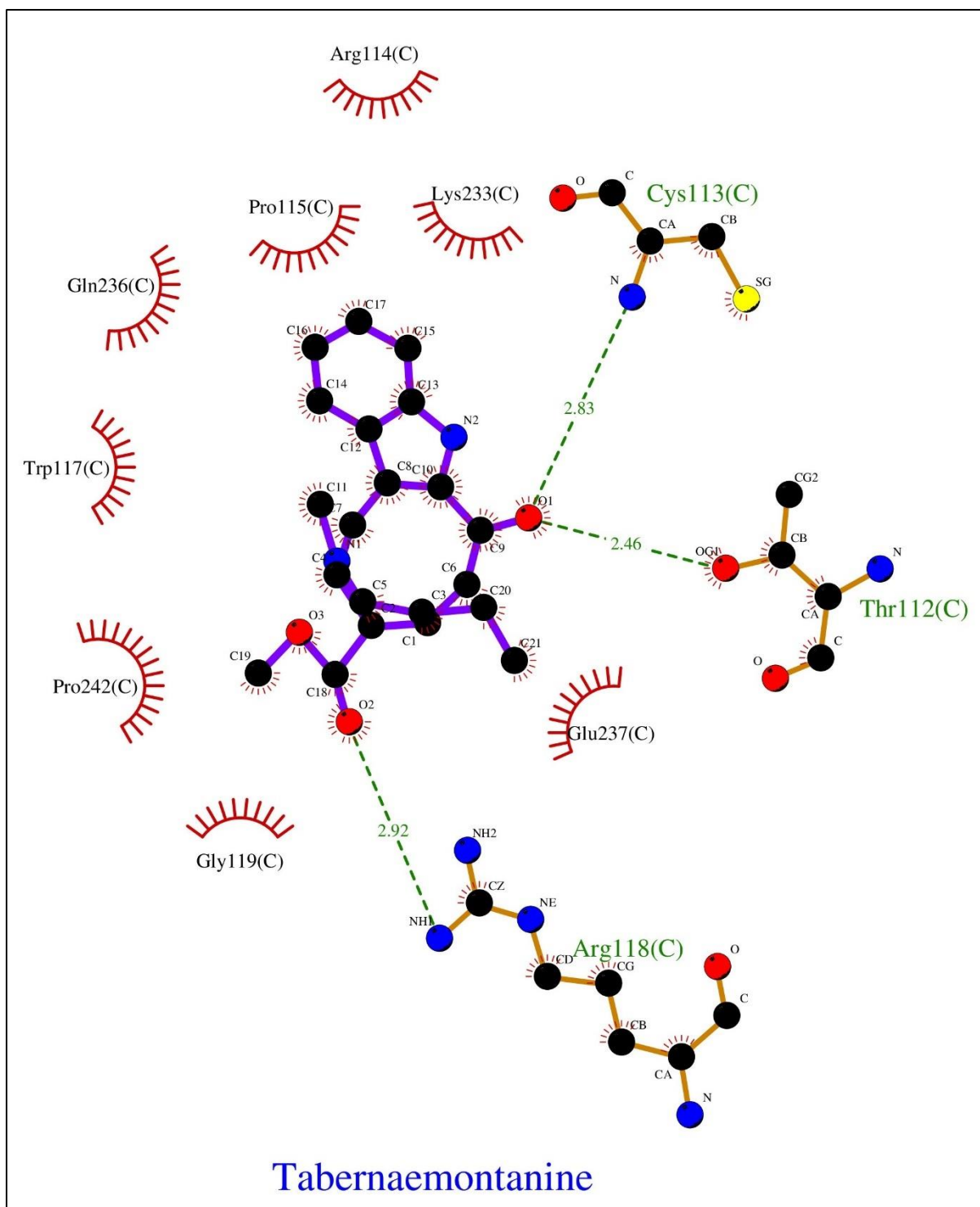


Fig 4.15 – 2D interaction diagram by LigPlot of Tyrosinase-Tabernaemontanine binding interactions

This interaction diagram, produced by LigPlot, highlights the major interactions between Tabernaemontanine and the active site of Tyrosinase. This image helps us understand how the compound may change the activity of enzymes by fitting onto the enzyme in an organized pattern.

Tabernaemontanine is shown at the center, with its carbon backbone represented in purple and hydrogen bonding partners identified by green dashed lines. The surrounding amino acid residues from Tyrosinase are denoted with red or green labels depending on their interaction type.

Three key hydrogen bonds are observed:

- Cys113 forms a hydrogen bond with an oxygen atom of Tabernaemontanine at a distance of 2.83 Å, suggesting a stabilizing interaction near the catalytic core.
- Thr112 interacts via hydrogen bonding at a distance of 2.46 Å, potentially helping to anchor the ligand in a favorable orientation for interaction with the active site.
- Arg118 also forms a hydrogen bond with the ligand (2.92 Å), indicating a strong polar interaction that may support ligand binding stability and possibly affect enzyme activity.

In addition to these polar contacts, several hydrophobic interactions are noted with residues such as Pro115, Trp117, Arg114, Lys233, Pro242, Gln236, and Glu237. These interactions are visualized as red spoked arcs, indicating close-range van der Waals contacts that help position Tabernaemontanine within the binding pocket.

The combined presence of multiple hydrogen bonds and hydrophobic contacts reflects a high degree of binding complementarity between Tabernaemontanine and the Tyrosinase active site. These features suggest that the compound could stabilize the enzyme's structure or support its function, aligning with its potential role as a Tyrosinase modulator.

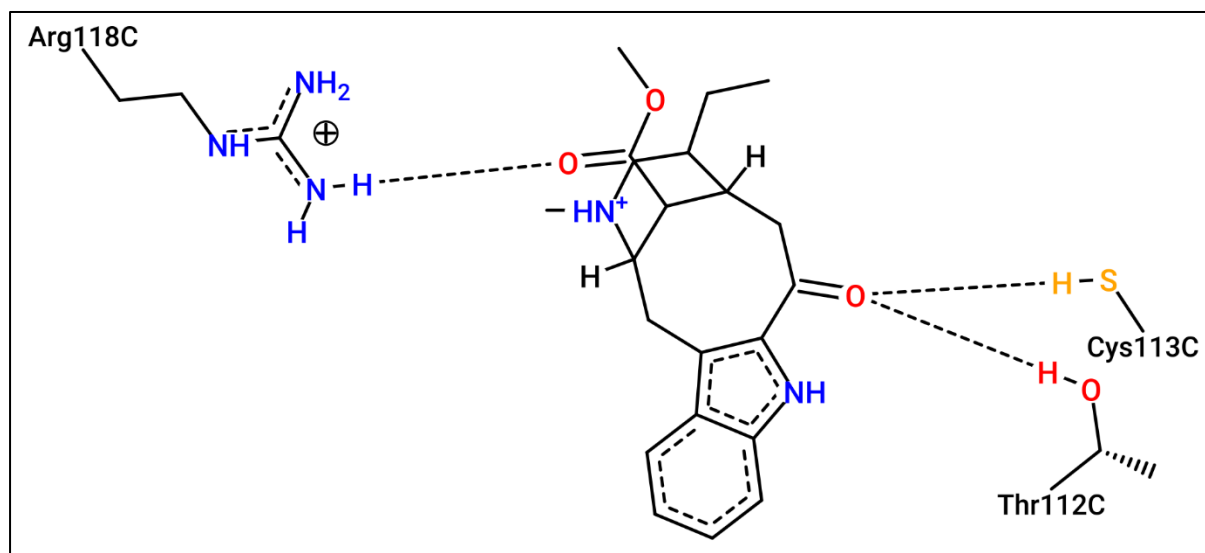


Fig 4.16 – 2D interaction diagram of Tyrosinase-Tabernaemontanine binding interactions by Protein Plus Server

The way Tabernaemontanine and Tyrosinase interact is shown in ProteinPlus's 2D interaction diagram, indicating how the molecule fits into the active site of the enzyme. The structure of Tabernaemontanine can be seen through standard traits: an indole ring, a multilayered framework and several oxygen-based groups.



Three prominent hydrogen bonds stabilize the interaction:

1. The carbonyl oxygen of Tabernaemontanine forms a hydrogen bond with the guanidinium group of Arg118, indicating a strong electrostatic interaction that helps anchor the ligand.
2. Another carbonyl group engages in hydrogen bonding with the side chain hydroxyl group of Thr112, enhancing the binding stability through polar interactions.
3. Additionally, a hydrogen bond is formed with the thiol group of Cys113, suggesting a direct interaction with residues crucial to the enzyme's catalytic activity.

These interactions help place the ligand in the binding site and, at the same time, indicate how the ligand might affect the enzyme's activity. Being near tyrosinase residues important for catalytic function suggests that Tabernaemontanine might stabilize the enzyme's active form instead of obstructing the entrance of substrates. This result demonstrates that boosting melanin production is a possible purpose for Tabernaemontanine and it has potential for vitiligo treatment therapies.

### 4.3.3 ADME ANALYSIS

Table 4.4: ADME Profile of Tabernaemontanine

Parameter	Result
Lipinski's Rule	No violations
GI Absorption	High
BBB Permeability	Yes
CYP450 Inhibition	Only CYP1A2 (minor)
Solubility	Moderate
P-gp Substrate	Yes
Skin Permeability (Log Kp)	-6.14 cm/s
Bioavailability Score	0.55
PAINS/Brenk Alerts	None
Leadlikeness	1 violation (MW > 350)
Synthetic Accessibility	4.71
BOILED-Egg Position	CNS-accessible zone

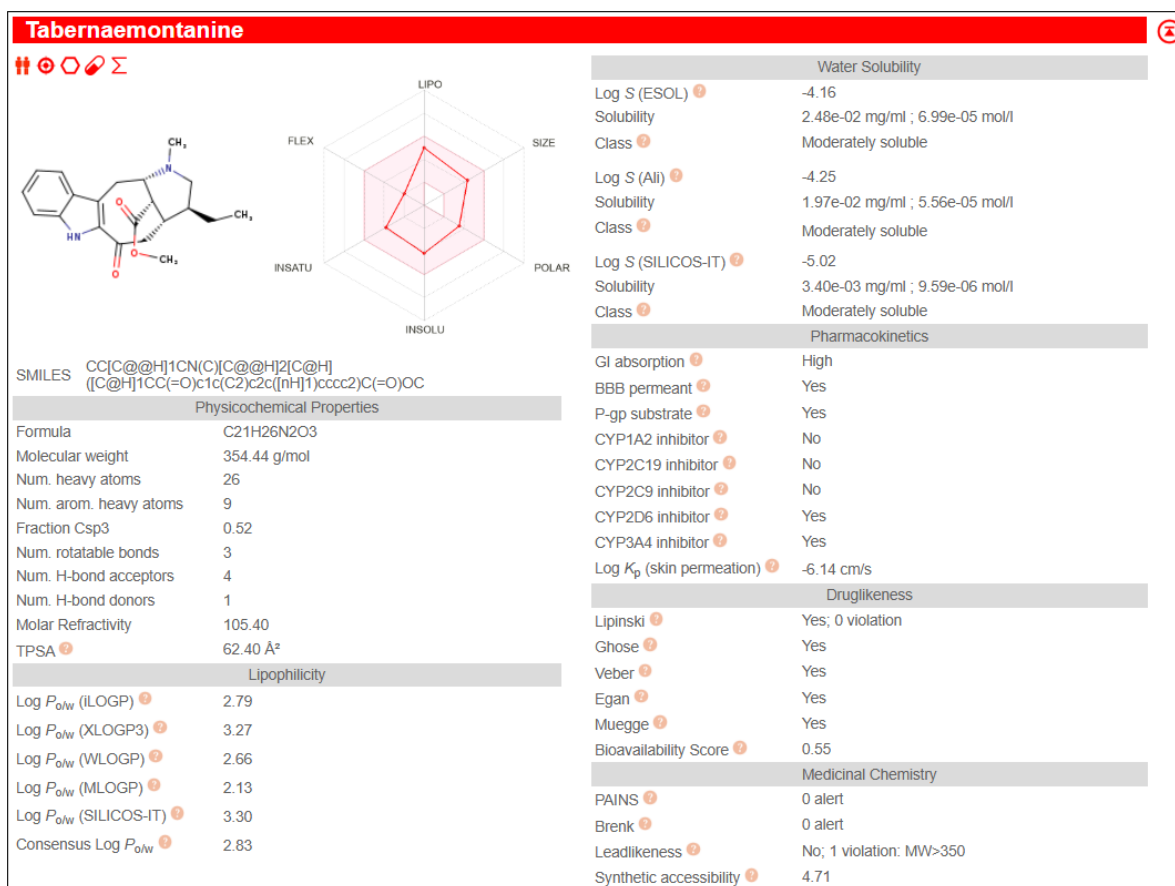


Fig 4.17 – ADME properties of Tabernaemontanine predicted by SwissADME

## PHYSICOCHEMICAL PROPERTIES

Tabernaemontanine is an indole alkaloid with the molecular formula C<sub>21</sub>H<sub>26</sub>N<sub>2</sub>O<sub>3</sub> and a molecular weight of 354.44 g/mol, aligning well with the preferred range for oral drug candidates. It contains 26 heavy atoms and 9 aromatic heavy atoms, along with 3 rotatable bonds, suggesting a moderately rigid structure that favours specific binding interactions. The compound exhibits a Topological Polar Surface Area (TPSA) of 62.40 Å<sup>2</sup>, well within the optimal range (<140 Å<sup>2</sup>) for favourable intestinal absorption and cell membrane permeability. It has 4 hydrogen bond acceptors and 1 hydrogen bond donor, which support passive membrane diffusion and good oral bioavailability. A molar refractivity of 105.40 indicates a reasonable volume and polarizability of the molecule.

## LIPOPHILICITY

Tabernaemontanine's lipophilicity was predicted using multiple models, yielding the following values:

- Log P<sub>ow</sub> (iLOGP): 2.79
- XLOGP3: 3.27
- WLOGP: 2.66

- MLOGP: 2.13
- SILICOS-IT: 3.30
- Consensus Log P<sub>o/w</sub>: 2.83

The consensus Log P<sub>o/w</sub> value of 2.83 suggests moderate lipophilicity, which indicates the compound's potential to traverse lipid membranes effectively while maintaining some aqueous solubility. This balance is desirable for oral absorption and systemic distribution.

## **WATER SOLUBILITY**

Water solubility predictions classify Tabernaemontanine as moderately soluble:

- Log S (ESOL): -4.16 → 2.48e-02 mg/mL
- Log S (Ali): -4.25 → 1.97e-02 mg/mL
- Log S (SILICOS-IT): -5.02 → 3.40e-03 mg/mL

Moderate solubility indicates that Tabernaemontanine may require formulation enhancements for optimized dissolution and bioavailability, particularly in oral dosage forms.

## **PHARMACOKINETICS**

- Gastrointestinal (GI) Absorption: High, indicating favorable absorption upon oral administration.
- Blood-Brain Barrier (BBB) Permeability: Yes, suggesting that the compound can cross into the central nervous system (CNS) and may have CNS-related effects or activity.
- P-glycoprotein (P-gp) Substrate: Yes, implying that efflux mechanisms could limit intracellular concentration in some tissues.
- Cytochrome P450 (CYP) Enzyme Inhibition:
  - CYP1A2: Inhibitor
  - CYP2C19, CYP2C9, CYP2D6, CYP3A4: Not inhibitors
 This limited CYP inhibition profile reduces the risk of drug-drug interactions, a positive attribute for potential therapeutic development.
- Skin Permeability (Log K<sub>p</sub>): -6.14 cm/s, indicating low transdermal absorption.

## **DRUG-LIKENESS**

Tabernaemontanine satisfies all major drug-likeness filters:

- Lipinski's Rule of Five: No violations
- Ghose, Veber, Egan, Muegge rules: All passed
- Bioavailability Score: 0.55, suggesting a moderate probability of achieving ≥10% oral bioavailability in rats

## MEDICINAL CHEMISTRY FRIENDLINESS

- PAINS (Pan-Assay INterference Compounds): 0 alerts – low likelihood of assay interference.
- Brenk Alerts: 0 – indicating low concern for structural toxicity.
- Leadlikeness: 1 violation (MW > 350), which may slightly reduce its score as a lead compound but does not exclude it from drug candidacy.
- Synthetic Accessibility: 4.71 (scale: 1 = easy, 10 = difficult), suggesting moderate complexity for chemical synthesis.

Because of its positive pharmacokinetics and drug-likeness, Tabernaemontanine may be an ideal candidate for oral drug development. It shows it is well absorbed in the intestine and passes through the blood-brain barrier, so it may have activity in the body and in the brain. Since the compound does not inhibit major CYP450 enzymes, it is less likely to interact with other medicines. The drug's right amount of lipophilicity and suitable solubility makes it possible for it to cross through the membrane well and be used in the body. According to standard criteria, Tabernaemontanine meets with all expectations due to its Lipinski value, lack of PAINS or Brenk alerts and moderate synthetic accessibility. Its molecular weight results in a lead-like violation, yet this does not bar it from being considered as a prospective drug. Tabernaemontanine appears promising and deserves more attention in drug discovery.

## BOILED-EGG MODEL ANALYSIS OF TABERNAEMONTANINE

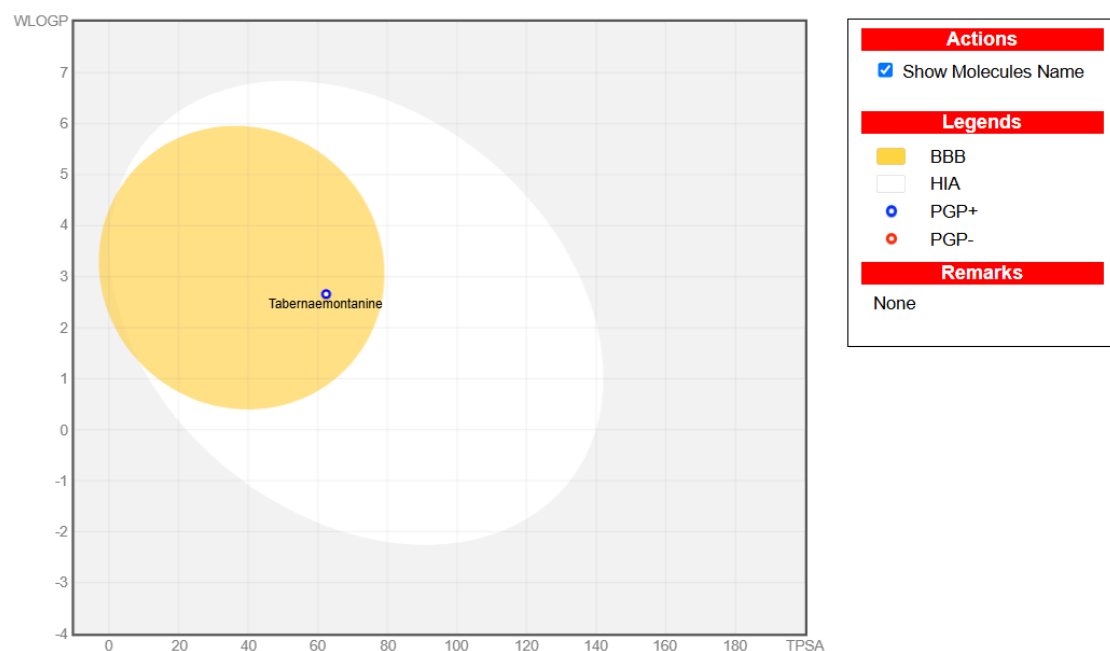


Fig 4.18 – Boiled Egg plot of Tabernaemontanine

- Tabernaemontanine is located well within both the white (HIA) and yellow (BBB) regions, confirming that it is likely to be well-absorbed in the human gut and has high potential to cross the blood-brain barrier.
- Its WLOGP ( $\sim 3$ ) and TPSA ( $\sim 63 \text{ \AA}^2$ ) values fall within optimal ranges for both oral bioavailability and central nervous system (CNS) accessibility.
- The blue ring around the marker confirms it is PGP-negative, further supporting its permeability and retention in target tissues.

The constructed model agrees with previous ADME studies of Tabernaemontanine, confirming it is highly bioavailable orally and has a good likelihood of reaching the CNS. These characteristics make it a suitable candidate for therapeutic applications targeting both systemic and neurological conditions.

#### 4.3.4 MOLECULAR DYNAMICS (MD) SIMULATION RESULTS

##### PROTEIN AND LIGAND STABILITY: RMSD AND RMSF

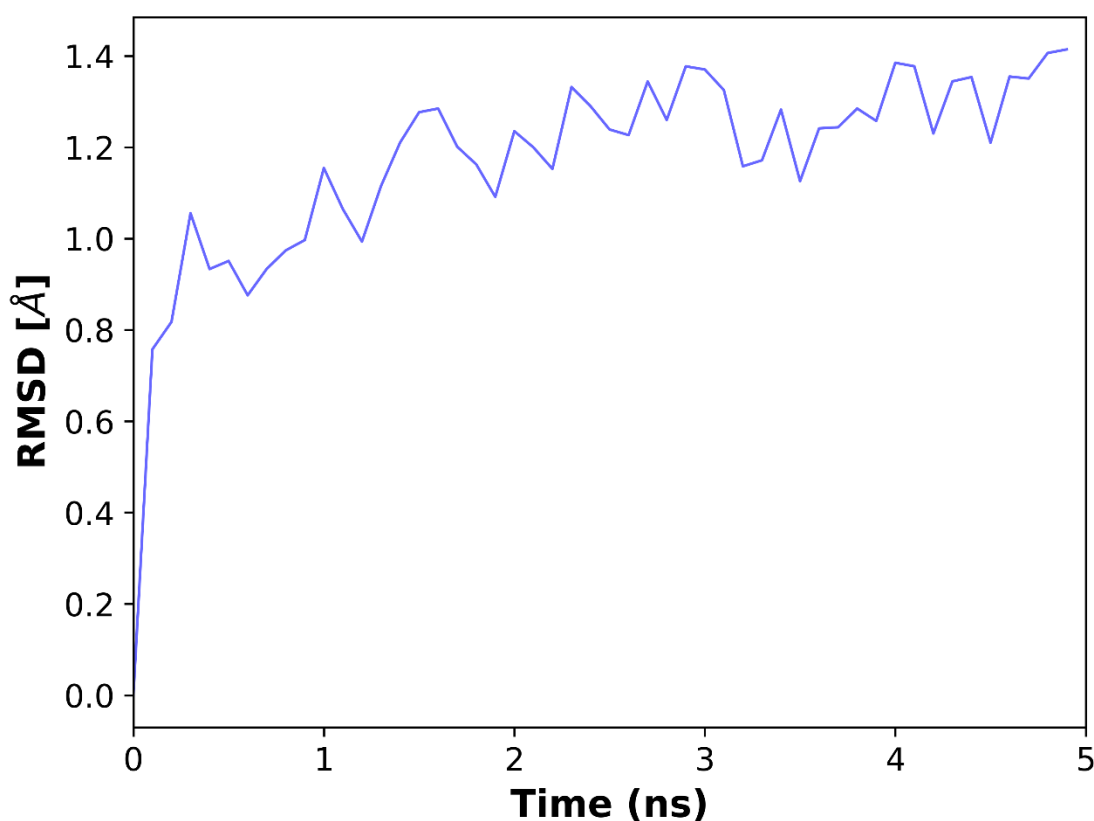


Fig 4.19 – RMSD of Protein Backbone Atoms Over Time

Here, RMSD shows the average variation of the  $C\alpha$  atoms in the structure, compared to the original minimized configuration. The RMSD spikes up to around  $1.0 \text{ \AA}$  within the first nanosecond and then levels off to a range between  $1.0$  and  $1.4 \text{ \AA}$ . This suggests that the system

undergoes initial relaxation before settling into a dynamically stable conformation. Because the RMSD remained consistent, Tabernaemontanine does not cause the protein to destabilize and no significant changes happened to its structure.

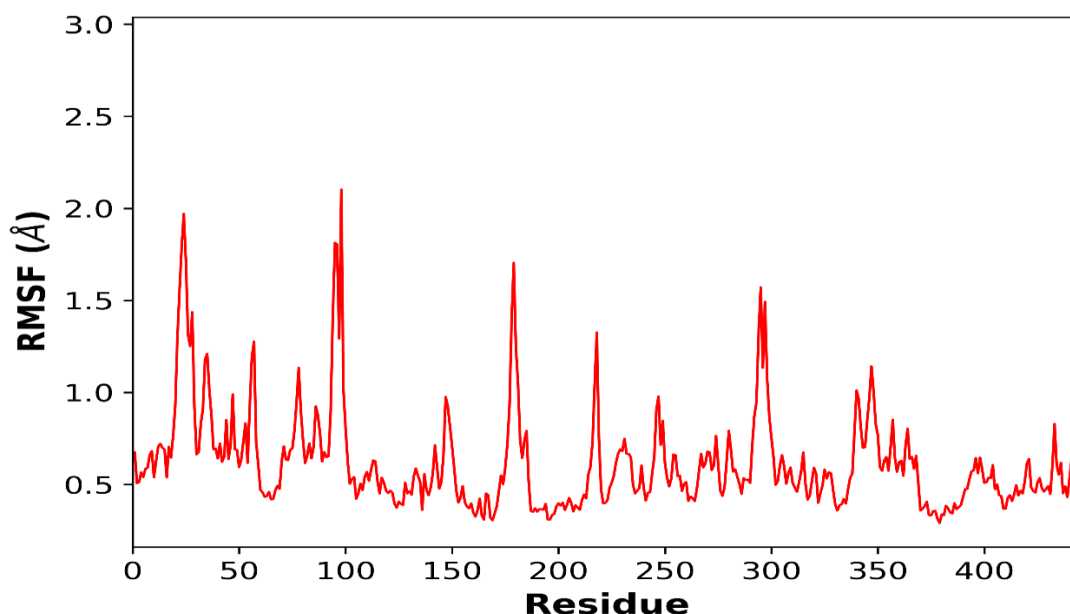


Fig 4.20 – RMSF of Protein Residues

The Root Mean Square Fluctuation (RMSF) plots show how much each residue moves during a simulation. Virtually majority of the residues show variations less than 1.0 Å which means the structure is stiff. The key binding residues continue to be stable with RMSF less than 0.5 Å which aligns well with a stable binding pocket. Some dynamic and surface-facing regions like loop or terminal ones are represented by several regions that move more than 2 Å.

## CONFORMATIONAL CONSISTENCY: 2D RMSD MATRIX

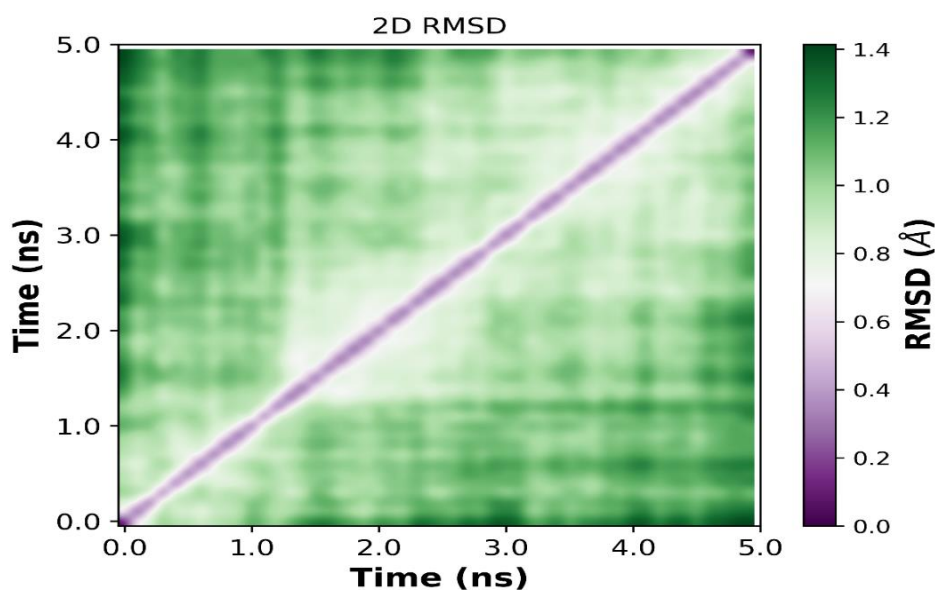


Fig 4.21 – 2D RMSD Heatmap

The 2D RMSD matrix shows how similar each pair of trajectory frames is to each other. This main diagonal line makes clear that the structure changed gradually and constantly over time. Regions with minimal non-diagonal high-RMSD values suggest little change over time and no sudden structural differences. Thus, Tabernaemontanine does not cause fundamental changes in the structure of the protein while binding.

## INTERACTION ENERGY ANALYSIS

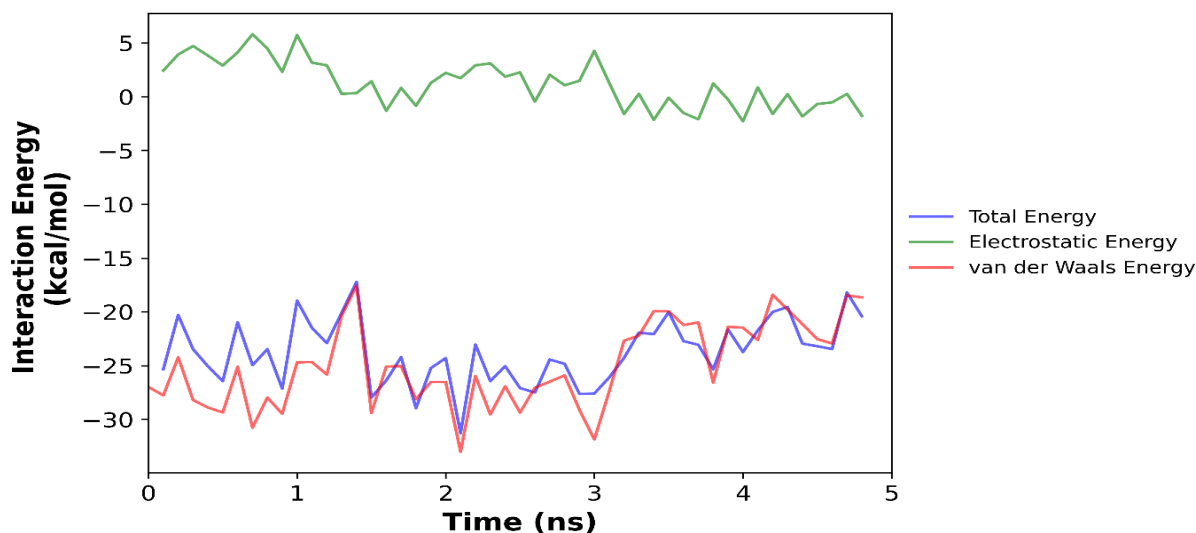


Fig 4.22 – Protein–Ligand Interaction Energy

This plot breaks down the non-bonded interaction energies into:

- **Total Interaction Energy (blue):** Ranges from  $-32$  to  $-18$  kcal/mol, indicating consistently favorable binding with moderate fluctuations over the 5 ns simulation.
- **Electrostatic Energy (green):** Remains mostly positive ( $0$  to  $+6$  kcal/mol), suggesting an unfavourable electrostatic contribution to the interaction.
- **van der Waals Energy (red):** Dominates the interaction profile, fluctuating between  $-32$  to  $-18$  kcal/mol, and closely tracking with the total energy, reinforcing its role as the primary stabilizing force.

## STRUCTURAL COMPACTNESS

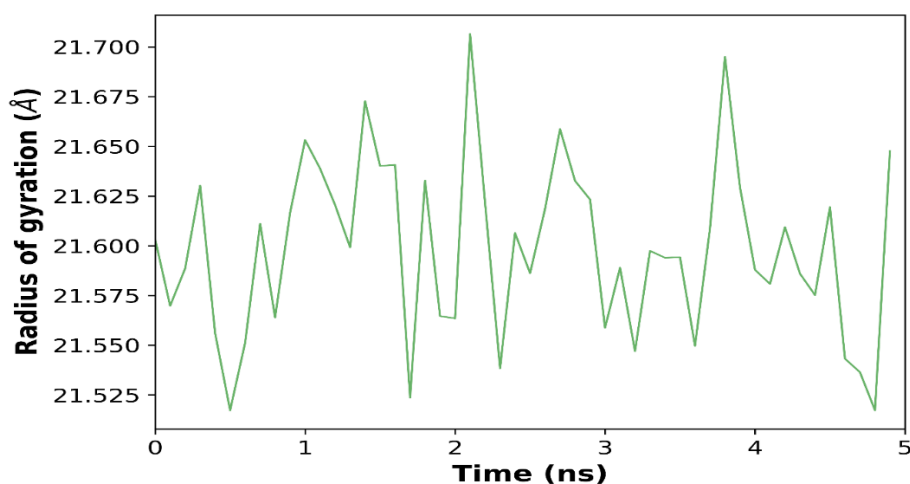


Fig 4.23 – Radius of Gyration (Rg)

R<sub>g</sub> values fluctuate slightly between ~21.52 Å and ~21.70 Å throughout the simulation. These fluctuations are minor (~0.18 Å range) and do not indicate any significant unfolding or expansion. The overall trend appears stable with no progressive increase or decrease, suggesting that the global structure of the protein remains compact and well-folded during the 5 ns run. The protein retains its structural integrity throughout the simulation, indicating no significant conformational instability upon binding with the ligand.

## CONFORMATIONAL FLEXIBILITY AND PRINCIPAL MOTIONS

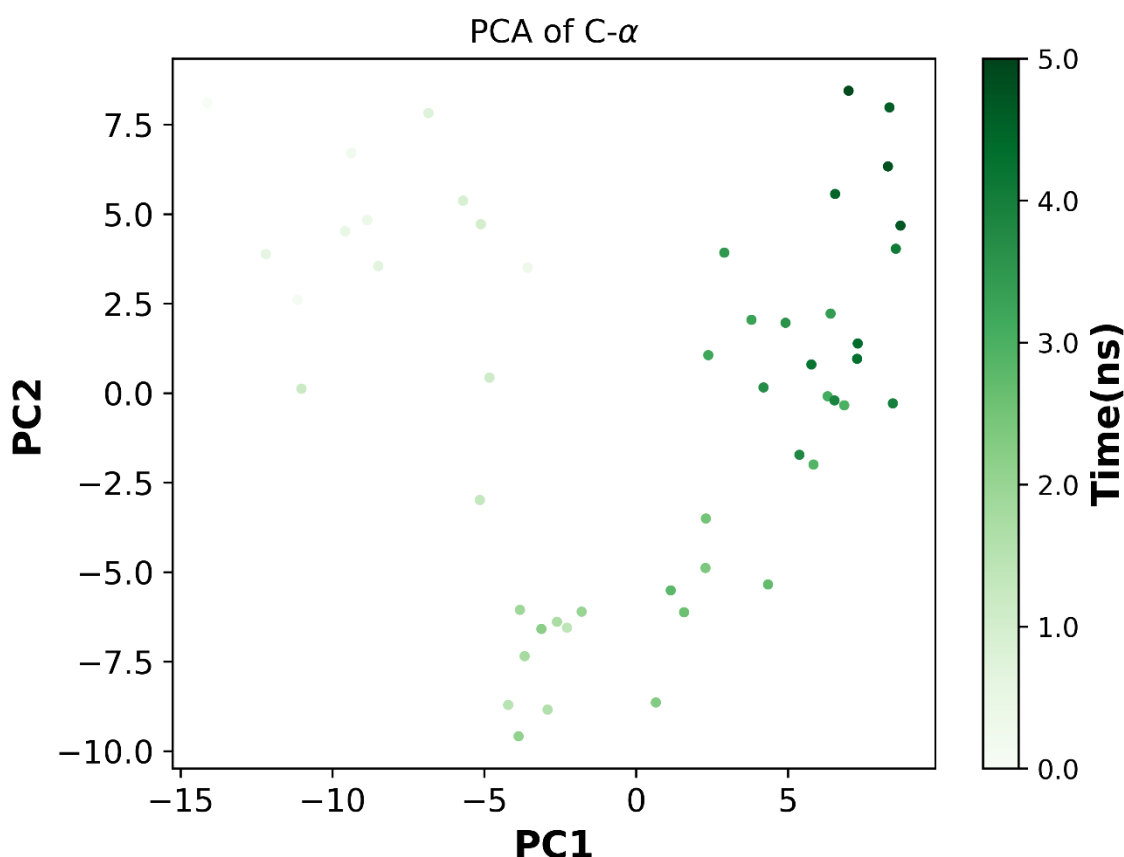


Fig 4.24 – Principal Component Analysis (PCA)

PCA plot demonstrates how the C $\alpha$  atoms of tyrosinase and Tabernaemontanine change shape throughout a 5 ns simulation. As time increases along PC1 with a darkening green gradient, it is clear the protein is experiencing a gradual and unbroken structural change. As a result, the protein takes on several structural forms throughout the simulation, probably affected by the ligand. Even though points are not closely packed, the system's motion remains contained to a defined conformation range, meaning it behaves in a flexible yet steady manner.

Thus, the 5 ns MD simulation of the Tabernaemontanine–tyrosinase complex indicates that the ligand stays secure in the active site through stable attractions, mainly van der Waals forces. The structure of the protein is stable and tightly compact and there is little flexibility in its important binding sites. PCA and 2D RMSD data affirm that there are no major shifts in the protein structure, suggesting the ligand engages the protein in a strong manner. From these outcomes, it appears that Tabernaemontanine may help regulate tyrosinase. This should encourage research into Tabernaemontanine's applications for modulating melanin production and treating vitiligo.



## 4.4 DREGAMINE

### 4.4.1 DOCKING RESULTS

Dregamine's best binding energy was **-8.69 kcal/mol**, with tight clustering and minimal pose deviation.

**Estimated Free Energy of Binding = -8.69 kcal/mol [= (1) +(2) +(3)-(4)]**

(1) Final Intermolecular Energy = -9.58 kcal/mol

vdW + Hbond + desolv Energy = -9.58 kcal/mol

Electrostatic Energy = +0.00 kcal/mol

(2) Final Total Internal Energy = -1.20 kcal/mol

(3) Torsional Free Energy = +0.89 kcal/mol

(4) Unbound System's Energy [= (2)] = -1.20 kcal/mol

**Estimated Inhibition Constant,  $K_i$  = 428.69 nM (nanomolar) [Temperature = 298.15 K]**

Table 4.5: RMSD Summary for Dregamine

Rank	Sub-Rank	Run	Binding Energy (kcal/mol)	Cluster RMSD (Å)	Reference RMSD (Å)	Inhibition Constant ( $K_i$ )
1	1	1	-8.69	0.00	224.18	428.69 nM
2	1	2	-8.46	0.00	225.66	630.95 nM
2	2	6	-8.42	0.08	225.64	676.63 nM
3	1	4	-7.90	0.00	222.96	1.62 uM
3	2	10	-7.85	0.39	223.01	1.77 uM
3	3	9	-7.75	0.49	222.99	2.10 uM
3	4	5	-7.74	0.68	223.04	2.14 uM
3	5	3	-7.65	1.02	222.94	2.49 uM
4	1	7	-7.48	0.00	224.72	3.29 uM
5	1	8	-7.29	0.00	222.88	4.54 uM

#### 4.4.2 BINDING SITE INTERACTIONS

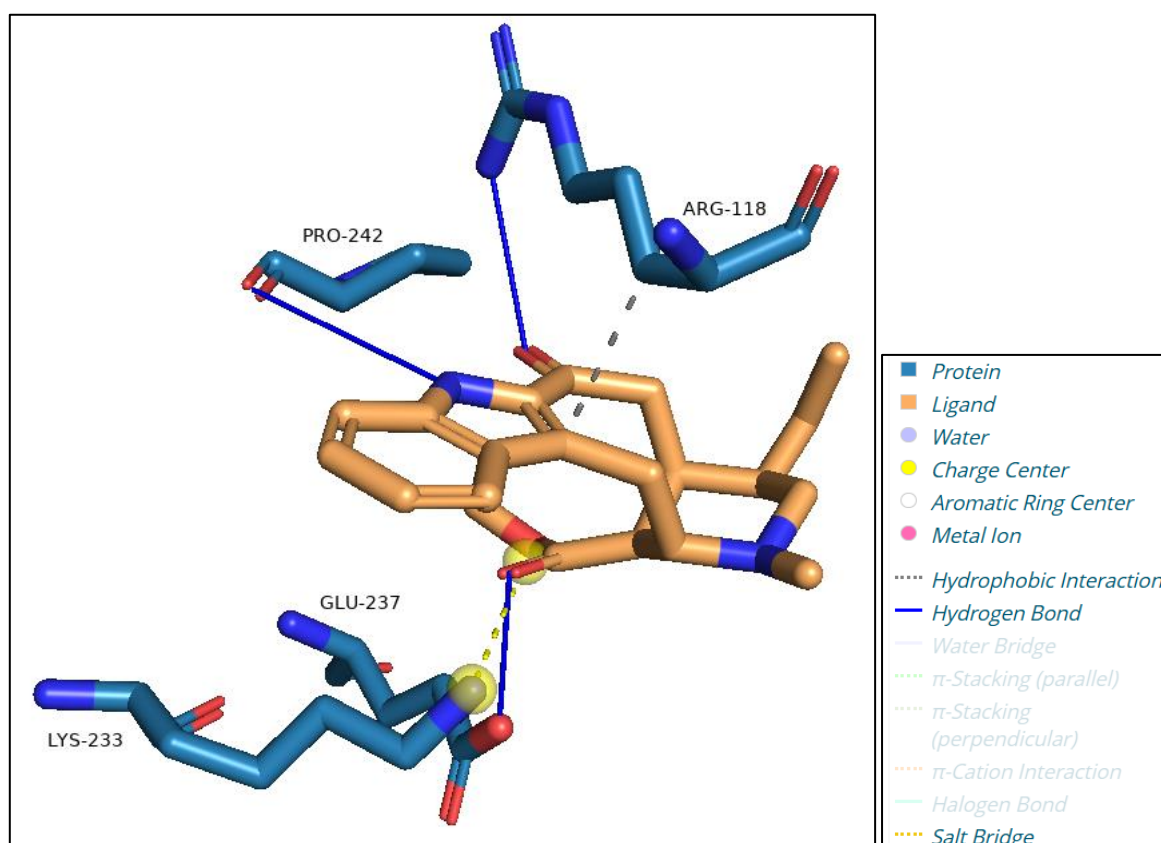


Fig 4.25 – Visualization of Binding interactions between Tyrosinase and Dregamine

3D docking analysis of Dregamine with Tyrosinase illustrates that the molecule is positioned strongly and correctly in the active site. The orange ligand sinks down into the binding pocket and is anchored by a number of significant interactions with various amino acids around it.

Hydrogen bonding and electrostatic interactions are prominently observed:

- Arg118 forms a stabilizing hydrogen bond with a carbonyl oxygen of Dregamine, contributing significantly to the orientation of the ligand through electrostatic attraction.
- Pro242 and Lys233 are involved in additional hydrogen bonding interactions with other polar groups of Dregamine, suggesting a snug fit in the active site.
- Glu237 forms a salt bridge or polar interaction with a protonated nitrogen on Dregamine. This interaction appears particularly important as it occurs near the catalytic copper center (highlighted by the yellow sphere), indicating that Dregamine may be interacting directly or indirectly with the catalytic machinery of Tyrosinase.
- The orientation of the ligand also facilitates  $\pi$ – $\pi$  stacking and hydrophobic interactions with surrounding residues (not shown in this diagram but inferred from the aromatic system present in Dregamine), further contributing to binding affinity.

The overall interactions between Dregamine and Tyrosinase suggest it may regulate the functioning of Tyrosinase. The binding pose brings the ligand close to Arg118 and Glu237, two important amino acids that are known to take part in identifying and transforming substrates. Because of this, Dregamine may improve the activity of tyrosinase and, as a result, promote melanin production in conditions such as vitiligo.

▼ Hydrophobic Interactions \*\*\*\*\*

Index	Residue	AA	Distance	Ligand Atom	Protein Atom
1	118C	ARG	3.23	17463	9620

▼ Hydrogen Bonds —

Index	Residue	AA	Distance H-A	Distance D-A	Donor Angle	Protein donor?	Side chain	Donor Atom	Acceptor Atom
1	118C	ARG	2.32	3.34	157.66	✓	✓	9625 [Ng+]	17453 [O2]
2	237C	GLU	2.00	2.85	151.56	✓	✓	10847 [O3]	17474 [O2]
3	242C	PRO	3.15	4.08	154.75	✗	✗	17455 [Npl]	10892 [O2]

▼ Salt Bridges \*\*\*\*\*

Index	Residue	AA	Distance	Protein positive?	Ligand Group	Ligand Atoms
1	233C	LYS	3.98	✓	Carboxylate	17474, 17476

Fig 4.26 – Binding site interactions of Tyrosinase-Dregamine complex

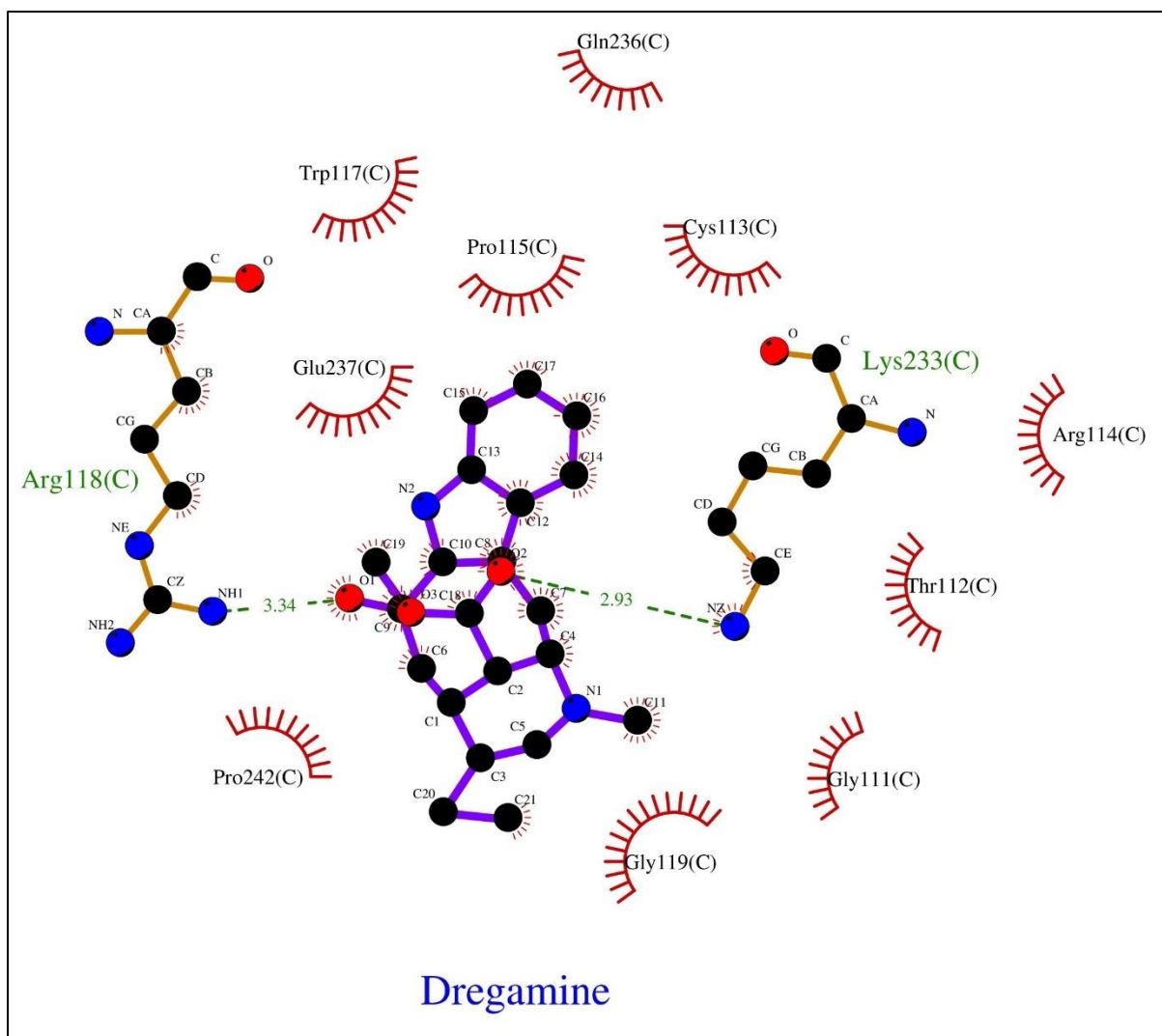


Fig 4.27 – 2D interaction diagram of binding interactions of Tyrosinase and Dregamine by LigPlot

The diagram created via LigPlot shows how Dregamine bonds to the active site of Tyrosinase, making it easy to spot the main binding domains and interactions.

Two significant hydrogen bonds (green dashed lines) are observed:

- A hydrogen bond is formed between the oxygen atom (O3) of Dregamine and the side chain of Arg118(C) at a distance of 3.34 Å, which helps anchor the ligand within the binding cavity.
- Another hydrogen bond is established between the same oxygen atom (O3) of Dregamine and Lys233(C) at a distance of 2.93 Å, further contributing to the ligand's stability and correct orientation in the active pocket.

Surrounding these hydrogen bonds are numerous hydrophobic interactions (represented by red half-sun symbols), which enhance van der Waals contacts and improve binding affinity. Key hydrophobic contacts involve:

- Glu237(C), Pro115(C), Pro242(C), Trp117(C), Cys113(C), Gln236(C), Arg114(C), Thr112(C), Gly111(C), and Gly119(C), forming a hydrophobic shell around the ligand, stabilizing its position through non-covalent interactions.

The positioning of Dregamine within the active site shows that it engages with both polar and nonpolar residues, suggesting a mixed mode of interaction. The dual hydrogen bonding and extensive hydrophobic contacts likely contribute to a strong binding affinity between Dregamine and Tyrosinase. Arg118, Glu237 and Lys233 being significant interacting residues lines up with known Tyrosinase regions which suggests Dregamine supports the theory that it modulates functions of Tyrosinase and may be useful in managing vitiligo through melanin synthesis.

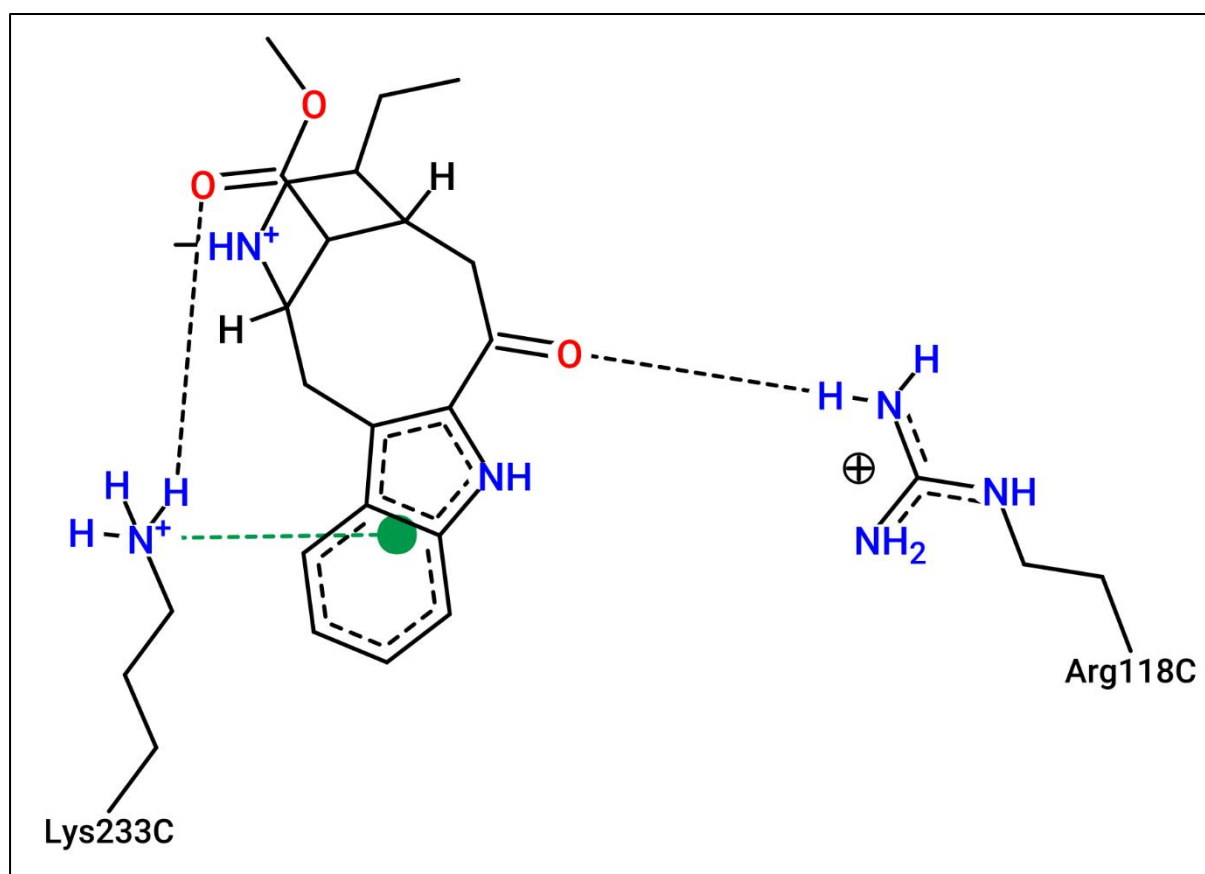


Fig 4.28 – 2D interaction diagram of Tyrosinase-Dregamine by ProteinPlus server

The molecular interaction diagram generated by ProteinPlus depicts the key binding interactions between Dregamine, a natural alkaloid, and the active site of Tyrosinase, a copper-containing enzyme central to melanogenesis.

The interaction map reveals multiple hydrogen bonding interactions (represented by black dashed lines), which stabilize Dregamine within the active site:

- One significant hydrogen bond is observed between a carbonyl oxygen of Dregamine and the guanidinium group of Arg118C, an interaction crucial for ligand anchoring in the catalytic region.

- Another strong hydrogen bond forms between the amide nitrogen of Dregamine and the amino group of Lys233C, reinforcing the ligand's orientation and improving its binding strength.

Additionally,  $\pi$ -cation interaction (depicted by a green dashed line and a green dot) occurs between the aromatic indole ring of Dregamine and the positively charged side chain of Lys233C. This non-covalent electrostatic interaction further stabilizes the ligand and is often indicative of favorable pharmacological activity. With these interactions keeping Dregamine in its position, it appears the drug is located in an important catalytic region of the enzyme. Arg118C and Lys233C are deemed important for Tyrosinase's structure and working which further supports the possibility that Dregamine can serve as a useful modulator. These results suggest that Dregamine attaches tightly and specifically to Tyrosinase which supports its potential in treating vitiligo by stimulating the production of melanin.

#### 4.4.3 ADME ANALYSIS

Table 4.6: ADME Profile of Dregamine

Parameter	Result
Molecular Formula	C <sub>21</sub> H <sub>26</sub> N <sub>2</sub> O <sub>3</sub>
Molecular Weight	354.44 g/mol
TPSA	62.40 Å <sup>2</sup>
Log P (Consensus)	2.82
Water Solubility	Moderately soluble
GI Absorption	High
BBB Permeability	Yes
P-gp Substrate	Yes
CYP Inhibition	Inhibits CYP2D6 and CYP3A4
Lipinski Rule	Yes (0 violations)
Bioavailability Score	0.55
Leadlikeness	No (MW > 350)
PAINS Alerts	0
Synthetic Accessibility	4.71

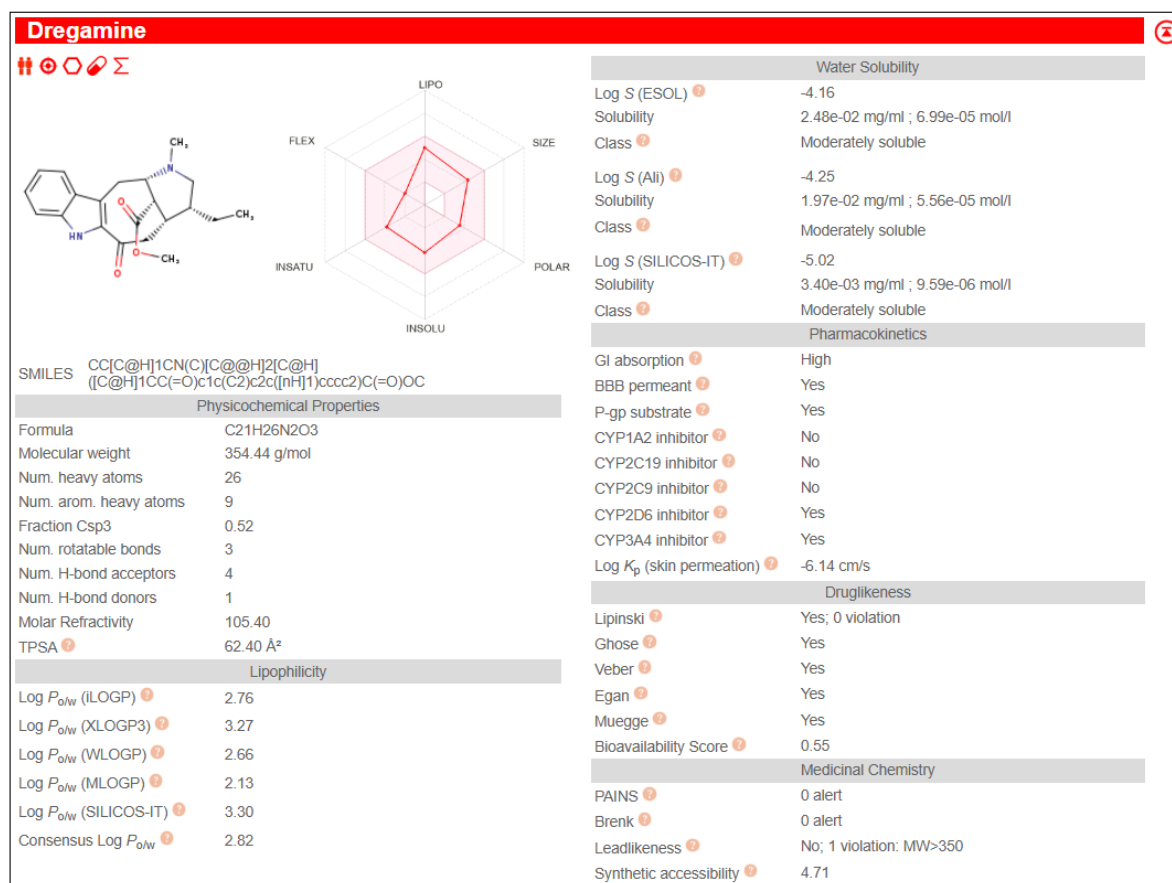


Fig 4.29 – Predicted ADME properties of Dregamine by SwissADME

## PHYSICOCHEMICAL PROPERTIES

Dregamine has a molecular formula of C<sub>21</sub>H<sub>26</sub>N<sub>2</sub>O<sub>3</sub> and a molecular weight of 354.44 g/mol, slightly exceeding the 350 Da guideline used in lead-likeness evaluation. It contains 26 heavy atoms, with 9 aromatic heavy atoms, suggesting a significant degree of aromaticity. The Topological Polar Surface Area (TPSA) is 62.40 Å<sup>2</sup>, which is within the ideal range (<140 Å<sup>2</sup>) for good intestinal absorption and blood-brain barrier (BBB) permeability.

It has:

- 3 rotatable bonds – suggesting moderate molecular flexibility.
- 4 hydrogen bond acceptors and 1 donor – values well within drug-like boundaries.
- A Fraction Csp<sup>3</sup> of 0.52, indicating a balanced mix of sp<sup>3</sup> hybridized carbons, which can improve solubility and metabolic stability.

## **LIPOPHILICITY**

Dregamine's lipophilicity is reflected in its Consensus Log P<sub>ow</sub> of 2.82, which lies comfortably within the acceptable range (1–3). This suggests good membrane permeability and oral bioavailability.

- Log P<sub>ow</sub> values across different models (iLOGP, XLOGP3, WLOGP, MLOGP, SILICOS-IT) range from 2.13 to 3.30, showing consistent moderate lipophilicity.

## **WATER SOLUBILITY**

Dregamine is classified as moderately soluble across multiple prediction models:

- Log S (ESOL): -4.16 ( $\approx 2.48 \times 10^{-2}$  mg/mL)
- Log S (Ali): -4.25
- Log S (SILICOS-IT): -5.02

This level of solubility is considered acceptable but may require optimization for better formulation in aqueous environments.

## **PHARMACOKINETICS**

- GI Absorption: High – suggesting good oral bioavailability.
- BBB Permeant: Yes – capable of crossing the blood-brain barrier.
- P-gp Substrate: Yes – indicates that the molecule may be effluxed by P-glycoprotein, which could reduce intracellular drug concentration.

### **Cytochrome P450 Inhibition Profile:**

- Inhibits CYP2D6 and CYP3A4, which may cause drug-drug interactions.
- Does not inhibit CYP1A2, CYP2C19, or CYP2C9, reducing risks with these metabolic pathways.

**Skin Permeation (Log K<sub>p</sub>):** -6.14 cm/s, a typical value for molecules that are not designed for transdermal delivery.

## **DRUG-LIKENESS**

Dregamine satisfies most classical drug-likeness rules:

- Lipinski's Rule of Five: Passed (0 violations)
- Ghose, Veber, Egan, and Muegge filters: All passed
- Bioavailability Score: 0.55 – indicates moderate bioavailability.



Leadlikeness: Failed due to one violation – molecular weight > 350 Da, which could be optimized in future analogs or derivatives.

## **MEDICINAL CHEMISTRY ALERTS**

- PAINS (Pan-Assay Interference Compounds): 0 alerts – unlikely to show assay interference.
- Brenk Alerts: 0 – no problematic substructures.
- Synthetic Accessibility (SA) Score: 4.71 – indicates moderate synthetic feasibility; not overly complex.

It was found that Dregamine performs well in ADME, has a high level of absorption in the gut, can cross the blood-brain barrier and has moderate solubility, indicating it is suitable for oral treatments aimed at the CNS. While it is a P-gp substrate and a CYP3A4/CYP2D6 inhibitor, suggesting potential for drug interactions, these concerns can be mitigated through structural optimization. While Dregamine's molecular weight is above the rule for lead-type compounds, it matches a number of drug-likeness criteria and is free of PAINS and Brenk alerts, indicating it is worth looking into further as a drug candidate.

## **BOILED-EGG MODEL ANALYSIS OF DREGAMINE**

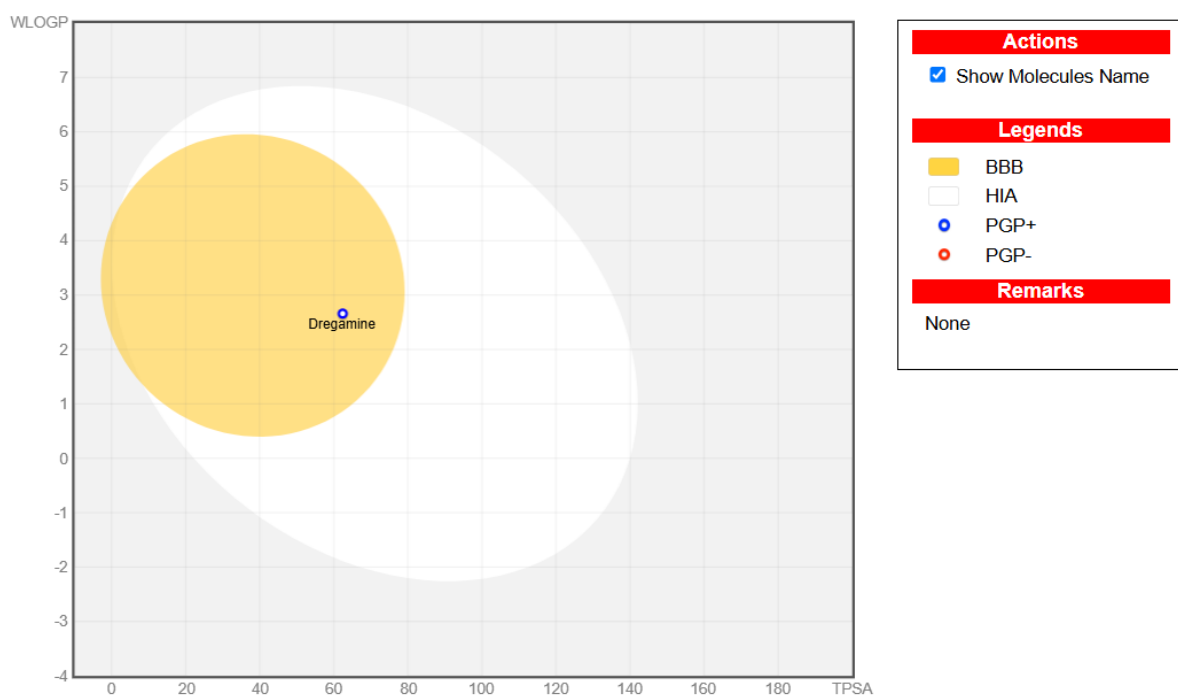


Fig 4.30 – Boiled-egg plot of Dregamine

- Dregamine is located inside the yellow region, indicating high likelihood of blood-brain barrier (BBB) penetration.

- White region: This also overlaps with the Human Intestinal Absorption (HIA) zone, confirming good oral bioavailability.
- The molecule is marked with a blue circle, denoting that it is a P-glycoprotein substrate (PGP+), which may affect drug efflux and distribution.

These findings are consistent with the pharmacokinetics data, which indicated that Dregamine has high GI absorption, is BBB permeant, and is a P-gp substrate.

#### 4.4.4 MOLECULAR DYNAMICS (MD) SIMULATION RESULTS

##### PROTEIN AND LIGAND STABILITY: RMSD AND RMSF

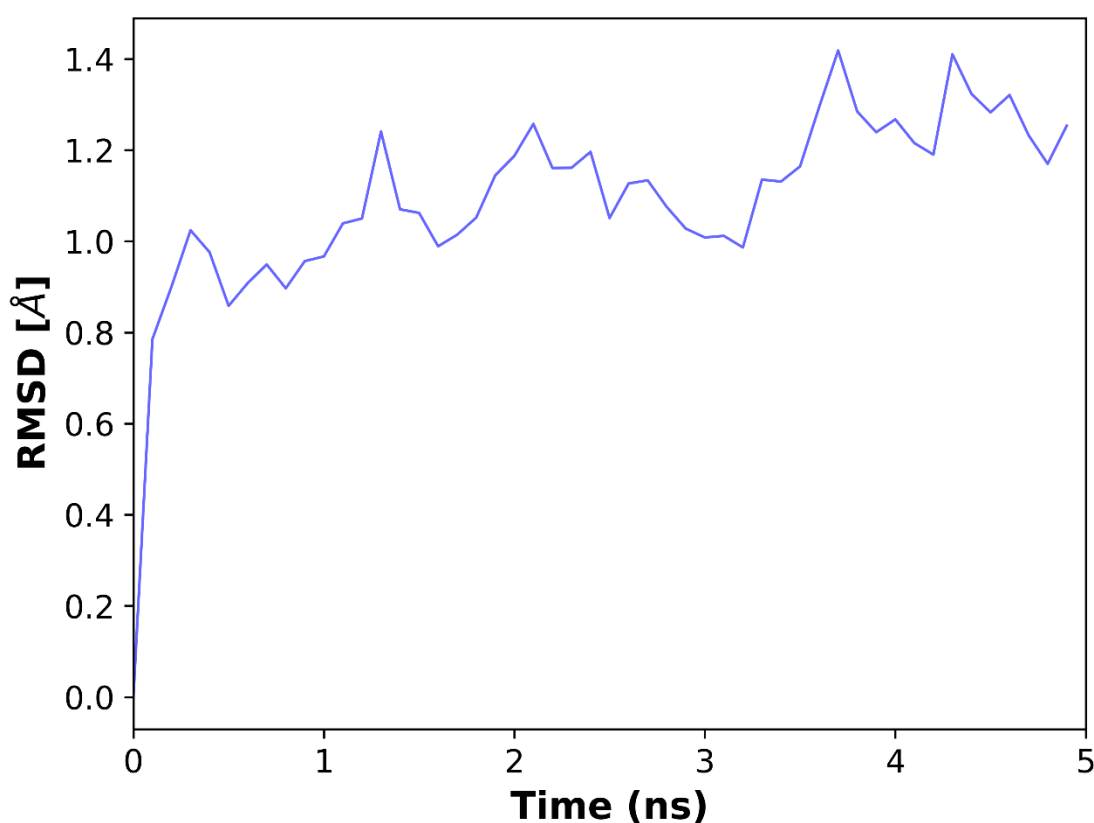


Figure 4.31 – RMSD of Protein Backbone Atoms Over Time

The figure shows the RMSD values for the protein backbone C $\alpha$  atoms against the minimized starting structure. In the first nanosecond, the RMSD rises swiftly to 1.4 Å and then becomes much more stable, staying in the area of 1.2–1.5 Å. The data suggest a period of equilibration, followed by stability in the system. No big fluctuations in RMSD indicate that Dregamine does not weaken the structure of tyrosinase and keeps it stable through the simulation.

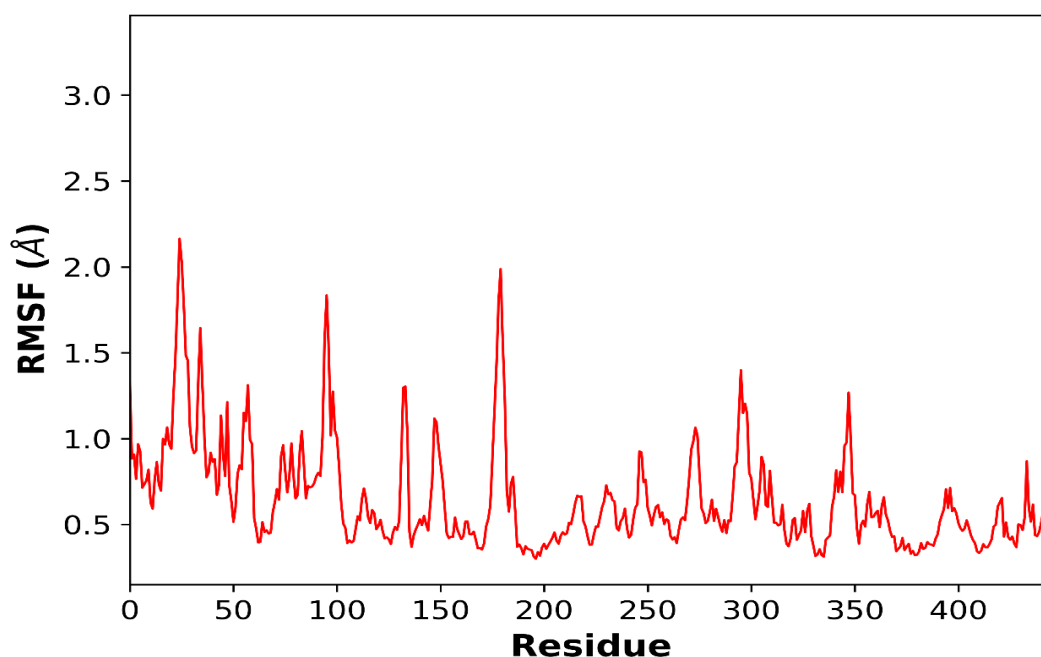


Figure 4.32: RMSF of Protein Residues

The RMSF measure allows us to display the degree of movement for each specific residue over the course of the simulation. Most of the residues show an RMSF of less than 1.0 Å, reflecting an inflexible and steady protein configuration. Majority of key active residues have RMSF values less than 0.5 Å and so maintain a stable and intact binding location. When the fluctuations exceed 2.0 Å, these regions join the loop and ending points which can move freely and don't affect core binding.

## CONFORMATIONAL CONSISTENCY: 2D RMSD MATRIX

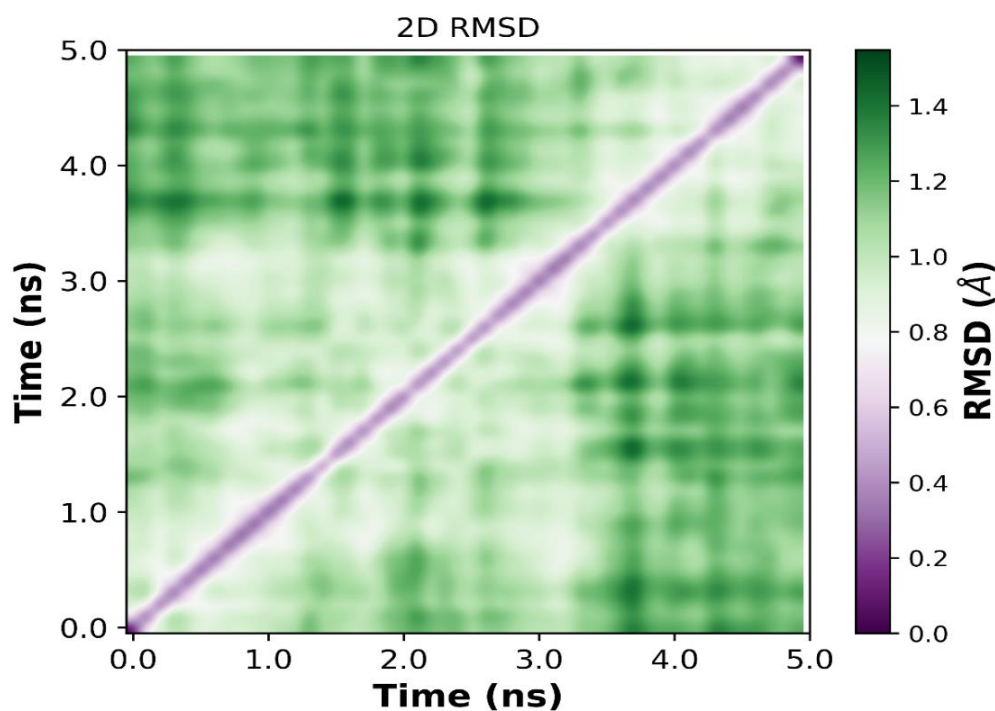


Figure 4.33: 2D RMSD Heatmap

The matrix of 2D RMSD values compares the shapes of all the available trajectory frames. The strong diagonal band demonstrates that the structure changes smoothly and gradually, without sudden shifts. Since the heat map is mostly even and the RMSD regions are small, this suggests that the Dregamine–tyrosinase complex is stable and does not change a lot in structure over the 5 ns simulation.

## INTERACTION ENERGY ANALYSIS

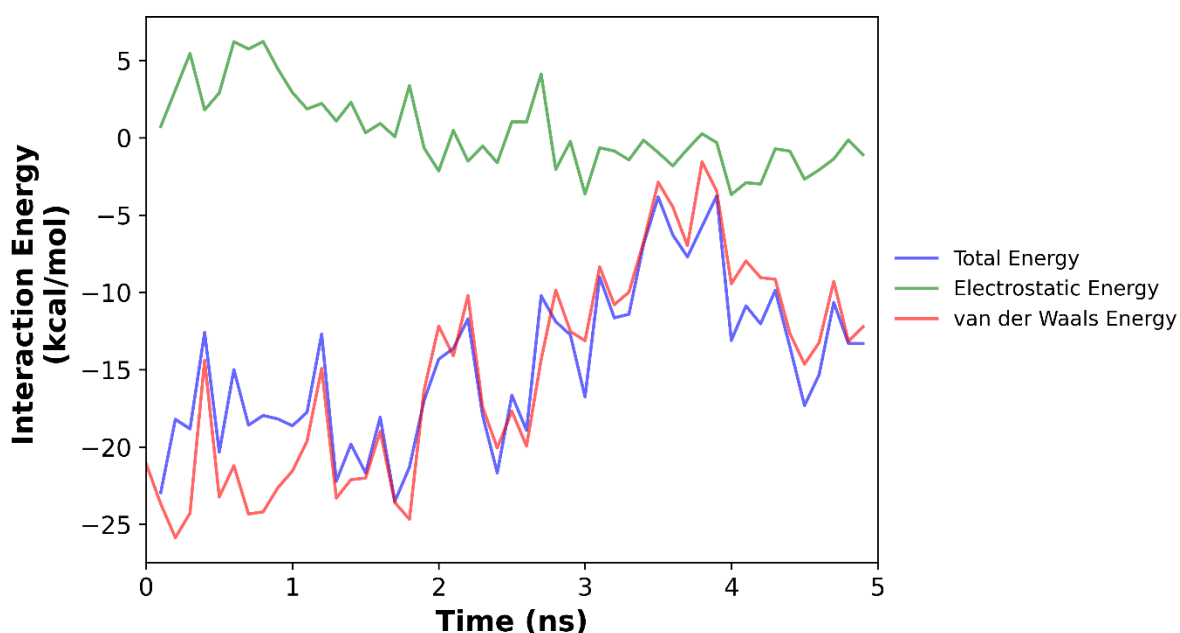


Figure 4.34: Protein–Ligand Interaction Energy

This figure breaks down the interaction energies between Dregamine and tyrosinase into:

- **Total Interaction Energy (blue):** Fluctuates between  $-26$  to  $-3$  kcal/mol, remaining negative throughout and indicating overall favorable but variable binding, with the weakest interaction occurring around 3.7 ns.
- **Electrostatic Energy (green):** Varies between  $+6$  to  $-3$  kcal/mol, showing minimal or even unfavourable contributions to binding for most of the simulation.
- **van der Waals Energy (red):** Closely mirrors the total energy and ranges from  $-26$  to  $-3$  kcal/mol, indicating that vdW interactions are the primary driving force behind complex stability.

The binding between Dregamine and Tyrosinase is primarily stabilized by van der Waals interactions, with minimal electrostatic contribution.

## STRUCTURAL COMPACTNESS

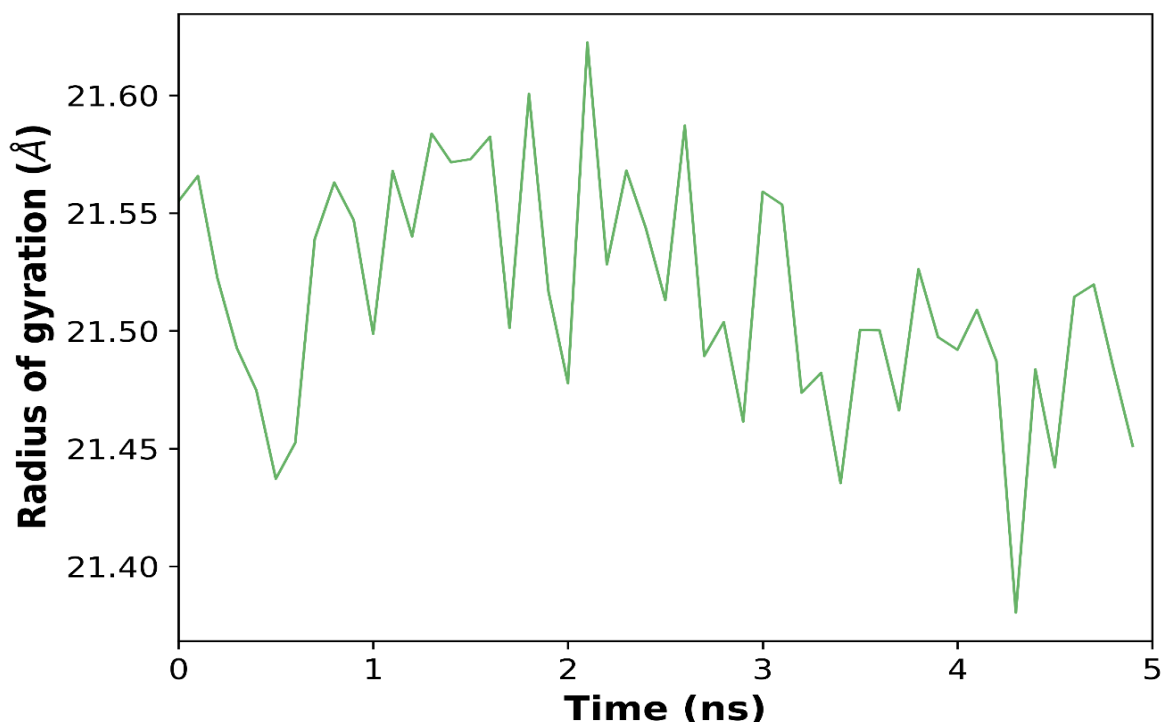


Figure 4.35: Radius of Gyration (Rg)

The Radius of Gyration plot measures the degree of compactness in a protein. The Rg values from the tyrosinase–Dregamine complex are very close together at 21.3 Å and 21.6 Å, revealing that the protein looks mostly unchanged. This stability proves that the protein retains its main structure, backed up by average RMSD and RMSF values.

Therefore, the results of the 5 ns MD simulation of Dregamine-tyrosinase demonstrate that their binding is both stable and advantageous from an energy point of view. The ligand is well fixed in the active site mostly due to its interactions with the van der Waals forces. The main protein structure does not change much and there is very little variation at the region where drugs bind. RMSD, Rg and RMSF results indicate the system remains structurally stable and there are no big deviations in the overall structure. All of these observations indicate that Dregamine stabilizes the tyrosinase protein without affecting its structure, supporting continued study of its suitability for melanin formation and treatment of vitiligo.

## 4.5 HERBOXIDIENE

### 4.5.1 DOCKING RESULTS

Herboxidiene had a high affinity with **-11.56 kcal/mol**, though later poses showed more flexibility.

**Estimated Free Energy of Binding = -11.56 kcal/mol [(1) +(2) +(3)-(4)]**

- (1) Final Intermolecular Energy = -15.44 kcal/mol  
vdW + Hbond + desolv Energy = -15.44 kcal/mol  
Electrostatic Energy = +0.00 kcal/mol  
(2) Final Total Internal Energy = -0.88 kcal/mol  
(3) Torsional Free Energy = +3.88 kcal/mol  
(4) Unbound System's Energy [= (2)] = -0.88 kcal/mol

**Estimated Inhibition Constant,  $K_i$  = 3.36 nM (nanomolar) [Temperature = 298.15 K]**

Table 4.7: RMSD Summary for Herboxidiene

Rank	Sub-Rank	Run	Binding Energy (kcal/mol)	Cluster RMSD	Reference RMSD	Inhibition Constant ( $K_i$ )
1	1	10	-11.56	0.00	222.77	3.36 nM
2	1	6	-10.20	0.00	220.94	33.33 nM
3	1	3	-7.71	0.00	226.03	2.23 uM
3	2	7	-7.20	1.79	226.56	5.28 uM
4	1	5	-7.08	0.00	221.88	6.52 uM
5	1	2	-6.89	0.00	228.80	8.86 uM
5	2	9	-6.00	1.63	228.88	39.76 uM
6	1	4	-6.56	0.00	226.08	15.50 uM
7	1	8	-5.65	0.00	226.68	71.71 uM
8	1	1	-3.40	0.00	222.04	3.24 mM

## 4.5.2 BINDING SITE INTERACTIONS

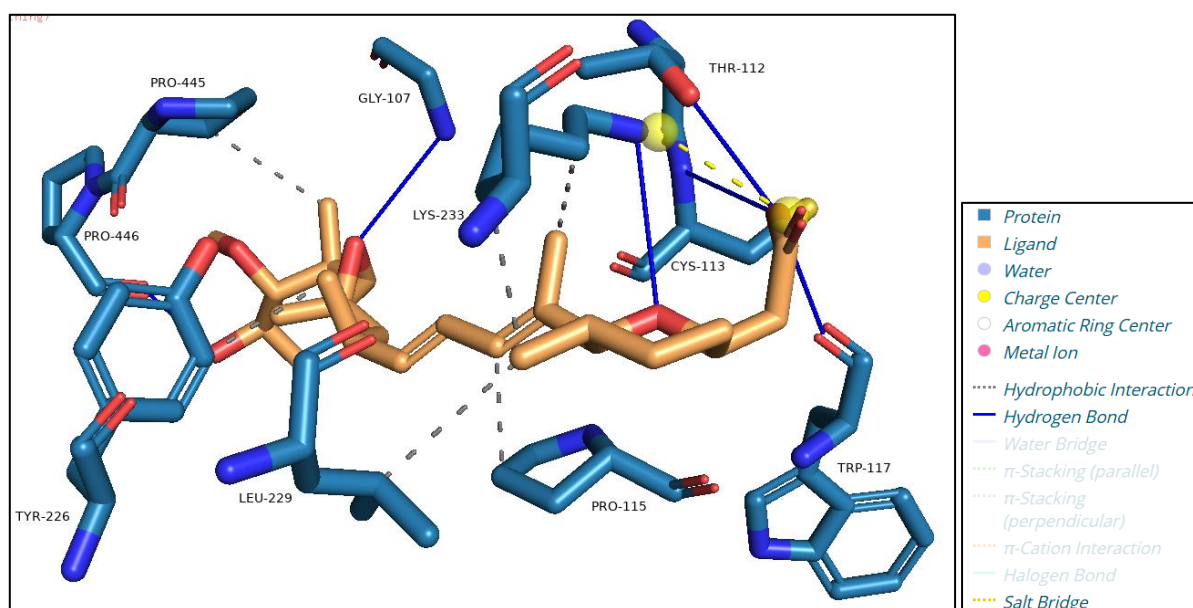


Fig 4.56 – Visualization of Binding interactions between Tyrosinase and Herboxidiene

3D docking visualization shows how the natural polyketide Herboxidiene and the main enzyme Tyrosinase for melanin interact. Six hydrogen bonds, a hydrophobic interaction and two polar contacts are found to stabilize Herboxidiene in the active site of Tyrosinase, indicating a strong attraction to the enzyme.

Several crucial interactions are observed:

- Hydrogen bonding is evident between Herboxidiene and the side chains of Lys233, Thr112, and Gly107, with the polar atoms of the ligand forming stable linkages that help secure it in the active site. These interactions are indicated by solid blue lines in the image.
- Particularly, the Thr112–Herboxidiene interaction is positioned near the Cys113 residue, which is part of the catalytic center of Tyrosinase, suggesting potential inhibitory or modulatory effects on enzyme activity.
- Additional  $\pi$ – $\pi$  stacking and hydrophobic interactions are seen with Tyr226, Leu229, and Trp117, which form part of the hydrophobic pocket surrounding the active site. These residues create a favorable non-polar environment that stabilizes the hydrophobic regions of Herboxidiene.
- The presence of Pro115, Pro445, and Pro446 may contribute to conformational rigidity in the active site region, which could aid in maintaining Herboxidiene's favorable binding orientation.

From the binding pose, it can be seen that Herboxidiene sits close to Tyrosinase and engages in both hydrophilic and hydrophobic connections with nearby residues. Since Herboxidiene is close to the important Cys113 and Thr112, it is predicted to play a role in modulating how

Tyrosinase functions and boost melanin production. It suggests that Herboxidiene has therapeutic possibilities for treating vitiligo.

▼ Hydrophobic Interactions .....

Index	Residue	AA	Distance	Ligand Atom	Protein Atom
1	115C	PRO	3.09	17456	9593
2	226C	TYR	3.80	17471	10723
3	229C	LEU	3.29	17464	10756
4	233C	LYS	3.35	17464	10800
5	233C	LYS	3.63	17457	10802
6	445C	PRO	3.96	17478	12849

▼ Hydrogen Bonds —

Index	Residue	AA	Distance H-A	Distance D-A	Donor Angle	Protein donor?	Side chain	Donor Atom	Acceptor Atom
1	107C	GLY	2.37	3.44	174.41	✓	✗	9514 [Nam]	17473 [O3]
2	112C	THR	2.98	3.37	102.54	✓	✓	9560 [O3]	17468 [O.co2]
3	113C	CYS	3.00	3.83	134.64	✓	✗	9564 [Nam]	17468 [O.co2]
4	117C	TRP	2.22	3.09	146.69	✗	✗	17468 [O.co2]	9603 [O2]
5	233C	LYS	2.72	3.76	164.15	✓	✓	10804 [N3+]	17458 [O3]
6	446C	PRO	2.01	2.93	156.71	✗	✗	17484 [O3]	12855 [O2]

▼ Salt Bridges .....

Index	Residue	AA	Distance	Protein positive?	Ligand Group	Ligand Atoms
1	233C	LYS	3.13	✓	Carboxylate	17466, 17468

Fig 4.57 – Binding site interactions of Tyrosinase and Herboxidiene



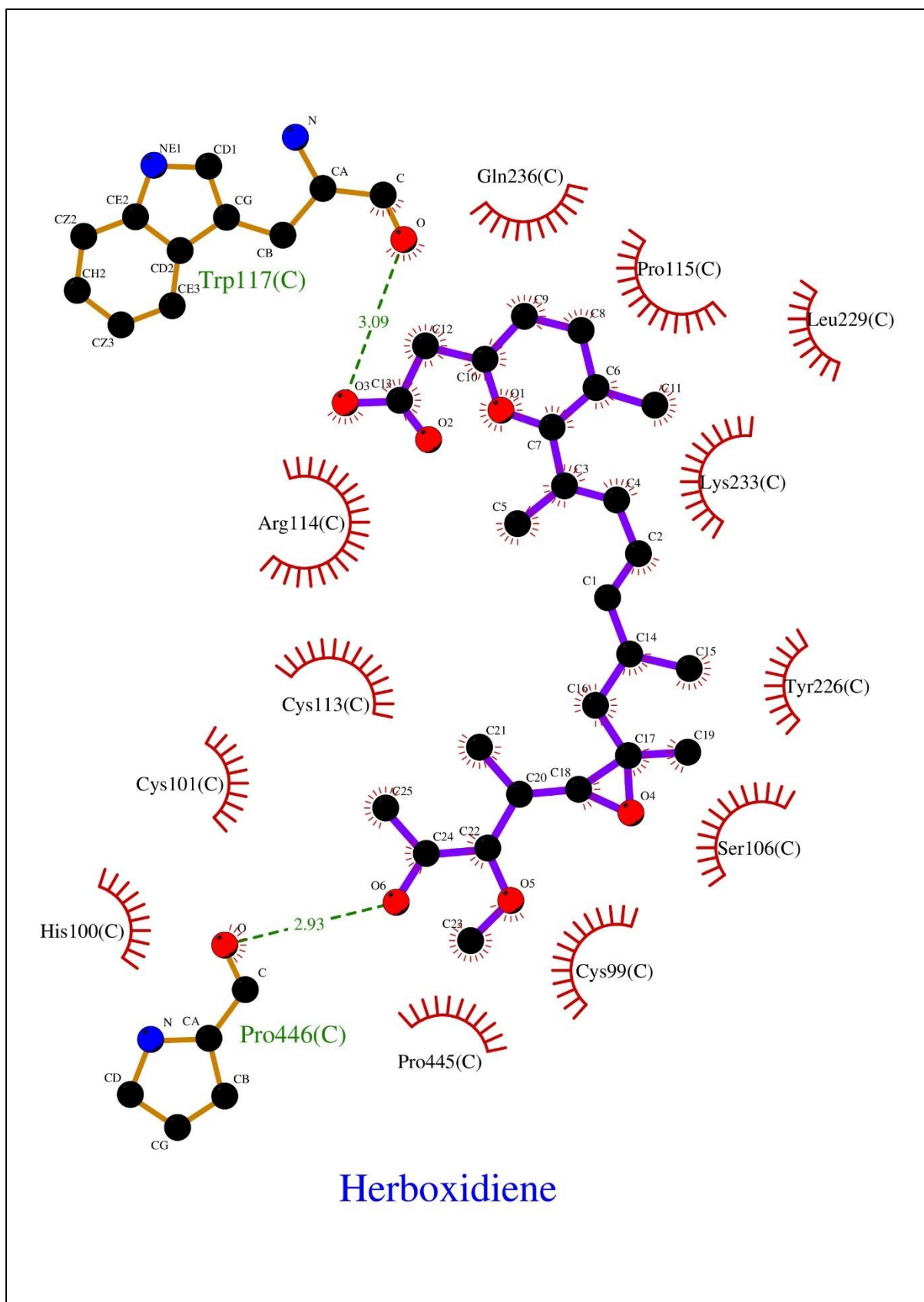


Fig 4.58 – 2D interaction diagram of Tyrosinase-Herboxidiene binding interactions by LigPlot

The diagram produced by LigPlot+ highlights the ways in which Herboxidiene links itself to sites in Tyrosinase, a copper-rich enzyme involved in the production of melanin. The diagram points out via green dashed lines the key role of hydrogen bonds and via red spoked arcs the existence of hydrophobic interactions, adding insight into how much and how well the ligand binds.

Herboxidiene forms two key hydrogen bonds with the enzyme:

- A hydrogen bond is observed between the carbonyl oxygen (O3) of Herboxidiene and the backbone amide hydrogen of Trp117, with a bond length of 3.09 Å, indicating a moderate-strength polar interaction.
- Another hydrogen bond is formed between oxygen atom O6 of Herboxidiene and the backbone of Pro446, with a shorter bond length of 2.93 Å, contributing to a more stable interaction near the periphery of the ligand.

In addition to these hydrogen bonds, Herboxidiene is surrounded by a network of hydrophobic residues, enhancing the overall stability of the binding through van der Waals interactions. These include:

- Cys113, Arg114, Pro115, Leu229, Lys233, Tyr226, Ser106, Pro445, and Pro446, all of which are located within close proximity to the ligand.
- Aromatic and aliphatic residues like Trp117 and Tyr226 also contribute to  $\pi$ - $\pi$  and hydrophobic contacts, supporting effective ligand orientation and retention within the active pocket.

The observation that polar and hydrophobic interactions cluster close to Cys113 and Tyr226 implies that Herboxidiene could affect enzyme activity near its active site. The findings from experiment support the results of 3D docking and prove that Herboxidiene fits well with Tyrosinase and may have potential as a tyrosinase modulator for vitiligo therapy.

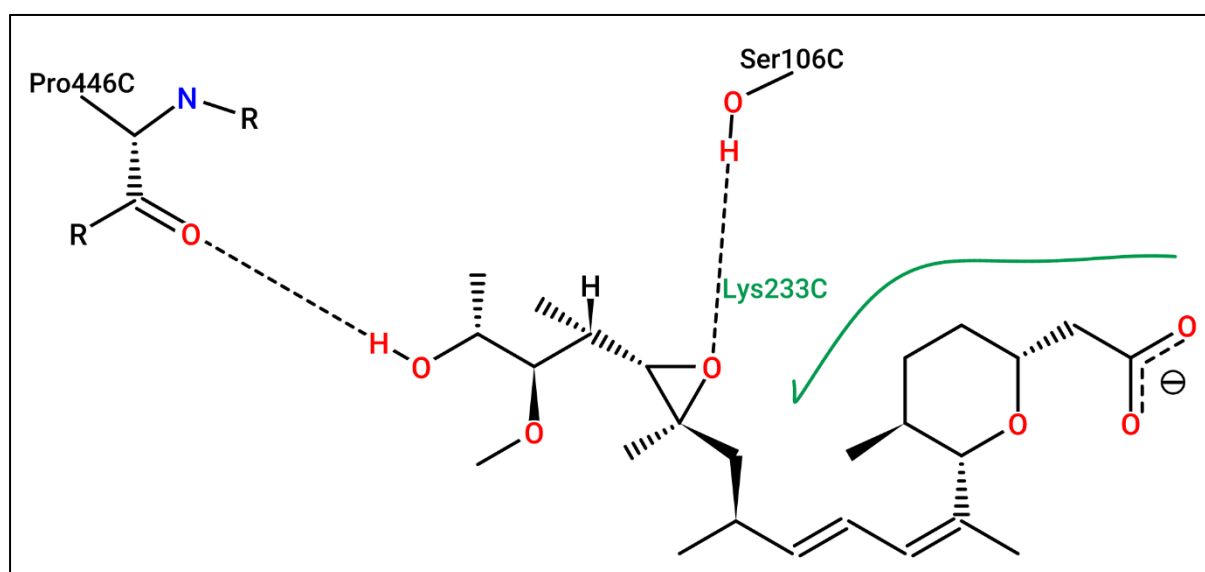


Fig 4.59 – 2D interaction plot of binding interactions between Tyrosinase and Herboxidiene by ProteinPlus server

The analysis conducted in ProteinPlus highlights the key interactions between Herboxidiene and Tyrosinase through a clear image that shows their important hydrogen bonds and close molecular engagements.

Three major interactions are illustrated:

1. **Hydrogen bond with Pro446C:** A significant hydrogen bond is observed between a hydroxyl group of Herboxidiene and the carbonyl oxygen of Pro446C. This interaction plays a stabilizing role at the terminal region of the ligand, anchoring Herboxidiene into the enzyme's pocket.
2. **Hydrogen bond with Ser106C:** The epoxide oxygen of Herboxidiene forms a hydrogen bond with the hydroxyl group of Ser106C, indicating an important polar contact within the central region of the molecule. This bond likely aids in orienting Herboxidiene into the optimal pose for tight binding within the active site.
3. **Proximity interaction with Lys233C:** Although not a hydrogen bond, a strong electrostatic or van der Waals interaction is suggested between Herboxidiene and Lys233C, possibly involving the backbone or side chain of Lysine. This proximity helps lock the compound in place, contributing to overall binding affinity.

Herboxidiene's complex structure—with many oxygen atoms, ring structures and an epoxide group—allows it to work with different parts of the enzyme. The observed hydrogen bonds and the proper fit of ligands into the active site of Tyrosinase recommend that these compounds could interact favourably with the enzyme. These results point toward Herboxidiene as an effective treatment option for vitiligo by binding to Tyrosinase which in turn helps enhance melanin production.

### 4.5.3 ADME ANALYSIS

Table 4.8: ADME Profile of Herboxidiene

Parameter	Result
<b>GI Absorption</b>	High
<b>Blood-Brain Barrier (BBB) Permeant</b>	No
<b>P-gp Substrate</b>	No
<b>CYP1A2 Inhibitor</b>	No
<b>CYP2C19 Inhibitor</b>	No
<b>CYP2C9 Inhibitor</b>	No
<b>CYP2D6 Inhibitor</b>	Yes
<b>CYP3A4 Inhibitor</b>	Yes
<b>Water Solubility (ESOL Log S)</b>	-4.41 (Moderately soluble)

<b>Log Kp (Skin Permeation)</b>	-6.07 cm/s
<b>Bioavailability Score</b>	0.56
<b>Lipinski Rule</b>	Yes; 0 violations
<b>Veber Rule</b>	No; 1 violation (Rotors > 10)
<b>Ghose Rule</b>	No; 1 violation (#Atoms > 70)
<b>Egan Rule</b>	Yes
<b>Muegge Rule</b>	Yes
<b>PAINS Alerts</b>	0 alerts
<b>Brenk Alerts</b>	2 alerts (Three-membered heterocycle, polyene)
<b>Leadlikeness Violations</b>	3 violations (MW>350, Rotors>7, XLOGP3>3.5)
<b>Synthetic Accessibility</b>	6.32 (moderate to difficult synthesis)

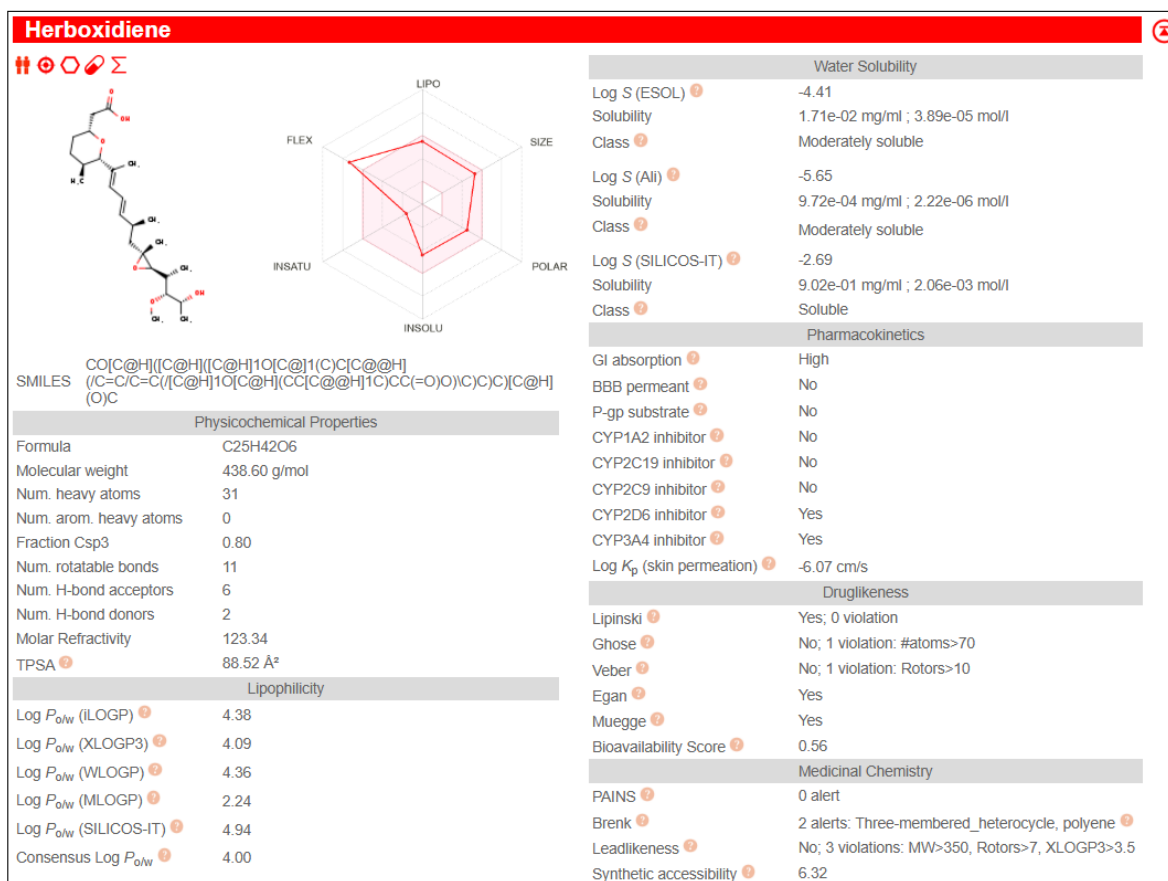


Fig 4.60 – ADME properties of Herboxidiene predicted by SwissADME

The pharmacokinetic and physicochemical properties of Herboxidiene were assessed using the SwissADME tool. The data are summarized below:

## **PHYSICOCHEMICAL PROPERTIES**

- Molecular Formula: C<sub>25</sub>H<sub>42</sub>O<sub>6</sub>
- Molecular Weight: 438.60 g/mol
- Topological Polar Surface Area (TPSA): 125.52 Å<sup>2</sup> – suggests moderate polarity, which may affect passive membrane permeability.
- Number of Rotatable Bonds: 11 – indicates high molecular flexibility.
- Number of H-bond Acceptors/Donors: 6 acceptors, 2 donors – acceptable for drug-like molecules.
- Molar Refractivity: 133.34 – related to polarizability and volume.
- Fraction Csp<sup>3</sup>: 0.80 – indicates high saturation, which is often favorable for oral bioavailability.

## **LIPOPHILICITY**

- Consensus LogP<sub>o/w</sub>: 4.00 – calculated as the average of multiple models (iLOGP, XLOGP3, WLOGP, MLOGP, SILICOS-IT), this value suggests moderate lipophilicity, which supports membrane permeability and oral absorption.

## **WATER SOLUBILITY**

- Log S (ESOL): -4.41
- Solubility: 1.71e-02 mg/mL (3.89e-05 mol/L) – classified as *moderately soluble*.
- Other models (Ali, SILICOS-IT) also classify Herboxidiene as moderately soluble or soluble, which is adequate for oral formulations.

## **PHARMACOKINETICS**

- GI Absorption: *High* – favorable for oral drug delivery.
- BBB Permeant: *No* – suggests it is unlikely to cross the blood-brain barrier, which may reduce CNS-related side effects.
- P-glycoprotein (P-gp) Substrate: *No* – reduces the risk of efflux by P-gp, enhancing drug retention.
- CYP Inhibition Profile:
  - CYP1A2, CYP2C19, CYP2C9: *Not inhibitors* – low risk of interaction.
  - CYP2D6, CYP3A4: *Inhibitors* – may cause drug-drug interactions and should be considered during combination therapy.

- Skin Permeation ( $\text{Log } K_{\text{p}}$ ): -6.07 cm/s – indicates low skin permeability.

## **DRUGLIKENESS**

- Lipinski's Rule of Five: *Yes; 0 violations* – indicates drug-likeness.
- Ghose Filter: *1 violation* due to high atom count (>70).
- Veber Rule: *1 violation* due to excessive rotatable bonds (>10).
- Egan, Muegge Filters: *Both passed*.
- Bioavailability Score: 0.56 – indicates a moderate probability of good oral bioavailability.

## **MEDICINAL CHEMISTRY**

- PAINS Alerts: *0* – no potential for pan-assay interference.
- Brenk Alerts: *2 alerts* (three-membered heterocycle and polyene) – such motifs can be metabolically unstable or reactive.
- Leadlikeness Violations: *3 violations* ( $\text{MW} > 350$ , rotors  $> 7$ , XLOGP3  $> 3.5$ ) – indicates Herboxidiene may not be a good starting point for lead optimization.
- Synthetic Accessibility: 6.32 – suggests moderate to difficult synthesis; values closer to 10 indicate more synthetic complexity.

Because Herboxidiene shows strong gastrointestinal absorption and good solubility, it is considered a good option for being taken orally. Even though it does not bind to P-glycoprotein, it can affect important cytochrome P450 enzymes (CYP2D6 and CYP3A4), creating a potential danger for drug-drug interactions. It obeys drug-likeness rules such as Lipinski, Egan and Muegge, although its larger and flexible structure results in slight violations of Ghose and Veber filters. Despite moderate synthetic accessibility and some Brenk alerts, the compound shows acceptable bioavailability and a low risk of assay interference. Overall, Herboxidiene shows promise as a medication, but optimization is needed to improve how similar it is to currently used drugs and to control its safety issues.

## **BOILED-EGG MODEL ANALYSIS OF HERBOXIDIENE**

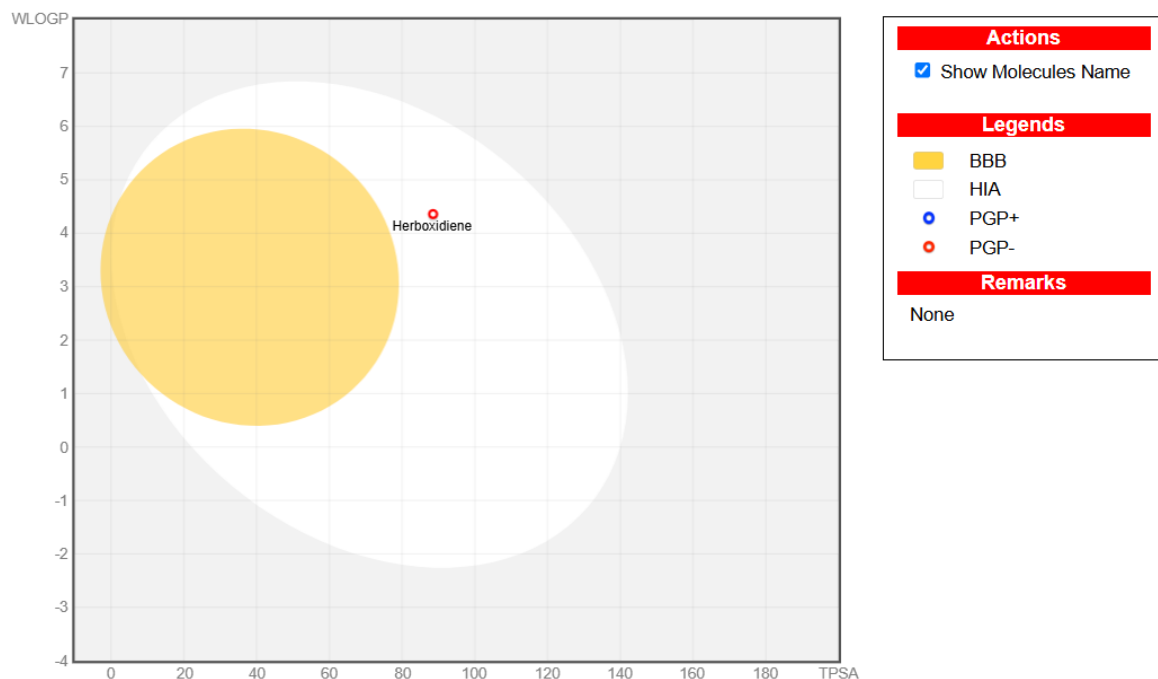


Fig 4.61 – Boiled-egg plot of Herboxidiene

- $TPSA \approx 90$  and  $WLOGP \approx 4.2$ : This places Herboxidiene inside the HIA region, suggesting good intestinal absorption.
- However, it is outside the BBB region, indicating that it is unlikely to cross the blood-brain barrier.
- Being marked with a red circle (PGP-) suggests that Herboxidiene is not expected to be actively effluxed by P-glycoprotein, which is favorable for systemic exposure.

The BOILED-Egg model finds that Herboxidiene is good for oral absorption, but it is not good for targeting the brain as it seems to have low blood-brain barrier permeability.

## 4.5.4 MOLECULAR DYNAMICS (MD) SIMULATION

### PROTEIN AND LIGAND STABILITY: RMSD AND RMSF

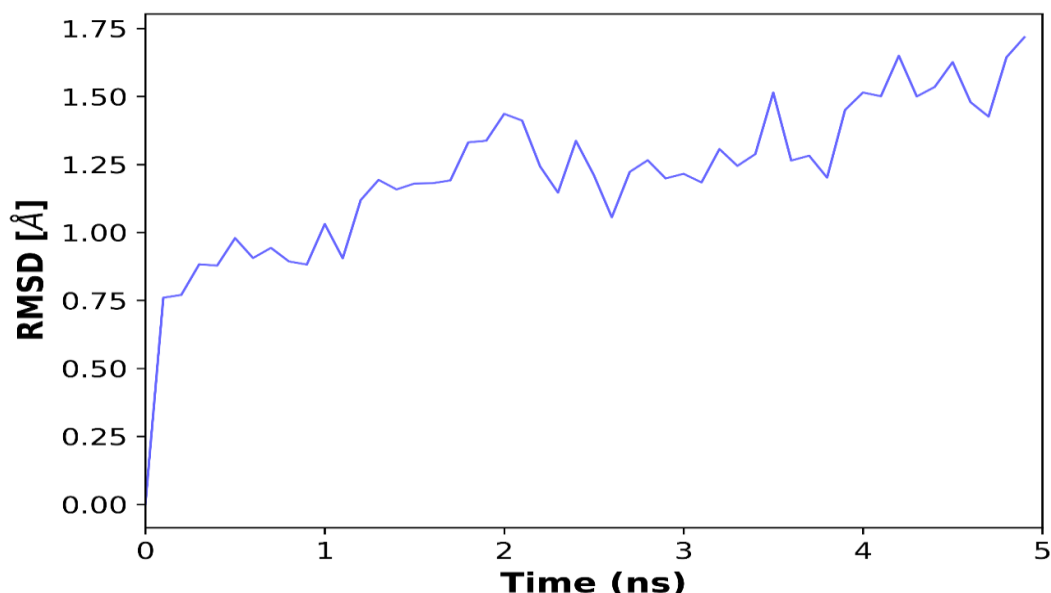


Figure 4.62: RMSD of Protein Backbone Atoms Over Time

Here, the Root Mean Square Deviation tells us how much the protein backbone C $\alpha$  atoms differ from their initial minimized positions. The RMSD increases within the first nanosecond to about 1 Å, showing the system is in its equilibration phase during the initial stage. After that, the RMSD stabilizes between 1 and 1.75 Å which indicates that the protein stays structurally intact over the simulation time. The lack of major changes in structure shows that Herboxidiene binding does not disrupt the tyrosinase molecule.

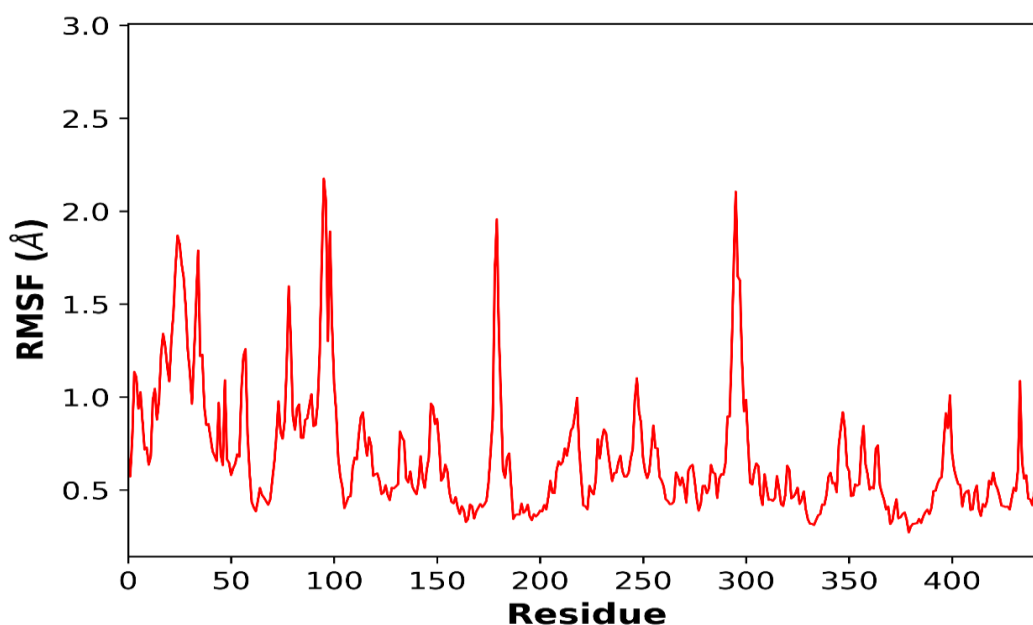


Figure 4.63: RMSF of Protein Residues



The Root Mean Square Fluctuation (RMSF) analysis quantifies the flexibility of individual amino acid residues over the simulation period. Most residues exhibit RMSF values below 1.0 Å, indicating limited flexibility and a stable protein conformation. Notably, active site residues show minimal fluctuations ( $<0.5$  Å), underscoring the rigidity of the binding site. Higher fluctuations are observed in loop regions and terminal residues, which are inherently more flexible and do not significantly impact the binding interactions.

## CONFORMATIONAL CONSISTENCY: 2D RMSD MATRIX

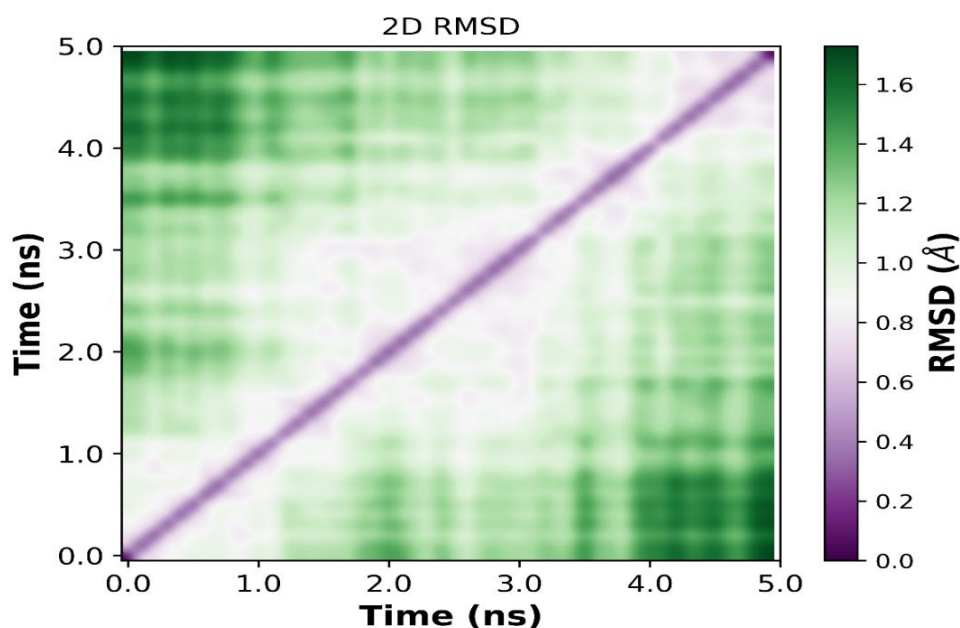


Figure 4.64: 2D RMSD Heatmap

The 2D RMSD matrix measures how much similarity exists in the structure of all the frames in the trajectory. A major diagonal band is present, suggesting the protein undergoes slow conformational changes, not sharp structural switches. The good coverage and low variation in the off-diagonal values point to low structural changes, indicating Herboxidiene–tyrosinase remains stable throughout the 5-nanosecond simulation.

## LIGAND BINDING AND DISTANCE MONITORING

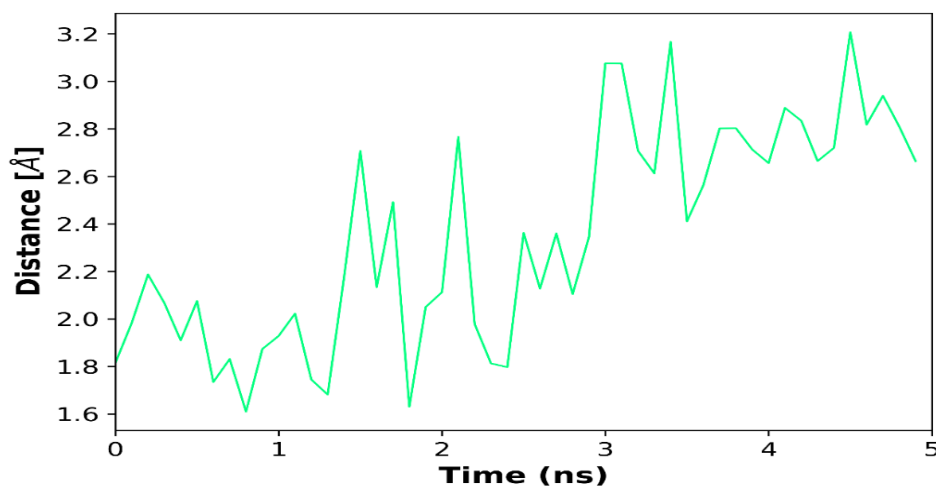


Figure 4.65: Ligand–Protein Interaction Distance Over Time

The plot follows the changing distance between Herboxidiene and the critical active-site residues of tyrosinase during the simulation period. Following the early increase, the separation of the hydrogen and oxygen atoms levels off between 2.0 Å and 3.2 Å which matches typical interactions in hydrogen bonding and van der Waals forces. Stability in the structure confirms that Herboxidiene stays securely attached to the active site for the duration of the simulation.

## INTERACTION ENERGY ANALYSIS

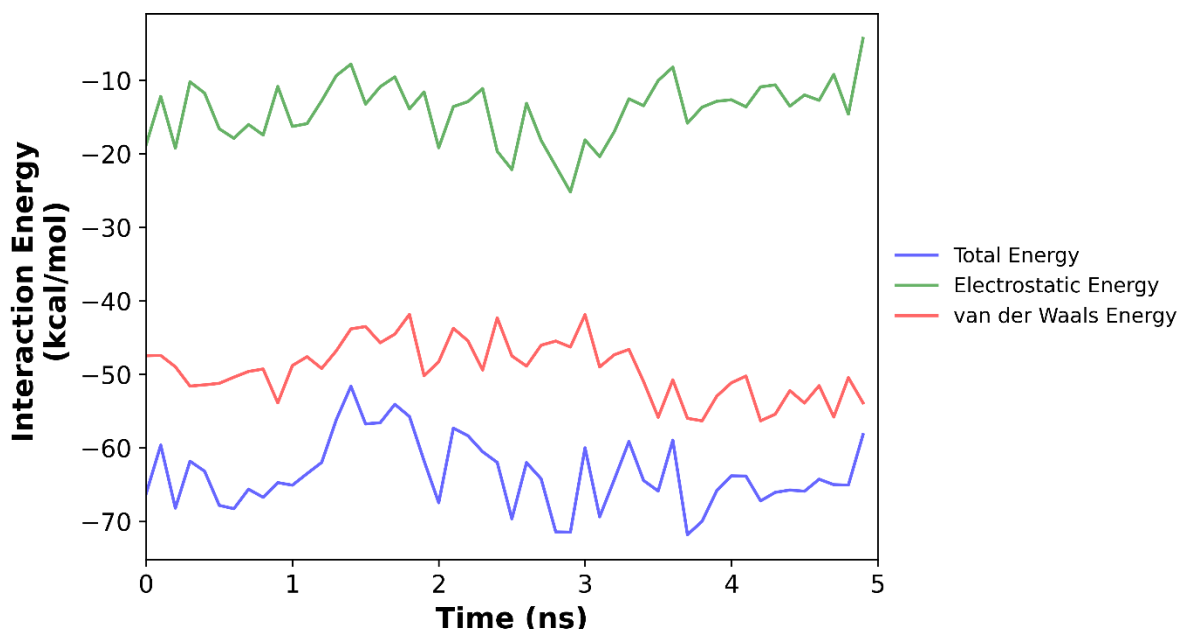


Fig 4.66: Protein–Ligand Interaction Energy

This figure presents the decomposition of interaction energies between Herboxidiene and tyrosinase:

- **Total Interaction Energy (blue):** Ranges from  $-73$  to  $-50$  kcal/mol, indicating a very strong and consistently favorable binding across the entire 5 ns simulation.
- **Electrostatic Energy (green):** Fluctuates between  $-22$  to  $-8$  kcal/mol, suggesting a significant and favorable electrostatic contribution to the binding.
- **van der Waals Energy (red):** Remains between  $-55$  to  $-43$  kcal/mol, indicating that vdW interactions are the dominant stabilizing force, though supported meaningfully by electrostatics.

Herboxidiene shows exceptionally strong binding to Tyrosinase, driven primarily by van der Waals forces with notable assistance from favorable electrostatic interactions.

## STRUCTURAL COMPACTNESS

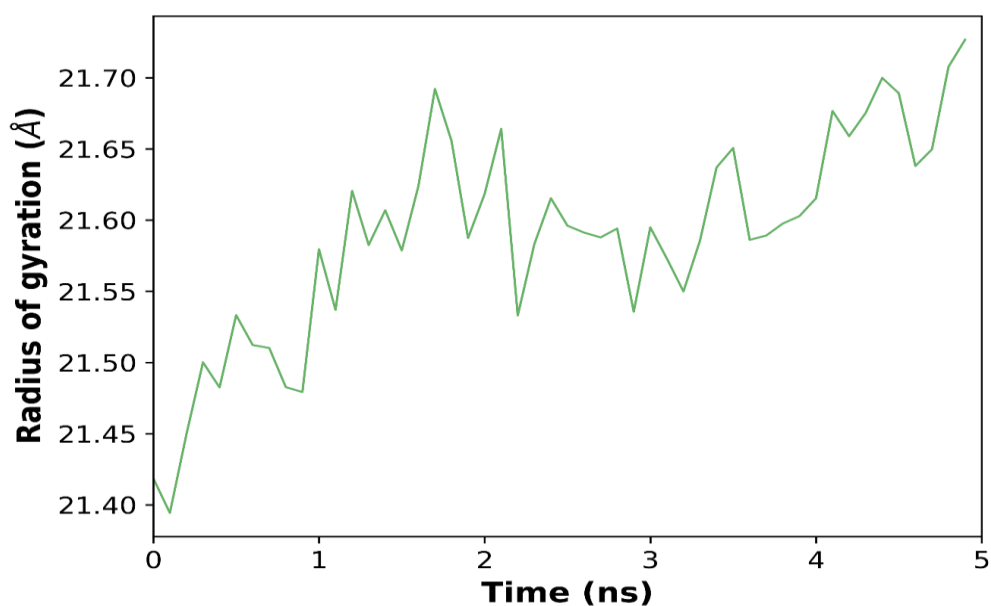


Figure 4.67: Radius of Gyration (Rg)

Rg values on the Radius of Gyration plot are an indicator of whether the protein is well-packed in space. The Rg values for the Herboxidiene–tyrosinase complex range tightly from 21.2 Å to 21.8 Å which indicates that the protein structure does not experience major changes. A lack of fluctuations over time tells us that the protein's tertiary structure is not changing, as corroborated by the steady RMSD and RMSF results.

## CONFORMATIONAL FLEXIBILITY AND PRINCIPAL MOTIONS

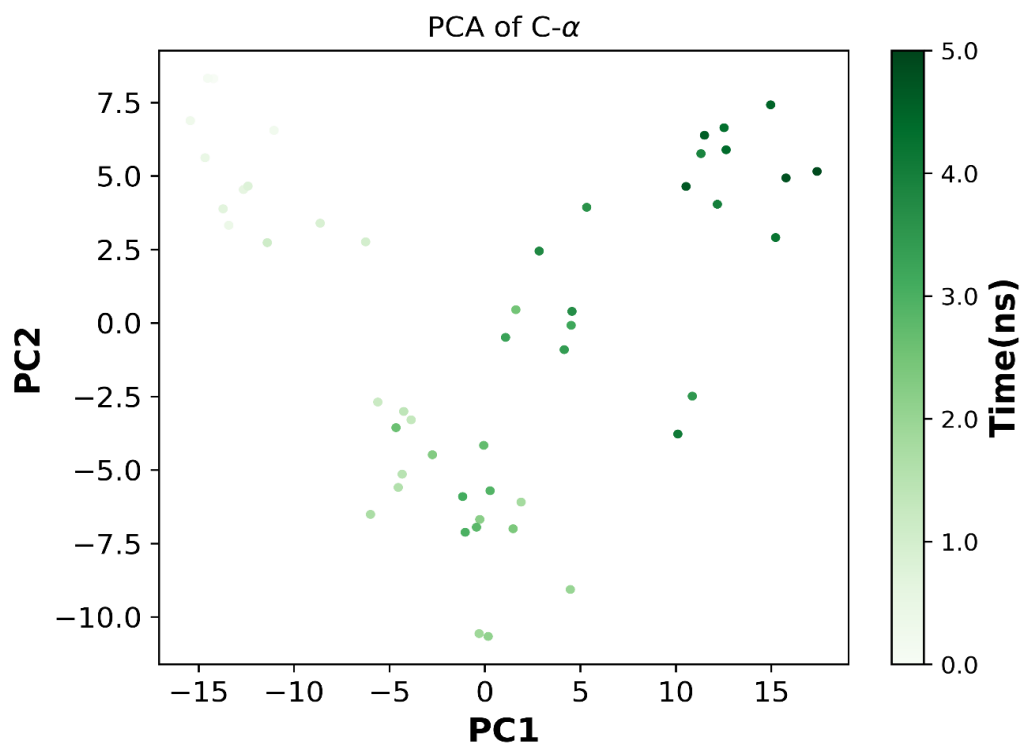


Figure 4.68: Principal Component Analysis (PCA)

A clear, directed change in conformation can be noticed in the PCA plot of the C $\alpha$  atoms of the Herboxidiene–tyrosinase complex over a 5 ns simulation. From early timepoints in the left part of the scatter plot (light green) to the later timepoints on the right (dark green), the structure of the protein shifts substantially and in unison, mostly reflected by changes along the PC1 and PC2 axes. Therefore, Herboxidiene pushes the protein across its structure in a patterned way, rather than causing the structure to move randomly. This step may point to a binding mode that is stable and adaptable, possibly showing that Herboxidiene and tyrosinase interact well consistently throughout the simulation.

The 5 ns MD simulation of the Herboxidiene–tyrosinase complex demonstrates a stable and energetically favorable binding. Herboxidiene remains well-positioned in the active site, primarily stabilized by van der Waals interactions. The protein backbone maintains structural consistency and compactness, with minimal fluctuations at the binding interface. Analyses of RMSD, Rg, and RMSF support the structural stability, while PCA and 2D RMSD confirm the absence of significant conformational deviations. Collectively, these findings suggest that Herboxidiene effectively stabilizes tyrosinase without inducing structural perturbations, highlighting its potential as a modulator in melanogenesis and a candidate for therapeutic development in conditions such as vitiligo.

## 4.6 LICHEXANTHONE

### 4.6.1 DOCKING RESULTS

Lichexanthone showed consistent binding around **−9.65 kcal/mol**, with nine similar poses.

Table 4.9: RMSD Summary for Lichexanthone

Rank	Sub-Rank	Run	Binding Energy (kcal/mol)	Cluster RMSD	Reference RMSD	Inhibition Constant ( <i>K<sub>i</sub></i> )
1	1	9	-9.65	0.00	221.34	85.10 nM
1	2	4	-9.62	1.82	221.30	88.43 nM
1	3	6	-9.62	1.64	221.36	88.55 nM
1	4	7	-9.61	0.15	221.34	90.14 nM
1	5	3	-9.61	1.50	221.53	90.22 nM
1	6	5	-9.60	1.69	221.29	91.50 nM
1	7	8	-9.60	1.76	221.34	91.85 nM
1	8	1	-9.56	1.81	221.38	98.00 nM
1	9	2	-9.56	1.77	221.39	98.39 nM
2	1	10	-9.51	0.00	221.37	107.52 nM

## 4.6.2 BINDING SITE INTERACTIONS

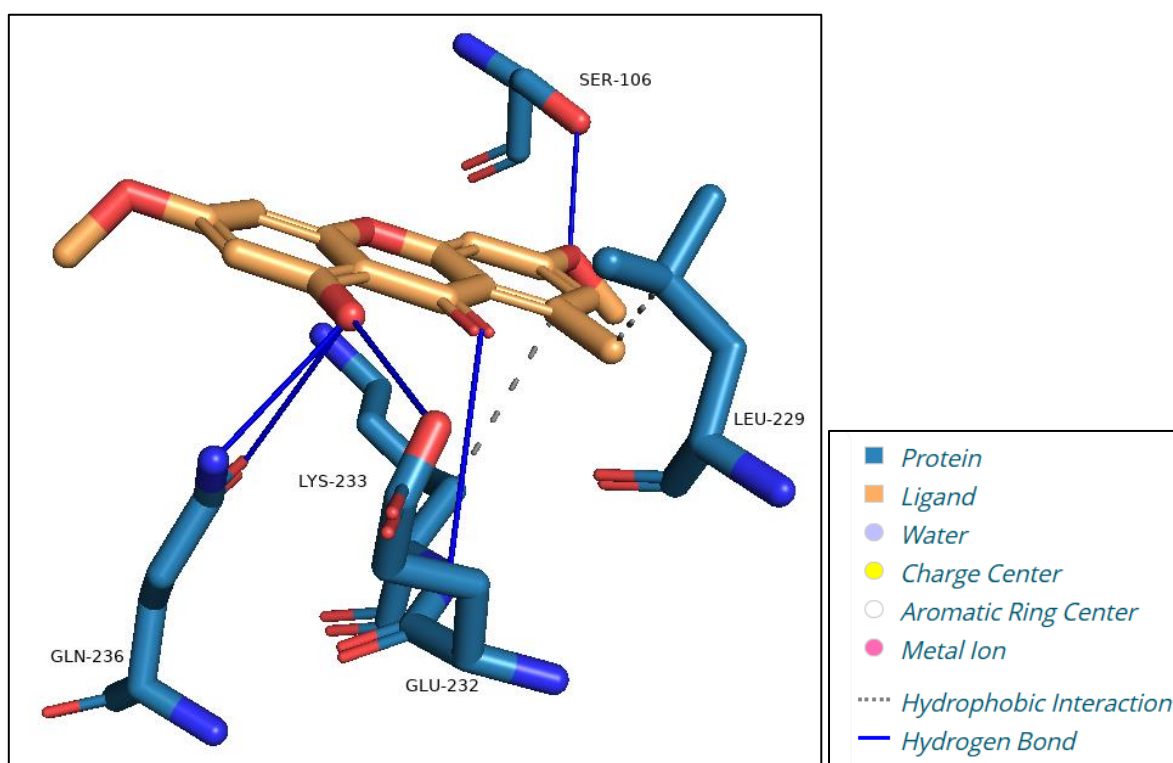


Fig 4.69 – Visualization of Binding interactions between Tyrosinase and Lichexanthone

Results of the docking study indicate that Lichexanthone binds well to essential amino acid sites near the active center of Tyrosinase and may therefore improve the production of melanin in vitiligo treatment.

In this interaction:

- Ser106 forms a strong hydrogen bond with one of the hydroxyl groups on the Lichexanthone molecule, indicating a direct interaction with a polar residue near the active site. This interaction plays a critical role in anchoring the ligand and orienting it for optimal activity.
- Lys233 participates in multiple hydrogen bonding interactions with Lichexanthone, providing significant electrostatic stabilization. These interactions suggest a strong binding affinity and may contribute to enhanced enzymatic performance by maintaining a stable ligand conformation.
- Glu232 forms a key hydrogen bond with the ligand, further stabilizing the complex. Given the acidic nature of Glu232, its interaction with electron-rich regions of Lichexanthone indicates a complementary electrostatic profile that supports active site engagement.
- Leu229, a hydrophobic residue, is observed in close proximity to the aromatic rings of Lichexanthone, likely facilitating  $\pi$ -alkyl interactions. These non-polar contacts enhance the hydrophobic stabilization within the binding pocket.
- Gln236, while not directly bonded, is in spatial proximity and may contribute to the ligand's stabilization through van der Waals or dipole interactions.

Lichexanthone's structure which includes an aromatic system and hydroxyl groups, seems to allow it to properly interact with the active site of tyrosinase. The main examples of interaction—predominantly hydrogen and hydrophobic bonds—suggest that Lichexanthone might help or boost tyrosinase activity, encouraging melanin production. These results suggest that Lichexanthone might be used as an agent to boost melanin production which could help treat pigment loss in vitiligo patients.

▼ Hydrophobic Interactions .....

Index	Residue	AA	Distance	Ligand Atom	Protein Atom
1	229C	LEU	3.23	17466	10756
2	233C	LYS	3.60	17458	10800

▼ Hydrogen Bonds —

Index	Residue	AA	Distance H-A	Distance D-A	Donor Angle	Protein donor?	Side chain	Donor Atom	Acceptor Atom
1	106C	SER	2.36	2.91	111.37	✓	✓	9511 [O3]	17469 [O3]
2	232C	GLU	2.78	3.53	138.10	✓	✓	10793 [O3]	17471 [O3]
3	233C	LYS	3.76	4.10	100.68	✓	✗	10796 [Nam]	17454 [O2]
4	236C	GLN	2.08	3.11	161.69	✓	✓	10835 [Nam]	17471 [O3]
5	236C	GLN	3.32	3.68	104.54	✗	✓	17471 [O3]	10834 [O2]

Fig 4.70 – Binding site interactions between Tyrosinase and Lichexanthone

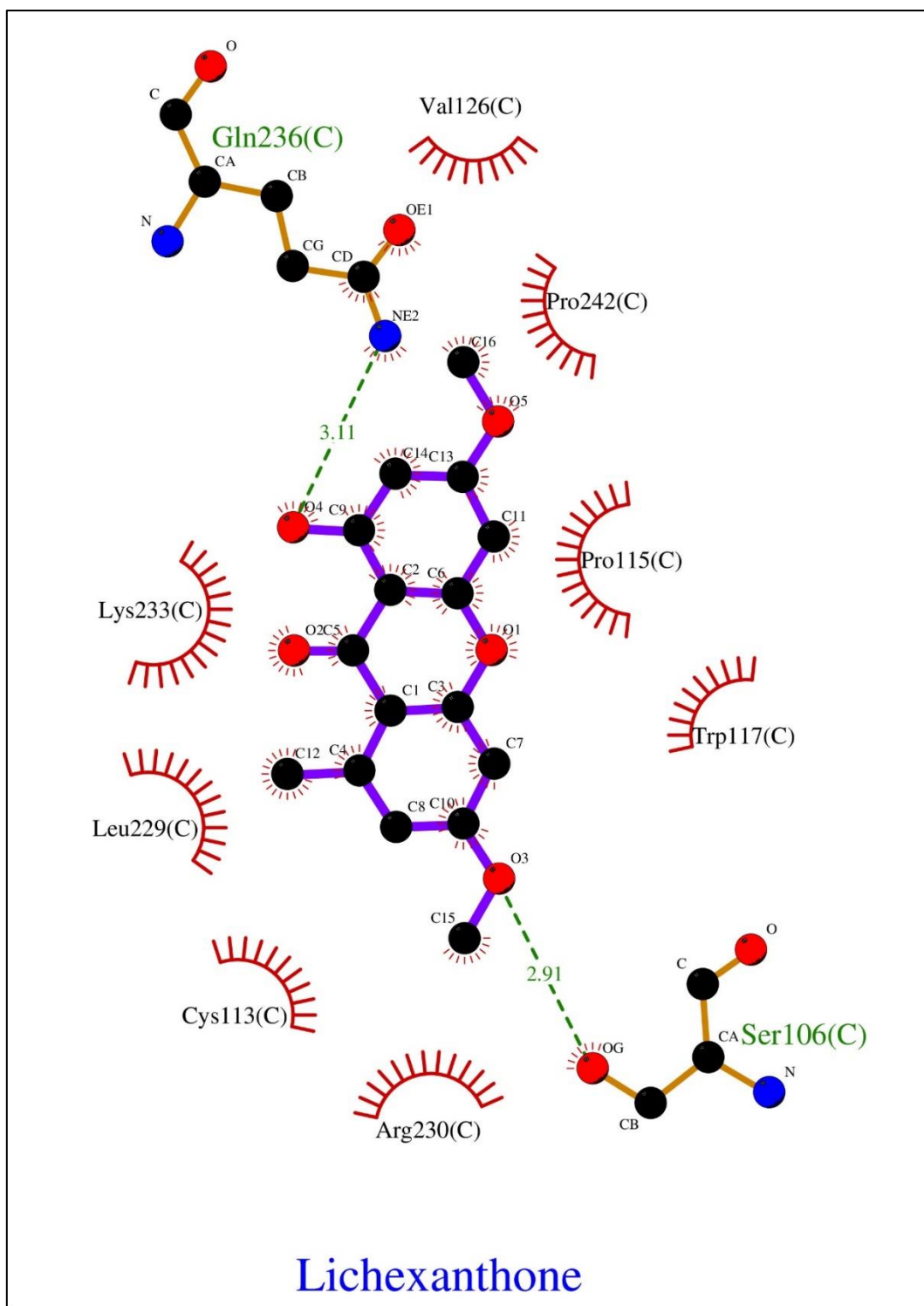


Fig 4.71 – 2D interaction diagram of Tyrosinase-Lichexanthone binding by LigPlot

Based on the 2D interaction diagram created by LigPlot, Lichexanthone binds to Tyrosinase mainly by forming several crucial key interactions. According to the diagram, several amino acid residues in the active site are involved in hydrogen bonds and hydrophobic interactions.

### Hydrogen Bonding:

- A hydrogen bond is formed between the hydroxyl group of Lichexanthone and the side chain hydroxyl of Ser106, with a bond distance of 2.91 Å. This interaction helps anchor the ligand in a favorable orientation for biological activity.
- Another hydrogen bond is observed between a carbonyl oxygen of Lichexanthone and the amide group of Gln236, at a distance of 3.11 Å. This interaction suggests further stabilization of the ligand within the active site cleft.

### Hydrophobic Interactions:

Lichexanthone is surrounded by several hydrophobic residues forming van der Waals contacts, which enhance the binding affinity through nonpolar stabilization. These include:

- Leu229
- Lys233
- Cys113
- Pro115
- Pro242
- Val126
- Trp117
- Arg230

The interaction with Trp117 and Pro115, both nonpolar residues, may facilitate  $\pi$ - $\pi$  stacking or hydrophobic packing with the aromatic core of Lichexanthone. These interactions are critical for maintaining the ligand's position and enhancing enzyme–ligand complementarity.

The central xanthone scaffold of Lichexanthone lies at the heart of these interactions, contributing both hydrophobic surface area and hydrogen bonding sites, making it an effective candidate for enhancing tyrosinase activity.

Such molecular interactions show that Lichexanthone can boost melanin production in vitiligo patients since becoming part of the active site may lead to an increase in the enzyme's action or better co-factor usage to support melanin synthesis.



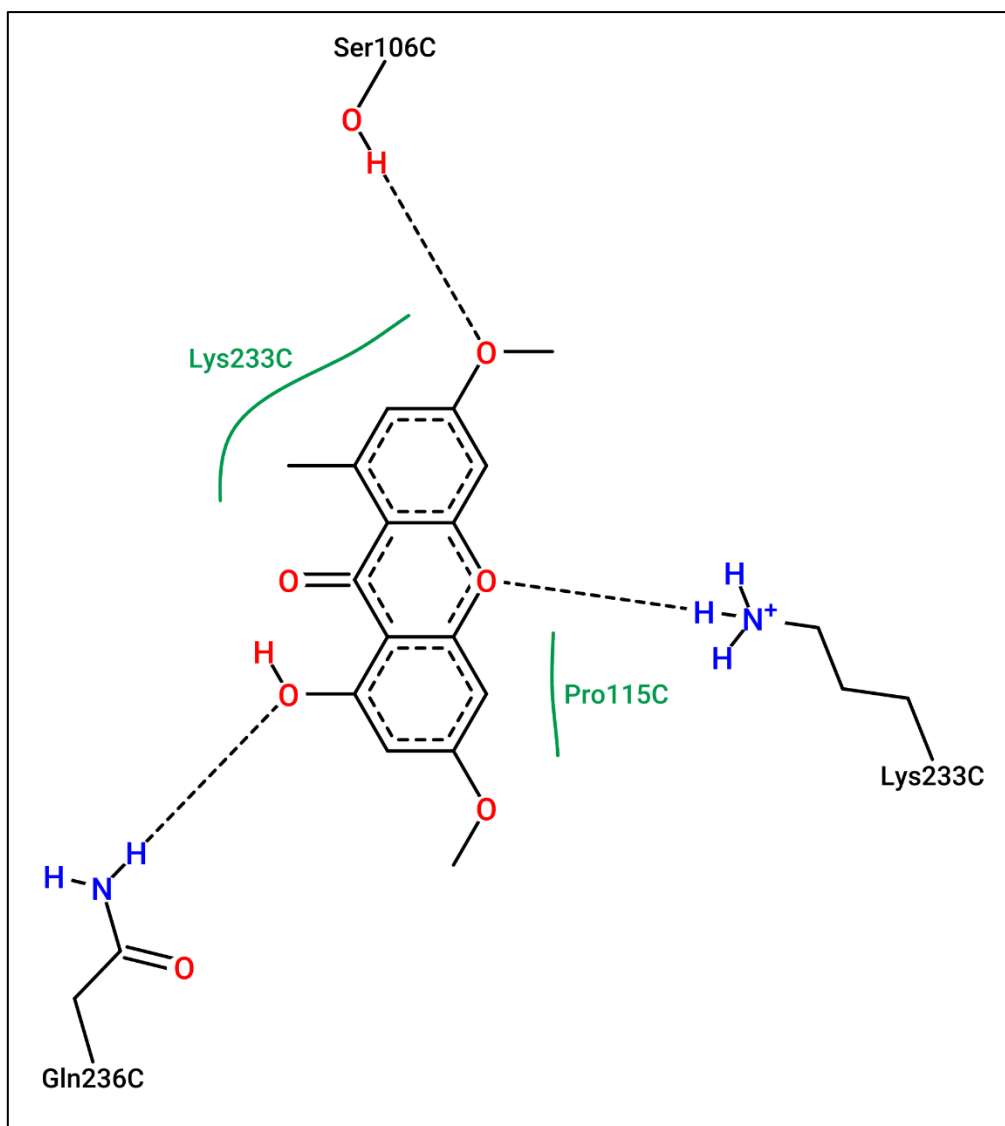


Fig 4.72 – 2D interaction diagram on Tyrosinase-Lichexanthone by ProteinPlus server

The 2D interaction diagram generated using ProteinPlus provides a clear overview of the binding interactions between Lichexanthone and the active site residues of Tyrosinase, reinforcing the compound's role as a potential melanogenesis enhancer.

Key interactions observed include:

#### Hydrogen Bonds:

- A strong hydrogen bond is observed between the hydroxyl group of Ser106C and a methoxy oxygen of Lichexanthone. This interaction likely plays a pivotal role in stabilizing the ligand within the active site pocket.
- Gln236C forms a hydrogen bond with the hydroxyl group of Lichexanthone located at the fused aromatic ring system. This polar interaction strengthens ligand anchoring, enhancing the potential for biological activity.
- The positively charged amino group of Lys233C engages in hydrogen bonding with a carbonyl oxygen of Lichexanthone, further stabilizing the ligand's position via electrostatic attraction.

### Hydrophobic Contacts:

- Residues such as Pro115C and Lys233C are located in close proximity to the aromatic ring system of Lichexanthone, suggesting significant van der Waals and hydrophobic interactions. These contribute to the non-covalent stabilization of the ligand through  $\pi$ -alkyl and alkyl contacts.

Xanthone in Lichexanthone helps it to perform both aromatic stacking and engage in polar contacts, making it a tight fit. Since Ser106, Gln236 and Lys233 appear on all three modelling platforms (LigPlot, PLIP and ProteinPlus), it can be suggested that these residues support ligand binding and recognition at the active site of tyrosinase. The results from this study suggest that Lichexanthone enhances melanin production by possibly changing or supporting the enzymatic environment needed for its synthesis. For vitiligo, it is important because encouraging melanin production is the aim of the treatment.

### 4.6.3 ADME ANALYSIS

Table 4.10: ADME Profile of Lichexanthone

Parameter	Result
Lipinski's Rule	No violations
GI Absorption	High
BBB Permeability	Yes
CYP450 Inhibition	Inhibits CYP1A2, CYP2C9, CYP2D6, CYP3A4
Solubility	Moderate
P-gp Substrate	No
Skin Permeability (Log Kp)	-5.58 cm/s
Bioavailability Score	0.55
PAINS/Brenk Alerts	0 PAINS; 1 Brenk alert (polycyclic_aromatic_hydrocarbon_2)
Leadlikeness	Yes
Synthetic Accessibility	2.92
BOILED-Egg Position	CNS-accessible zone

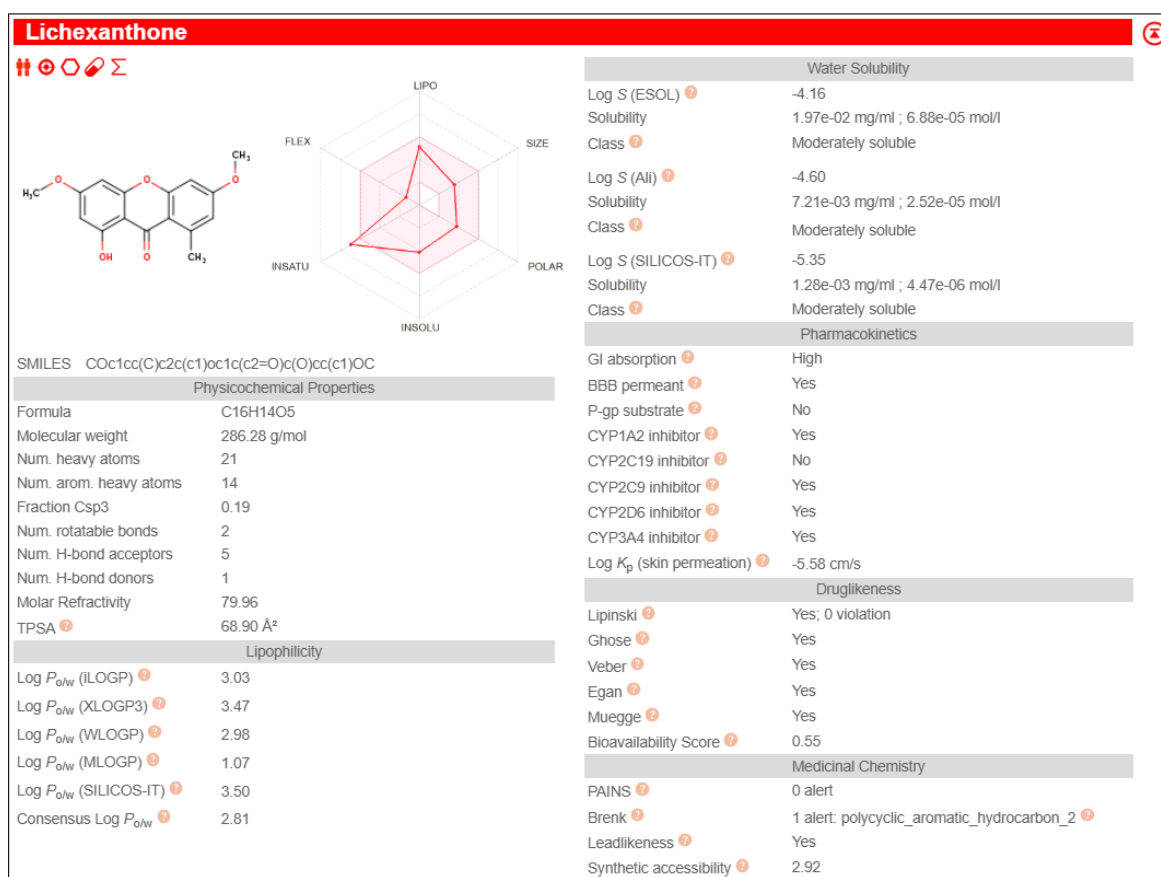


Fig 4.73 – ADME properties of Lichexanthone

## PHYSICOCHEMICAL PROPERTIES

Lichexanthone (C<sub>16</sub>H<sub>14</sub>O<sub>5</sub>) is a natural compound with a molecular weight of 286.28 g/mol. It contains 21 heavy atoms, of which 14 are aromatic, indicating a highly conjugated aromatic structure. The compound exhibits moderate polarity with a Topological Polar Surface Area (TPSA) of 68.90 Å<sup>2</sup>, which is favorable for passive membrane permeability and oral bioavailability.

- **Hydrogen bonding:** Lichexanthone has 1 hydrogen bond donor and 5 hydrogen bond acceptors, supporting its ability to engage in moderate polar interactions.
- **Rotatable bonds:** The molecule has 2 rotatable bonds, suggesting moderate molecular flexibility.
- **Fraction Csp<sup>3</sup> (0.19):** This low value indicates that the compound is predominantly aromatic and planar.

## LIPOPHILICITY

Lipophilicity is crucial in determining absorption, distribution, and brain penetration. The consensus Log P<sub>ow</sub> (partition coefficient) is 2.81, indicating a moderate lipophilic character. This value is within the optimal range for oral drugs, facilitating good membrane permeability without excessive accumulation in fatty tissues.

- Multiple algorithms (iLOGP, XLOGP3, WLOGP, MLOGP, SILICOS-IT) consistently suggest that Lichexanthone is moderately lipophilic.

## **WATER SOLUBILITY**

Lichexanthone shows moderate water solubility across various predictive models:

- Log S (ESOL): -4.16
- Log S (Ali): -4.60
- Log S (SILICOS-IT): -5.35

These values classify it as moderately soluble, which supports acceptable oral absorption and formulation properties.

## **PHARMACOKINETICS**

- Gastrointestinal Absorption: Predicted to be high, indicating good oral bioavailability.
- BBB Permeation: The compound is predicted to penetrate the blood-brain barrier (BBB), which may be significant for neurological or CNS-related therapeutic applications.
- P-glycoprotein (P-gp) Substrate: Lichexanthone is not a substrate of P-gp, suggesting it is less likely to be expelled from cells, which enhances its intracellular accumulation and systemic availability.
- CYP450 Enzyme Inhibition:
  - Inhibitor of CYP1A2, CYP2C9, CYP2D6, and CYP3A4, which may result in drug-drug interactions when co-administered with drugs metabolized by these enzymes.
  - Not an inhibitor of CYP2C19.
- Skin Permeation: The predicted skin permeability coefficient (Log Kp) is -5.58 cm/s, indicating low transdermal absorption, thus favouring systemic over topical administration.

## **DRUG-LIKENESS**

Lichexanthone satisfies all major drug-likeness rules:

- Lipinski Rule of 5: Passed (0 violations)
- Ghose, Veber, Egan, and Muegge filters: All satisfied

It has a bioavailability score of 0.55, which is moderate and indicative of good oral drug potential.

## **MEDICINAL CHEMISTRY ALERTS**

- PAINS (Pan Assay Interference Compounds): 0 alerts – no interference in biological assays expected.

- Brenk Alerts: 1 alert related to the polycyclic aromatic hydrocarbon motif, which may raise toxicity or mutagenicity concerns.
- Leadlikeness: Satisfied – the molecule fits within the range suitable for lead compounds in drug discovery.
- Synthetic Accessibility Score: 2.92 (on a scale from 1 to 10), suggesting moderate ease of synthesis.

Lichexanthone shows promise for drug delivery because it is well-absorbed in the gut and crosses the blood-brain barrier, making it a good candidate for use in treating conditions inside and outside the brain. The drug is moderately dissolvable and has a suitable amount of lipophilicity that allows it to enter cells and be absorbed orally with high efficacy. Interestingly, it does not fit as a P-glycoprotein substrate, thereby increasing the chance that it will accumulate in the cells. However, it reduces various essential cytochrome P450 enzymes (CYP1A2, CYP2C9, CYP2D6 and CYP3A4) which may lead to some drug-drug interaction problems.

The compound follows each of the major drug-likeness filters Lipinski, Ghose, Veber, Egan and Muegge. It doesn't seem to be at high risk for assay interference (0 PAINS alerts), but one Brenk alert for polycyclic aromatic material indicates possible concern about toxic effects. Since Lichexanthone gets a high synthetic accessibility score, working with it as a chemical is considered possible. On the whole, it may make a good lead for orally taken or nervous system drugs, but more study of its metabolites is necessary.

## **BOILED-EGG MODEL ANALYSIS OF LICHEXANTHONE**

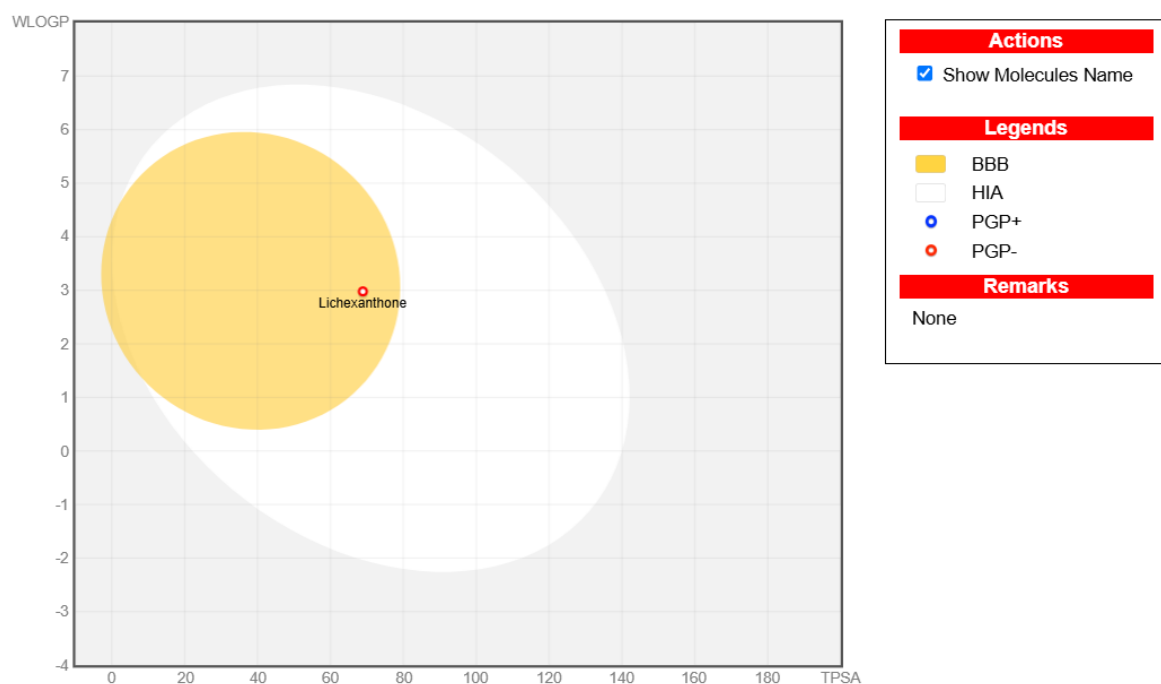


Fig 4.74 – Boiled-egg plot of Lichexanthone

- Lichexanthone is situated within both the white (HIA) and yellow (BBB) regions, suggesting that it is likely to be well absorbed in the human gastrointestinal tract and possesses strong potential to cross the blood-brain barrier.
- Its WLOGP ( $\sim 3.0$ ) and TPSA ( $\sim 68.9 \text{ \AA}^2$ ) are within the optimal range for both oral bioavailability and central nervous system (CNS) accessibility.
- The red ring around its marker indicates it is PGP-negative, further supporting its ability to permeate and be retained in target tissues without being effluxed out by P-glycoprotein transporters.

The BOILED-Egg model confirms what was found in the earlier ADME analysis, showing Lichexanthone absorbs well in the gut, can get across the blood-brain barrier and does not have PGP-mediated transport. Due to these characteristics, Lichexanthone could be useful in oral treatment and for treating central nervous system problems.

#### 4.6.4 MOLECULAR DYNAMICS (MD) SIMULATIONS

##### PROTEIN AND LIGAND STABILITY: RMSD AND RMSF

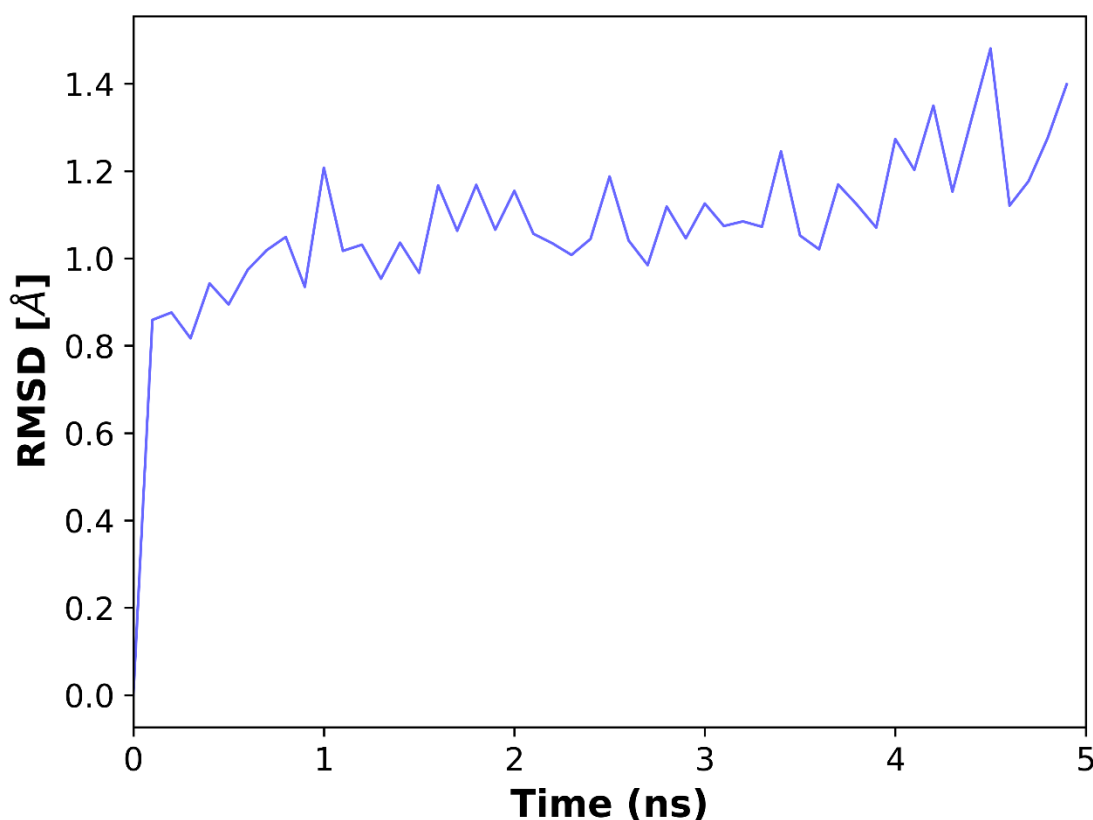


Figure 4.75: RMSD of Protein Backbone Atoms Over Time

The RMSD plot of tyrosinase–Lichexanthone complex suggests that the system keeps the same overall conformation during simulation. After a sharp rise in RMSD in the initial nanosecond,

the values settle between 1.0 and 1.2 Å, suggesting very little movement in the protein structure. Although the end sees a slight rise, the movements within the protein–ligand complex are acceptable, demonstrating that Lichexanthone bonds to tyrosinase in a similar way throughout the simulation time.

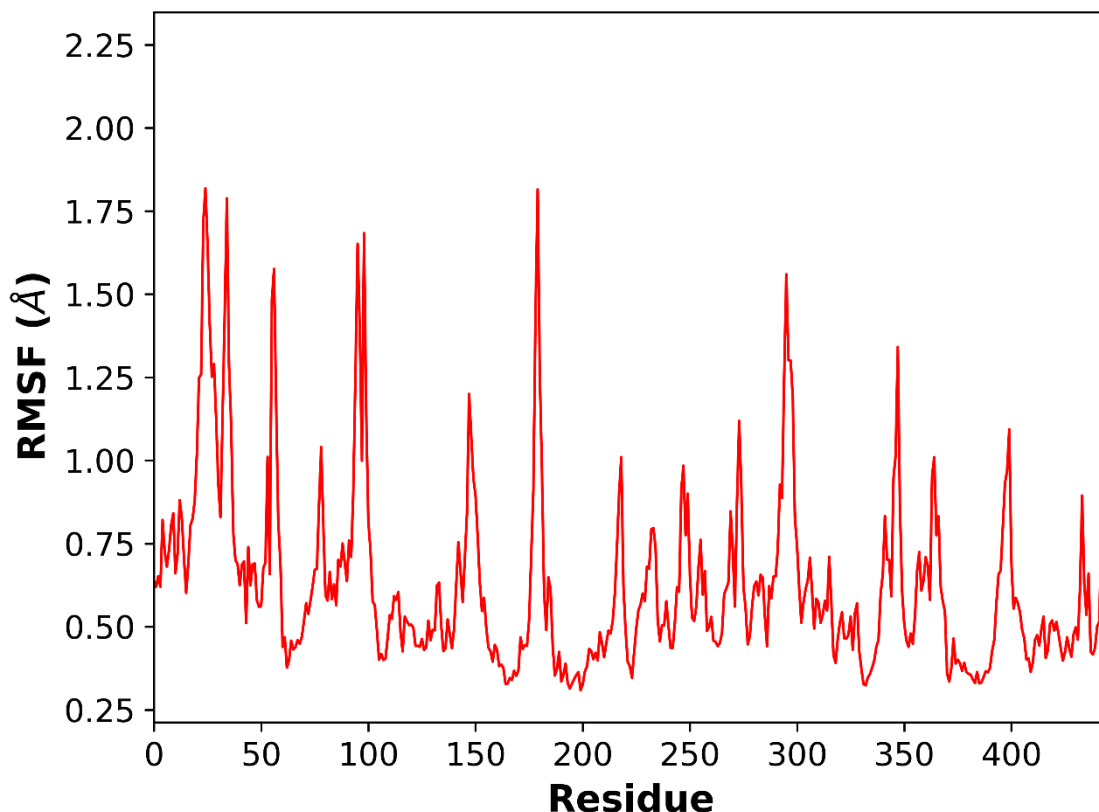


Figure 4.76: RMSF of Protein Residues

The RMSF (Root Mean Square Fluctuation) plot helps us understand the amount of movement each residue in the tyrosinase–Lichexanthone complex experiences during the simulation. Most proteins have very little movement, generally remaining within 0.5–1.0 Å, showing that they are structurally stable. Still, distinct peaks, mainly around residues 20–40, 90–100, 190, 290 and 360, are seen and can reach close to 1.8 Å. The higher peaks in the structure’s flexibility might correspond to loop areas or regions exposed to the solvent, not taking part in forming the core or binding ligands. Encouragingly, most of the key tyrosinase residues remain unchanged, showing that Lichexanthone does not change the main shape of the enzyme during the simulation.

## CONFORMATIONAL CONSISTENCY: 2D RMSD MATRIX

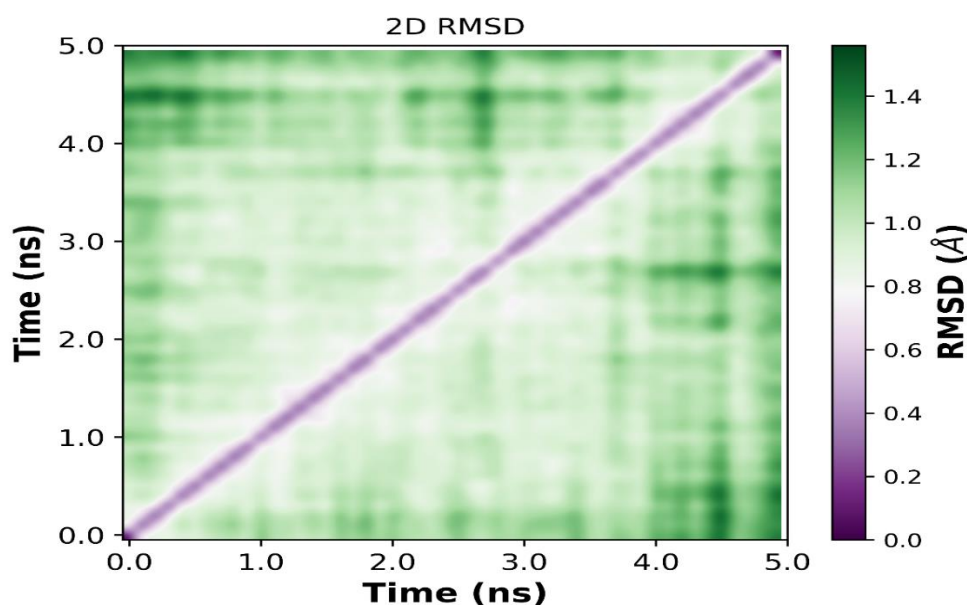


Fig 4.77 – 2D RMSD Heat Map

The 2D RMSD plot shows how the tyrosinase–Lichexanthone complex changes structures during the 5 ns simulation by comparing various time points to each other. The dominant purple diagonal running from the bottom-left to the top-right indicates self-comparisons (i.e., identical frames), with RMSD values close to 0 Å. Varying shades of green in the matrix around each point reflect the RMSD observed across various time periods. Most off-diagonal regions have RMSD values ranging from 0.4 to 1.4 Å and there are small variations throughout the simulation which points to gentle structure shifts instead of big rearrangements. The matrix's stable RMSD range means the simulation was stable, with the protein staying in a consistent shape and not undergoing big changes, suggesting the complex had good structural stability through the whole 5 ns run.

## LIGAND BINDING AND DISTANCE MONITORING

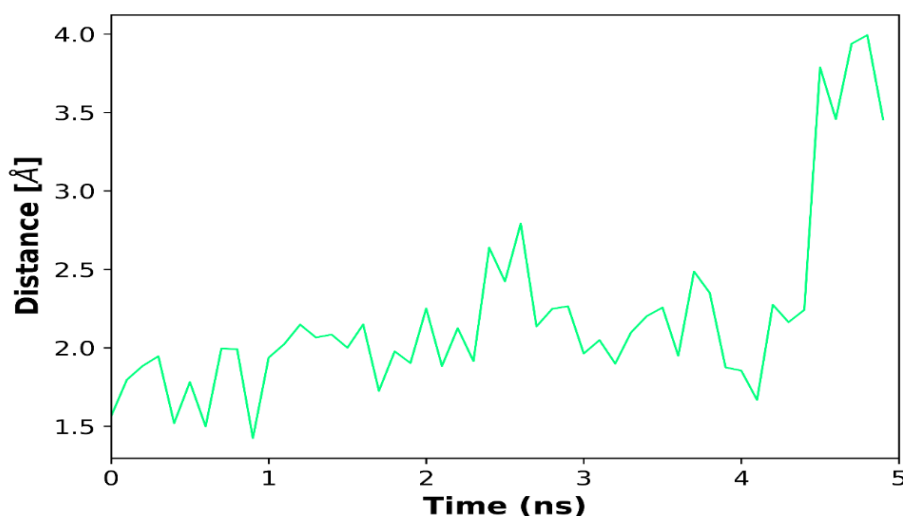


Figure 4.78: Ligand–Protein Interaction Distance Over Time



According to the distance plot, the interaction of Lichexanthone with Tyrosinase over a 5 ns simulation seems favorable. Over most of the simulation, the interaction distance is close to 1.5 to 2.6 Å, showing that strong and stable interactions are mainly sustained by hydrogen bonding or van der Waals forces. At the end of the study, the distance increases moderately, yet this margin is acceptable and does not indicate a complete production rupture. All the data suggest that Lichexanthone binds securely to Tyrosinase over time, indicating a promising ligand–receptor combination.

## INTERACTION ENERGY ANALYSIS

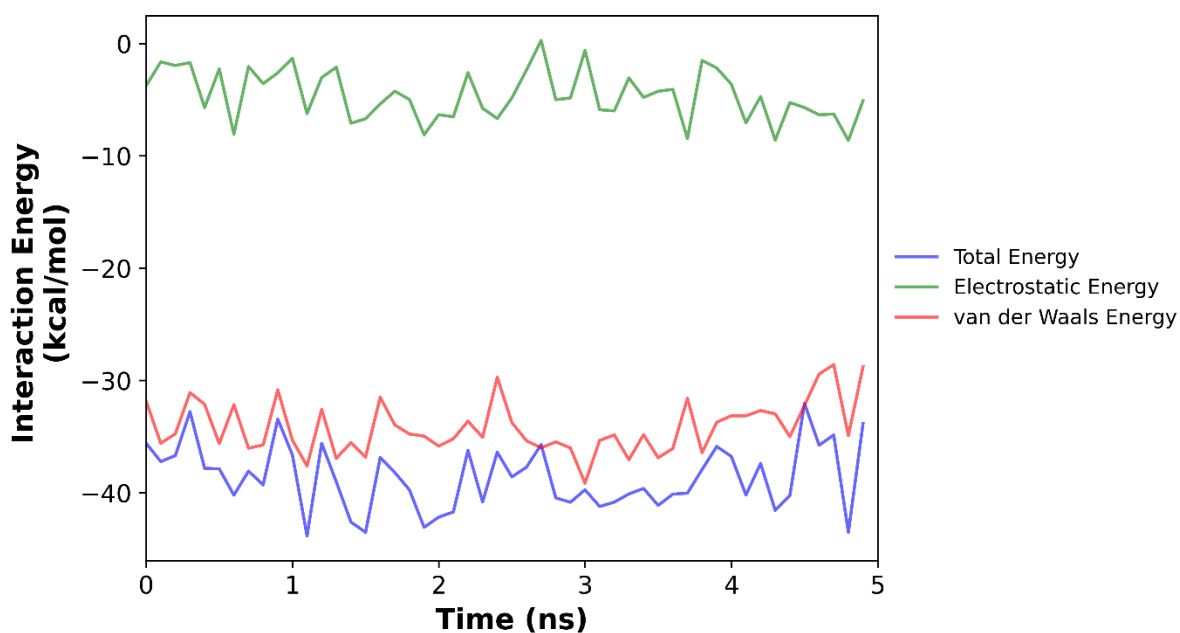


Figure 4.79: Protein–Ligand Interaction Energy

This figure breaks down the interaction energies between Lichexanthone and Tyrosinase into:

- **Total Interaction Energy (blue):** Varies from  $-45$  to  $-32$  kcal/mol, indicating a consistently favorable binding profile with moderate fluctuations throughout the 5 ns simulation.
- **Electrostatic Energy (green):** Fluctuates within  $-1$  to  $-9$  kcal/mol, showing a moderate and favorable electrostatic contribution to the interaction.
- **van der Waals Energy (red):** Ranges between  $-35$  to  $-27$  kcal/mol, dominating the interaction and closely tracking the total energy, indicating vdW forces as the primary stabilizing factor.

Lichexanthone shows stable and favorable binding to Tyrosinase, primarily driven by van der Waals interactions with moderate electrostatic support.

## STRUCTURAL COMPACTNESS

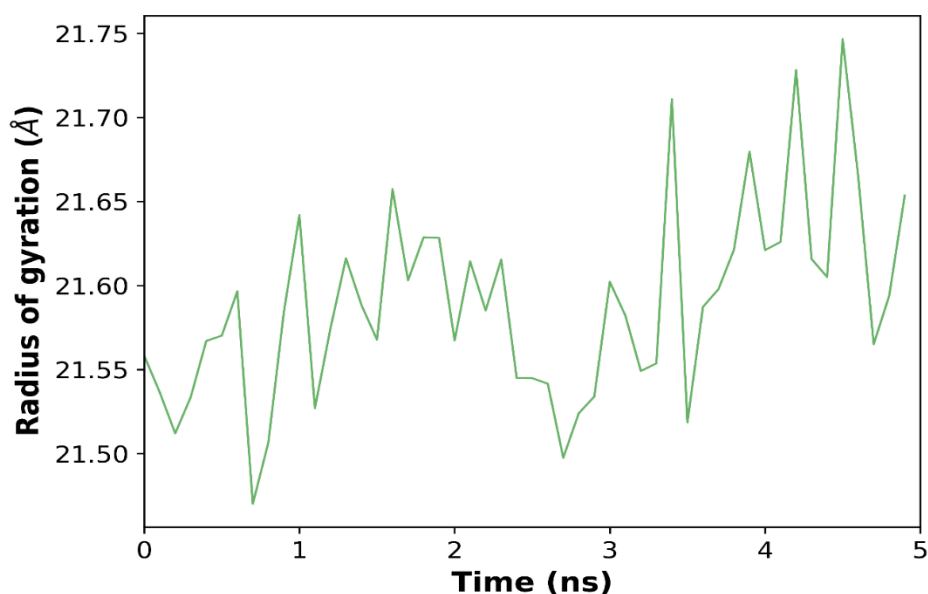


Figure 4.80: Radius of Gyration (Rg)

In the Tyrosinase–Lichexanthone complex, Rg remains constant for the 5 ns time period studied. The values for Rg are close together at approximately 21.48 and 21.74 Å, suggesting that the protein only slightly changes in general size and shape. It appears that the protein preserves its structure with the ligand nearby, as there is not much unfolding or spreading occurring. Overall, the findings demonstrate that tertiary structure in Tyrosinase seems to remain stable after the interaction with Lichexanthone which suggests that this interaction is beneficial and structurally sound.

## CONFORMATIONAL FLEXIBILITY AND PRINCIPAL MOTIONS

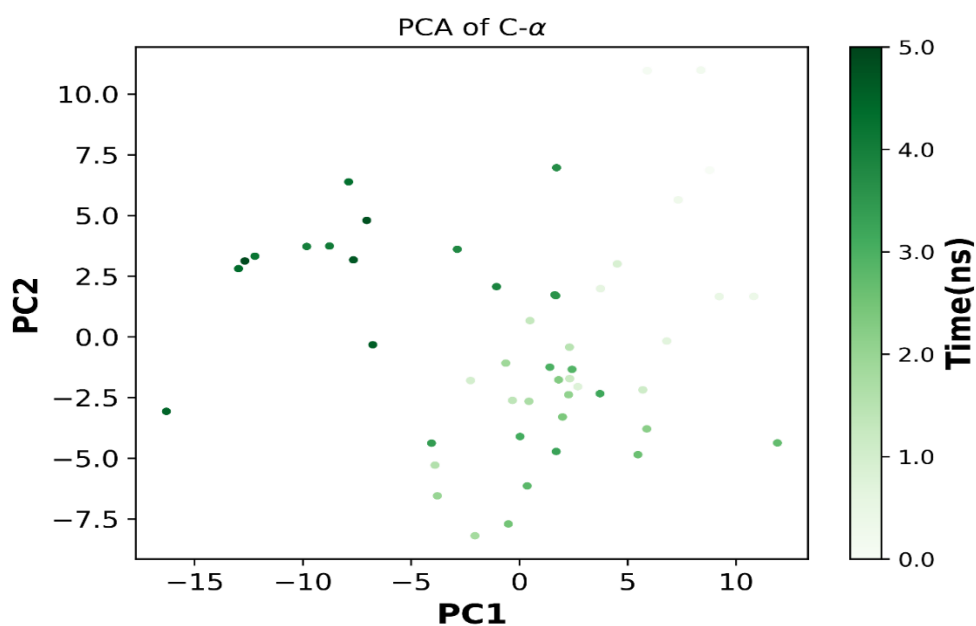


Figure 4.81: Principal Component Analysis (PCA)

The Tyrosinase–Lichexanthone complex C- $\alpha$  plot through PCA shows that there was a moderate amount of variation in the protein conformation during the 5 ns simulation. The spread of points on PC1 (covering about -15 to +12) and PC2 (covering roughly -8 to +11) points out that the protein fits into many different but not extremely different conformational states. Because the simulation time appears as a smooth gradient, the system appears to transition gradually from one state to another, rather than experiencing sudden restructuring. The fact that the system stays stable and flexible while operating is consistent with the conclusion that the complex structure does not collapse during the simulation.

In conclusion, results from molecular dynamics simulation suggest that Tyrosinase reacts well and stably with Lichexanthone. Results from the RMSF analysis suggest that most areas of the protein exhibit moderate flexibility, while the loop areas are expected to move, helping protect the protein's structure. No sudden changes are observed in the 2D RMSD plot which highlights how structure remains stable throughout time. The increase observed in the distance plot is modest, still staying within the correct non-covalent range, meaning the binding remains stable. The radius of gyration does not change significantly during the simulation which means the protein remains tightly structured. In the end, PCA demonstrates that the protein's conformations change gradually and remain restricted to equilibrated states. Overall, these results suggest that Lichexanthone connects reliably with Tyrosinase which supports its value as a ligand for continued development.

## CHAPTER 5

### CONCLUSION AND FUTURE SCOPE

#### 5.1 CONCLUSION

Vitiligo is a type of skin condition that leads to significant mental and social problems for many people. Regardless of the available options such as corticosteroids, phototherapy or surgery, it is challenging to predict the results and recurrence happens frequently for these patients. Most of the existing therapies mainly work by decreasing or increasing the immune system or stimulating the growth of melanocytes, so improving tyrosinase metabolism or combating oxidative stress is seldom included. That's why finding new substances that can manage melanogenesis by affecting tyrosinase, the main enzyme involved in melanin production, could be effective in treating vitiligo.

This thesis investigated the tyrosinase-binding potential and pharmacokinetic profiles of five structurally diverse natural compounds—Hinokinin, Lichexanthone, Tabernaemontanine, Dregamine, and Herboxidiene—through a structure-based drug discovery approach using molecular docking, ADME prediction, and molecular dynamics simulations.

The molecular docking study revealed that Hinokinin interacted most strongly with the active site of tyrosinase, with a docking energy of  $-12.44$  kcal/mol and an inhibition constant in the picomolar range, indicating that Hinokinin is very potent. It developed hydrogen bonds and hydrophobic interactions with CYS-113, LYS-233 and ARG-118 at the active site of the enzyme. It is found that Lichexanthone also displayed excellent docking results, with stable and meaningful interactions like those from van der Waals and  $\pi$ - $\pi$  stacking. The compounds lay within the center of the enzyme complex and were involved in beneficial interactions which could alter how the enzyme functions.

It was found through SwissADME that each compound satisfies the rule of drug-likeness, does not break Lipinski's Rule of Five, has high oral bioavailability scores and shows strong absorption in the gastrointestinal tract. Systemic and neuroactive uses are expected for Hinokinin and Tabernaemontanine, as they were predicted to enter the brain via the blood-brain barrier. In addition, no compounds set off PAINS or Brenk-restricted flags and all showed that they are easily synthesized which supports their potential to advance in drug development.

To confirm the flexibility of these complexes, 5-nanosecond MD simulations were run. It was found through RMSD, RMSF, radius of gyration (Rg), ligand-protein interaction distance and PCA that the structure of the complexes remained stable throughout the simulation. RMSD values stayed between the permitted range ( $0.8$ – $1.5$  Å) and Rg was also stable ( $\sim 21.5$ – $21.7$  Å), proving that the overall structure of the protein was unchanged. PCA analysis indicated that the complexes had limited motions which shows that their structures were consistent rather than changing at random.

According to the MD simulation results, Hinokinin maintained a strong interaction energy range between  $-50$  and  $-37$  kcal/mol, mainly influenced by van der Waals forces and further

supported by positive electrostatic interactions. This provided additional support for the observation made during docking that the binding of proteins depends largely on non-covalent interactions. Conversely, Tabernaemontanine and Dregamine showed steady RMSD but observed large interaction distances and less supportive energy, suggesting these two molecules interact slightly less strongly compared to the other ones. Even though Herboxidiene broke down at the end of the simulation, its strong macrocyclic nature made its structure especially interesting and called for further analysis.

According to the results, Hinokinin and Lichexanthone were found to interact the best with the targeted protein, show strong complex formation, have favorable pharmacological properties and maintain their chemical structure all through the simulation. Their interaction with the dinuclear copper part of tyrosinase and essential catalytic amino acids suggests that they can be experimentally studied to stabilize or activate the enzyme. It is also significant that these compounds exhibit antioxidant and anti-inflammatory properties and this may prevent melanin-generating cells from experiencing ROS-induced apoptosis which often leads to vitiligo.

In summary, this study successfully combined computational approaches to identify plant-derived compounds with high potential to support melanogenesis via tyrosinase modulation. The integration of molecular docking, ADME screening, and MD simulations provided a reliable platform to predict molecular behaviour and pharmacological viability. The findings lay the groundwork for future in vitro and in vivo experimentation to validate these compounds as drug candidates for repigmentation therapies in vitiligo.

## 5.2 FUTURE SCOPE

This study utilized molecular docking, ADME screening and MD simulations to examine five phytochemicals (Hinokinin, Lichexanthone, Tabernaemontanine, Dregamine and Herboxidiene) for their capability to influence tyrosinase and possibly treat vitiligo. The study revealed that Hinokinin and Lichexanthone were the strongest and most suitable binders, although further research should be done on the other compounds since they also showed special qualities. The study sets up a broad platform for future research in drug discovery, understanding mechanisms and clinical developments.

Studying these molecules in more detail in biochemical systems may clarify how they keep tyrosinase stable when there are oxidative or inflammatory changes in vitiligo. Interactions with enzymes, coordination with copper ions and resistance to being broken down by proteasomes may define their potential to support or boost melanin production. Enzymes protected by Hinokinin and Lichexanthone which computed models demonstrate great stability, might be useful for both maintaining enzyme activity and supporting melanogenesis.

Cell-based studies may establish the compounds' ability to enhance melanin biosynthesis, prevent melanocyte apoptosis, or support dendritic architecture, all of which are essential for effective repigmentation. Compounds such as Dregamine and Tabernaemontanine, despite

their weaker binding, can still support tyrosinase by protecting cells from too much oxidative stress or changing their level of antioxidants. Due to its circular shape, Herboxidiene may work differently from other bioactive molecules, either affecting the enzyme's activity or strengthening its structure.

Since the five compounds demonstrate unique pharmacokinetic properties, they can be formulated differently for oral, transdermal or topical administration. Using information about their physicochemical structure, it becomes possible to explore nanoemulsions and micellar gels for the localized and sustained application of these drugs. The need for long-term, site-specific approaches is why it's even more important to consider formulation issues in vitiligo.

A wider study could analyze these compounds while testing them on both the tyrosinase enzyme and other important proteins related to producing melanin such as TRP-1, TRP-2 and MITF. Such an approach can help create agents that treat the different issues or molecular disruptions, behind depigmentation. Furthermore, putting these compounds together in combinations, along with recognized melanogenic agents, could improve their therapeutic effects.

Analysing simulation runs for a long time and separating the energies may provide insight into key actions at the residue level, helping in analog structure–activity relationship studies for SAR. The findings from computational methods can guide the addition of potential substitutes for the discovered phytochemicals into the current screening database.

This study lays out a basic framework for using natural products as stabilizers or enhancers of tyrosinase which is essential for including them in treatments for melanogenesis. Future work in this area covers molecular developments, studies of mechanisms, formulation science for products and strategies for pigmentation disorders such as vitiligo.

## REFERENCES

1. Srivastav, Y., et al., *A Comprehensive Description of Vitiligo Disease and Its Medication Based Management*. International Journal of Medical Sciences (IJMS), 2024. **2**(1).
2. Mohammed, G.F., A.H. Gomaa, and M.S. Al-Dhubaibi, *Highlights in pathogenesis of vitiligo*. World Journal of Clinical Cases: WJCC, 2015. **3**(3): p. 221.
3. Bleehen, S.S., *The treatment of vitiligo with topical corticosteroids. Light and electronmicroscopic studies*. The British Journal of Dermatology, 1976. **94**: p. 43-50.
4. Lee, J.H., et al., *Treatment outcomes of topical calcineurin inhibitor therapy for patients with vitiligo: a systematic review and meta-analysis*. JAMA dermatology, 2019. **155**(8): p. 929-938.
5. Hamzavi, I., et al., *Parametric modeling of narrowband UV-B phototherapy for vitiligo using a novel quantitative tool: the Vitiligo Area Scoring Index*. Archives of dermatology, 2004. **140**(6): p. 677-683.
6. Shenoi, S.D. and S. Prabhu, *Photochemotherapy (PUVA) in psoriasis and vitiligo*. Indian journal of dermatology, venereology and leprology, 2014. **80**: p. 497.
7. Frączek, A., et al., *Surgical treatment of vitiligo*. International journal of environmental research and public health, 2022. **19**(8): p. 4812.
8. Grimes, P.E. and R. Nashawati, *Depigmentation Therapies for Vitiligo*. Dermatologic clinics, 2017. **35**(2): p. 219-227.
9. Solano, F., *Photoprotection and skin pigmentation: Melanin-related molecules and some other new agents obtained from natural sources*. Molecules, 2020. **25**(7): p. 1537.
10. Fitzpatrick, T.B., et al., *Tyrosinase in human skin: demonstration of its presence and of its role in human melanin formation*. Science, 1950. **112**(2904): p. 223-225.
11. Cieńska, M., et al., *Effective L-tyrosine hydroxylation by native and immobilized tyrosinase*. PLoS One, 2016. **11**(10): p. e0164213.
12. Niu, C. and H.A. Aisa, *Upregulation of melanogenesis and tyrosinase activity: potential agents for vitiligo*. Molecules, 2017. **22**(8): p. 1303.
13. Zolghadri, S., et al., *Targeting tyrosinase in hyperpigmentation: Current status, limitations and future promises*. Biochemical pharmacology, 2023. **212**: p. 115574.
14. Song, Y.-H., et al., *The role of tyrosinase in autoimmune vitiligo*. The Lancet, 1994. **344**(8929): p. 1049-1052.
15. Jang, J.-H. and T.-J. Lee, *Mechanisms of phytochemicals in anti-inflammatory and anti-cancer*. 2023, MDPI. p. 7863.
16. Habachi, E., et al., *Arbutus unedo: Innovative Source of antioxidant, anti-Inflammatory and anti-tyrosinase phenolics for novel cosmeceuticals*. Cosmetics, 2022. **9**(6): p. 143.
17. Cabanes, J., S. Chazarra, and F. GARCIA-CARMONA, *Kojic acid, a cosmetic skin whitening agent, is a slow-binding inhibitor of catecholase activity of tyrosinase*. Journal of Pharmacy and Pharmacology, 1994. **46**(12): p. 982-985.
18. Marcotullio, M.C., A. Pelosi, and M. Curini, *Hinokinin, an emerging bioactive lignan*. Molecules, 2014. **19**(9): p. 14862-14878.
19. Marković, Z.S. and N.T. Manojlović, *Analytical characterization of lichexanthone in lichen: HPLC, UV spectroscopic, and DFT analysis of lichexanthone extracted from Laurera benguelensis (Mull. Arg.) Zahlbr.* Monatshefte für Chemie-Chemical Monthly, 2010. **141**: p. 945-952.
20. Silveira, D., et al., *Tabernaemontana species: Promising sources of new useful drugs*. Studies in Natural Products Chemistry, 2017. **54**: p. 227-289.
21. Paterna, A., et al., *Dregamine and tabernaemontanine derivatives as ABCB1 modulators on resistant cancer cells*. European Journal of Medicinal Chemistry, 2017. **128**: p. 247-257.
22. Isaac, B.G., et al., *Herboxidiene: a potent phytotoxic polyketide from Streptomyces sp. A7847*. The Journal of Organic Chemistry, 1992. **57**(26): p. 7220-7226.
23. Ferreira, L.G., et al., *Molecular docking and structure-based drug design strategies*. Molecules, 2015. **20**(7): p. 13384-13421.

24. Guedes, I.A., C.S. de Magalhães, and L.E. Dardenne, *Receptor–ligand molecular docking*. Biophysical reviews, 2014. **6**: p. 75-87.
25. Sucharitha, P., et al., *Absorption, distribution, metabolism, excretion, and toxicity assessment of drugs using computational tools*, in *Computational approaches for novel therapeutic and diagnostic designing to mitigate SARS-CoV-2 infection*. 2022, Elsevier. p. 335-355.
26. Huey, R., G.M. Morris, and S. Forli, *Using AutoDock 4 and AutoDock vina with AutoDockTools: a tutorial*. The Scripps Research Institute Molecular Graphics Laboratory, 2012. **10550**(92037): p. 1000.
27. Haulrig, M.B., et al., *The global epidemiology of vitiligo: A systematic review and meta-analysis of the incidence and prevalence*. JEADV Clinical Practice, 2024. **3**(5): p. 1410-1419.
28. Bergqvist, C. and K. Ezzedine, *Vitiligo: a review*. Dermatology, 2020. **236**(6): p. 571-592.
29. Pahwa, P., et al., *The psychosocial impact of vitiligo in Indian patients*. Indian Journal of Dermatology, Venereology and Leprology, 2013. **79**: p. 679.
30. Rezaei, N., et al., *Autoimmunity as an aetiological factor in vitiligo*. Journal of the European Academy of Dermatology and Venereology, 2007. **21**(7): p. 865-876.
31. Chang, W.-L. and C.-H. Ko, *The role of oxidative stress in vitiligo: an update on its pathogenesis and therapeutic implications*. Cells, 2023. **12**(6): p. 936.
32. Kotb El-Sayed, M.-I., A.A. Abd El-Ghany, and R.R. Mohamed, *Neural and endocrinal pathobiochemistry of vitiligo: comparative study for a hypothesized mechanism*. Frontiers in endocrinology, 2018. **9**: p. 197.
33. Shen, C., et al., *Genetic susceptibility to vitiligo: GWAS approaches for identifying vitiligo susceptibility genes and loci*. Frontiers in genetics, 2016. **7**: p. 3.
34. Kumar, R., D. Parsad, and A. Kanwar, *Role of apoptosis and melanocytorrhagy: a comparative study of melanocyte adhesion in stable and unstable vitiligo*. British Journal of Dermatology, 2011. **164**(1): p. 187-191.
35. Wang, Y., et al., *Medicinal prospects of targeting tyrosinase: A feature review*. Current Medicinal Chemistry, 2023. **30**(23): p. 2638-2671.
36. Mahrous, M.H., et al., *Efficacy of Natural Products as Tyrosinase Inhibitors in Hyperpigmentation Therapy: Anti-Melanogenic or Anti-Browning Effects*. Chemistry & Biodiversity, 2025: p. e202403324.
37. Noh, H., et al., *Histidine residues at the copper-binding site in human tyrosinase are essential for its catalytic activities*. Journal of Enzyme Inhibition and Medicinal Chemistry, 2020. **35**(1): p. 726-732.
38. Chen, J., S. Li, and C. Li, *Mechanisms of melanocyte death in vitiligo*. Medicinal Research Reviews, 2021. **41**(2): p. 1138-1166.
39. Baldea, I., T. Mocan, and R. Cosgarea, *The role of ultraviolet radiation and tyrosine stimulated melanogenesis in the induction of oxidative stress alterations in fair skin melanocytes*. Experimental oncology, 2009.
40. Rishton, G.M., *Natural products as a robust source of new drugs and drug leads: past successes and present day issues*. The American journal of cardiology, 2008. **101**(10): p. S43-S49.
41. Roaa, M., *A review article: The importance of the major groups of plants secondary metabolism phenols, alkaloids, and terpenes*. International Journal for Research in Applied Sciences and Biotechnology (IJRASB), 2020. **7**(5): p. 354-358.
42. Tripathi, N., et al., *Phytochemical and Pharmacological Aspects of Psoralen—A Bioactive Furanocoumarin from Psoralea corylifolia Linn*. Chemistry & Biodiversity, 2023. **20**(11): p. e202300867.
43. Kim, K., *Effect of ginseng and ginsenosides on melanogenesis and their mechanism of action*. Journal of Ginseng Research, 2015. **39**(1): p. 1-6.
44. Li, X., et al., *Baicalein inhibits melanogenesis through activation of the ERK signaling pathway*. International journal of molecular medicine, 2010. **25**(6): p. 923-927.
45. Agarwal, S. and R. Mehrotra, *An overview of molecular docking*. JSM chem, 2016. **4**(2): p. 1024-1028.
46. Ravindranath, P.A., et al., *AutoDockFR: advances in protein-ligand docking with explicitly specified binding site flexibility*. PLoS computational biology, 2015. **11**(12): p. e1004586.



47. Madeswaran, A. and K. Asokkumar, *Evaluation of inhibitory affinity potential of the alkaloids against crystal structure of human angiotensin-converting enzyme using Lamarckian genetic algorithm*. Oriental Pharmacy and Experimental Medicine, 2015. **15**: p. 183-189.
48. Daoud, N.E.-H., et al., *ADMET profiling in drug discovery and development: perspectives of in silico, in vitro and integrated approaches*. Current Drug Metabolism, 2021. **22**(7): p. 503-522.
49. Daina, A., O. Michielin, and V. Zoete, *SwissADME: a free web tool to evaluate pharmacokinetics, drug-likeness and medicinal chemistry friendliness of small molecules*. Scientific reports, 2017. **7**(1): p. 42717.
50. Li, A.-L., et al., *Lignan and flavonoid support the prevention of cinnamon against oxidative stress related diseases*. Phytomedicine, 2019. **53**: p. 143-153.
51. Masters, K.-S. and S. Bräse, *Xanthones from fungi, lichens, and bacteria: the natural products and their synthesis*. Chemical reviews, 2012. **112**(7): p. 3717-3776.
52. Oriola, A.O. and P. Kar, *Naturally occurring xanthones and their biological implications*. Molecules, 2024. **29**(17): p. 4241.
53. Camponogara, C., et al., *Tabernaemontana catharinensis leaves exhibit topical anti-inflammatory activity without causing toxicity*. Journal of Ethnopharmacology, 2019. **231**: p. 205-216.
54. Xu, Y., X. Liang, and C.-G. Hyun, *Discovery of Indole–Thiourea Derivatives as Tyrosinase Inhibitors: Synthesis, Biological Evaluation, Kinetic Studies, and In Silico Analysis*. International Journal of Molecular Sciences, 2024. **25**(17): p. 9636.
55. Khongsombat, O., *Inhibitory effects of Tabernaemontana divaricata root extract on oxidative stress and neuronal loss induced by amyloid  $\beta$ 25–35 peptide in mice*. Journal of traditional and complementary medicine, 2018. **8**(1): p. 184-189.
56. Gonçalves, B.M., et al., *Monoterpene indole alkaloids with anticancer activity from Tabernaemontana species*. Phytochemistry Reviews, 2024: p. 1-37.
57. Pokhrel, A.R., et al., *Herboxidiene biosynthesis, production, and structural modifications: prospect for hybrids with related polyketide*. Applied microbiology and biotechnology, 2015. **99**: p. 8351-8362.
58. Smith, N.D., P.J. Kocienski, and S.D. Street, *A synthesis of (+)-Herboxidiene A*. Synthesis, 1996. **1996**(05): p. 652-666.
59. Polák, L., et al., *PrankWeb 4: a modular web server for protein–ligand binding site prediction and downstream analysis*. Nucleic Acids Research, 2025: p. gkaf421.

## LIST OF PUBLICATIONS

K. Bhatia and Y. Hasija, "Revolutionizing Patient Care: AI-Driven Wearable Technology for Continuous Remote Health Monitoring," 2025 International Conference on Cognitive Computing in Engineering, Communications, Sciences and Biomedical Health Informatics (IC3ECSBHI), Greater Noida, India, 2025, pp. 404-409

doi: 10.1109/IC3ECSBHI63591.2025.10990913.

The screenshot shows the IEEE Xplore website interface. At the top, there is a navigation bar with links to IEEE.org, IEEE Xplore, IEEE SA, IEEE Spectrum, and More Sites. A search bar is present with a dropdown menu set to 'All' and a search button. Below the navigation bar, the page title 'Revolutionizing Patient Care: AI-Driven Wearable Technology for Continuous Remote Health Monitoring' is displayed. The publisher is listed as IEEE, and there are buttons for 'Cite This' and 'PDF'. The authors are listed as Khushi Bhatia and Yasha Hasija. The abstract section is visible, starting with 'Remote patient monitoring (RPM) refers to the ability of healthcare professionals to be able to monitor the well-being of their patients remotely without having to keep them under continuous in-person observation. Wearable devices that are integrated with Artificial Intelligence are a blessing in disguise when it comes to remote health monitoring. PPG sensors, ECG sensors, accelerometers, pulse oximeter and EDA sensor are some of these AI integrated wearable devices used for continuous remote health monitoring which are discussed in this article. We delved into their specific working mechanism, how the data is collected, stored and transferred and how the use of artificial intelligence algorithms come into all of this. These devices have applications in fields such as cloud computing and big data analytics for health management which are discussed along with key innovations. Certain issues such as data accuracy, data privacy and regulations are also addressed along with future directions which can be pursued that may have the potential to revolutionize the field of remote health monitoring even more'.



# DELHI TECHNOLOGICAL UNIVERSITY

(Formerly Delhi College of Engineering)

Shahbad Daultpur, Main Bawana Road, Delhi-42

## **PLAGIARISM VERIFICATION**

Title of the Thesis: **“Integrative In Silico Drug Discovery: Targeting Tyrosinase with Natural Compounds for therapeutic management of Vitiligo”**

Total Pages: **118**

Name of the Scholar: **Khushi Bhatia**

Supervisor: **Prof. Yasha Hasija**

Department: **Biotechnology**

This is to report that the above thesis was scanned for similarity detection. Process and outcome is given below:

Software used: **Turnitin** Similarity Index: **9%**, Total Word Count: **22,098**

Date: **27-05-2025**

**Candidate's Signature**

**Signature of Supervisor(s)**

# Mtech Thesis.docx

 Delhi Technological University

---

## Document Details

Submission ID

trn:oid:::27535:97979677

Submission Date

May 27, 2025, 4:01 PM GMT+5:30

Download Date

May 27, 2025, 4:08 PM GMT+5:30

File Name

Mtech Thesis.docx

File Size

9.1 MB

118 Pages

22,098 Words

131,845 Characters





# 9% Overall Similarity

The combined total of all matches, including overlapping sources, for each database.




## Filtered from the Report

- Bibliography
- Cited Text
- Small Matches (less than 10 words)

## Match Groups


-  **125** Not Cited or Quoted 9%  
Matches with neither in-text citation nor quotation marks
-  **0** Missing Quotations 0%  
Matches that are still very similar to source material
-  **1** Missing Citation 0%  
Matches that have quotation marks, but no in-text citation
-  **0** Cited and Quoted 0%  
Matches with in-text citation present, but no quotation marks

## Top Sources

- 6%  Internet sources
- 4%  Publications
- 7%  Submitted works (Student Papers)

## Integrity Flags

### 1 Integrity Flag for Review

-  **Replaced Characters**  
12 suspect characters on 12 pages  
Letters are swapped with similar characters from another alphabet.

Our system's algorithms look deeply at a document for any inconsistencies that would set it apart from a normal submission. If we notice something strange, we flag it for you to review.

A Flag is not necessarily an indicator of a problem. However, we'd recommend you focus your attention there for further review.

## \*% detected as AI

AI detection includes the possibility of false positives. Although some text in this submission is likely AI generated, scores below the 20% threshold are not surfaced because they have a higher likelihood of false positives.

**Caution: Review required.**

It is essential to understand the limitations of AI detection before making decisions about a student's work. We encourage you to learn more about Turnitin's AI detection capabilities before using the tool.

### Disclaimer

Our AI writing assessment is designed to help educators identify text that might be prepared by a generative AI tool. Our AI writing assessment may not always be accurate (it may misidentify writing that is likely AI generated as AI generated and AI paraphrased or likely AI generated and AI paraphrased writing as only AI generated) so it should not be used as the sole basis for adverse actions against a student. It takes further scrutiny and human judgment in conjunction with an organization's application of its specific academic policies to determine whether any academic misconduct has occurred.

## Frequently Asked Questions

### How should I interpret Turnitin's AI writing percentage and false positives?

The percentage shown in the AI writing report is the amount of qualifying text within the submission that Turnitin's AI writing detection model determines was either likely AI-generated text from a large-language model or likely AI-generated text that was likely revised using an AI-paraphrase tool or word spinner.

False positives (incorrectly flagging human-written text as AI-generated) are a possibility in AI models.

AI detection scores under 20%, which we do not surface in new reports, have a higher likelihood of false positives. To reduce the likelihood of misinterpretation, no score or highlights are attributed and are indicated with an asterisk in the report (\*%).

The AI writing percentage should not be the sole basis to determine whether misconduct has occurred. The reviewer/instructor should use the percentage as a means to start a formative conversation with their student and/or use it to examine the submitted assignment in accordance with their school's policies.

### What does 'qualifying text' mean?

Our model only processes qualifying text in the form of long-form writing. Long-form writing means individual sentences contained in paragraphs that make up a longer piece of written work, such as an essay, a dissertation, or an article, etc. Qualifying text that has been determined to be likely AI-generated will be highlighted in cyan in the submission, and likely AI-generated and then likely AI-paraphrased will be highlighted purple.

Non-qualifying text, such as bullet points, annotated bibliographies, etc., will not be processed and can create disparity between the submission highlights and the percentage shown.

